Titre: Title:	Blending Ionic Liquids to Ir Complexes for Applications in Light-Emitting Electrochemical Cells (LEECs)
Auteur: Author:	Sareh Bayatpour
Date:	2014
Type:	Mémoire ou thèse / Dissertation or Thesis
Référence: Citation:	Bayatpour, S. (2014). Blending Ionic Liquids to Ir Complexes for Applications in Light-Emitting Electrochemical Cells (LEECs) [Mémoire de maîtrise, École Polytechnique de Montréal]. PolyPublie. https://publications.polymtl.ca/1387/

URL de PolyPublie: PolyPublie URL:	https://publications.polymtl.ca/1387/
Directeurs de recherche: Advisors:	Clara Santato, & Fabio Cicoira
Programme: Program:	Génie métallurgique

UNIVERSITÉ DE MONTRÉAL

BLENDING IONIC LIQUIDS TO Ir COMPLEXES FOR APPLICATIONS IN LIGHT-EMITTING ELECTROCHEMICAL CELLS (LEECs)

SAREH BAYATPOUR

DÉPARTEMENT DE GÉNIE PHYSIQUE
ÉCOLE POLYTECHNIQUE DE MONTRÉAL

MÉMOIRE PRÉSENTÉ EN VUE DE L'OBTENTION

DU DIPLÔME DE MAÎTRISE ÈS SCIENCES APPLIQUÉES
(GÉNIE MÉTALLURGIQUE)

AVRIL 2014

UNIVERSITÉ DE MONTRÉAL

ÉCOLE POLYTECHNIQUE DE MONTRÉAL

Ce mémoire intitulé

BLENDING IONIC LIQUIDS TO Ir COMPLEXES FOR APPLICATIONS IN LIGHT-EMITTING ELECTROCHEMICAL CELLS (LEECs)

présenté par : BAYATPOUR Sareh

en vue de l'obtention du diplôme de : Maîtrise ès sciences appliquées

a été dûment accepté par le jury d'examen constitué de :

M. SAVADOGO Oumarou, D.d'état., président

Mme SANTATO Clara, Doct., membre et directrice de recherche

M. CICOIRA Fabio, Ph. D., membre et codirecteur de recherche

Mme BADIA Antonella, Ph. D., membre

DEDICATION

To: Mohammad,
My lovely daughters
And my parents

ACKNOWLEDGMENTS

Foremost, I would like to thank my supervisor, Prof. Clara Santato and co-supervisor Prof. Fabio Cicoira for their constant support during my research, for their patient guidance, encouragement, enthusiasm, and knowledge. I would also like to express my sincere gratitude to Clara for giving me a chance to join her group, for her guidance through my study and research, for her constant encouragement and unending enthusiasm to explore new fields. I have been extremely lucky to have a supervisor who cared so much about my work. Without her guidance as a great mentor, this work would not have been possible.

I would also like to extend my appreciation to my committee members, Prof. Antonella Badia, and Prof. Oumarou Savadogo for taking their valuable time and providing great input into this work.

My special thanks also go to my fellow colleagues in the research laboratory, who helped me and shared their experiences and knowledge during my master project.

I am also very thankful to Patricia Moraille, Joël Bouchard, Jean-Paul Levesque and Yves Drolet for their generous technical support and for providing me with trainings on the instruments.

I am truly grateful to my parents and all my family. It would be impossible for me to finish this work without their endless support, encouragement, love and patience.

Lastly, I owe a big thank you to Mohammad. His love and support have made my life better in so many ways. I owe the completion of this work to his enthusiasm and fresh perspective when things looked down.

RÉSUMÉ

À l'heure actuelle, la recherche de nouvelles sources de lumière efficaces à bas cout connaît une progression impressionnante. Les cellules électrochimiques émettrices de lumière (LEECs) sont des sources de lumière à deux électrodes à base de complexes de métaux de transition ioniques (iTMCs) ou bien de polymères organiques, en tant que matériau pour l'émission. Le matériau émetteur peut être mélangé avec des électrolytes. Les électrolytes sont ajoutés pour diminuer la tension de fonctionnement du dispositif, à travers l'amélioration de l'efficacité du processus d'injection de porteurs de charge. Les avantages des polymères sont : faible coût, facilité de mise en œuvre, possibilité dé dépôt sur des grandes surfaces, flexibilité, et, surtout, possibilité de moduler la couleur d'émission en modifiant la structure moléculaire du polymère au moyen de la synthèse chimique. Néanmoins, les LEECs à base de iTMCs montrent une plus grande efficacité en raison de l'émission de lumière par phosphorescence en plus du processus de fluorescence. L'un des principaux défis dans le domaine des LEECs est leur long temps de commutation, en raison du transport ionique, relativement long, qui a lieu dans les dispositifs. Ce temps peut être réduit en utilisant, en tant qu'électrolyte, un liquide ionique (IL). Par rapport aux sels conventionnels, les liquides ioniques présentent une mobilité ionique plus élevée conduisant à son tour à un temps de commutation plus court. Cependant la présence de liquides ioniques dans la couche est accompagnée par une diminution de la stabilité du dispositif. Des études fondamentales sont nécessaires pour mieux comprendre le mécanisme de travail de LEECs et en améliorer les performances. A cette fin, l'architecture idéale est celle planaire, car elle permet la mesure directe de l'intensité de la lumière émise, par des sondes optiques. En plus de cela, la fabrication du dispositif planaire est beaucoup plus simple que la fabrication d'un dispositif analogue vertical. Des dispositifs LEECs planaires à base de iTMC n'ont jamais été construits. Dans ce travail, des couches minces de $Ir(ppy)_2(bpy)^+PF_6^-$ ou bien de mélanges de $Ir(ppy)_2(bpy)^+PF_6$/$BMIm^+PF_6^-$ ont été déposées par méthode spin-coating sur des substrats différents, y compris des motifs d'Au sur SiO_2, Au sur verre, verre conducteur, et verre conducteur modifié avec le polymère conducteur PEDOT : PSS. Nous avons étudié l'effet de la nature du substrat et des conditions de dépôt de la couche mince sur la morphologie de la couche mince, pour avancer les connaissances sur le mécanisme de fonctionnement de LEECs. La formation de la couche a été étudiée en utilisant l'imagerie de fluorescence hyperspectrale et la

microscopie à force atomique (AFM). Nous avons constaté que les couches sont constitués de particules dont la densité, la forme, la taille et la connectivité dépendent fortement de la composition chimique des couches et de la nature du substrat.

ABSTRACT

At present, the search for novel efficient and low cost solid state light sources is experiencing impressive progress.

Light emitting electrochemical cells (LEECs) are two-electrode light sources made of ionic transition metal complexes (iTMCs) or organic polymers as the light emitting material, in some cases blended with electrolytes. Electrolytes are intended for lowering the operating voltage of the device by improving the efficiency of the charge carrier injection process. The advantages of polymer semiconductors include low cost, easy processing in solution for use in large area and flexible devices, different colors of light emission tailorable by molecular synthesis. Nevertheless, LEECs based on iTMCs show higher efficiency due to light emission via phosphorescence in addition to fluorescence processes.

One of the main challenges in the field of LEECs is their long turn on time, due to *ionic* transport in the cell. The turn on time can be decreased by using as the electrolyte an ionic liquid (IL). Compared to conventional salts, ionic liquids exhibit higher ion mobility leading to lower turn on times. However, the presence of ILs in the film is unfortunately accompanied by a decrease in the stability of the device. Fundamental studies are needed to better understand the LEEC working mechanism and improve device performance. For this purpose, the ideal architecture for LEECs is a planar one since it enables the direct measurement of the intensity of the emitted light by optical probes as well as the imaging of the emission. In addition to that, planar device fabrication is much simpler than vertical.

LEECs with a *planar* configuration based on Ir complexes have not been reported. In this work, thin films of $Ir(ppy)_2(bpy)^+PF_6^-$ and blends of $Ir(ppy)_2(bpy)^+PF_6^-$/$BMIm^+PF_6^-$ were spin coated on different substrates, including Au-patterned SiO_2, Au-patterned glass, ITO, and PEDOT:PSS covered-ITO. The effect on the film morphology of the nature of the substrate and the film processing conditions was investigated, to shed light in to the LEEC working mechanism.

Film formation was studied using fluorescence hyperspectral imaging and Atomic Force Microscopy (AFM). We found that the films are constituted of particles whose density, shape,

size, and connectivity strongly depend on the substrate surface and chemical composition of thin films.

TABLE OF CONTENTS

LIST OF TABLES

LIST OF FIGURES

LIST OF ACRONYMS AND ABBREVIATIONS

AFM	Atomic Force Microscopy
$BMIM^{+}PF_6^{-}$	1-Butyl-3-methylimidazolium hexafluorophosphate
CC	Correlation coefficient
CVD	Chemical vapor deposition
DFT	Density functional theory
EL	Electroluminescence
FOV	Field of view
HOMO	Highest occupied molecular orbital
IL	Ionic liquid
IPA	Isopropyl alcohol
$Ir(ppy)_2(bpy)^{+}PF_6^{-}$	Bis(2-phenylpyridine-C,N)(2,2′-bipyridine-N,N′)iridium(III) hexafluorophosphate
ISC	Intersystem crossing
iTMC	Ionic transition metal complexes
ITO	Indium tin oxide
LC	Ligand centered
LEDs	Light emitting diodes
LEECs	Light emitting electrochemical cells

LUMO	Lowest unoccupied molecular orbital
MEH-PPV	Poly [2- methoxy-5-(2'-ethylhexyloxy)-p-phenylenevinylene]
MLCT	Metal-ligand charge transfer
MOs	Molecular Orbitals
OLEDs	Organic light emitting diodes
OLETs	Organic light emitting transistors
PARISS	Prism And Reflector Imaging Spectroscopy System
PEDOT:PSS	Poly (3, 4-ethylenedioxythiophene): poly (styrene sulfonate)
PL	Photoluminescence
PLECs	Polymer light emitting electrochemical cells
PPV	Poly (p-phenylenevinylene)
SOC	Spin-orbit coupling
SSL	Solid-state lighting

LIST OF APPENDICES

CHAPTER 1 INTRODUCTION

1.1 Overview

Solid-state lighting (SSL) is a technology of light generation using light emitting diodes (LEDs). Direct conversion of electricity to light with small heat generation makes these devices efficient. LEDs are supposed to reduce at least 10% of fuel consumption and carbon dioxide emissions from manufacturers within next years [1].

To improve LEDs, important parameters such as electroluminescence quantum efficiency [2], operating voltage [2], lifetime at high brightness [3][4] and fabrication costs should be considered. In Figure 1 is shown the progress trend of lighting devices from 1975.

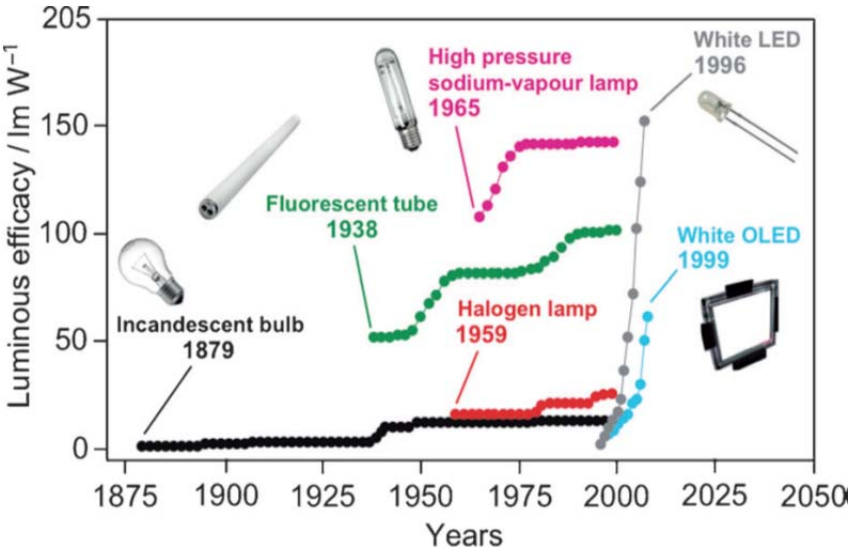

Figure 1: Progress trend of lighting device [5]

In LED fabrication, some innovative approaches are applied to increase the efficiency of devices [6-9]. For instance, flexible transparent electrodes such as graphene are used to have direct hole injection from the single-layer graphene anode into the emitter layers [6]. Substrate surface are modified to reduce charge carrier traps[10].

At present, high-performance small colorful thin displays based on organic LEDs (OLEDs) have already entered the market. However difficulty in multilayer device fabrication using vacuum deposition techniques, necessity of device encapsulation to prevent air exposure and the low

injection efficiency due to the mismatching between the work function of the electrodes and the energy levels of the light emitting materials are some disadvantages of these devices [11, 12].

In order to solve the difficulties associated to the OLEDs fabrication, light emitting electrochemical cells (LEECs) are an attractive alternative in electroluminescent lighting devices. In comparison with OLEDs, LEECs have very simple layer architecture and easy fabrication from solution. Moreover in LEECs, the work function of the metal electrodes does not have a remarkable effect on charge injection because of the presence of ions in the emissive layer [13]. The ions in LEECs are provided from either salts or ionic liquids (ILs) blended with emissive polymer in polymer light emitting electrochemical cells (PLECs) [14-17] or originate from the ionic transition metal complexes (iTMCs) used as the luminescent layer [5, 18-24].

A number of challenges still remain in the LEEC research area such as the mechanism of device operation, the synthesis of highly efficient electroluminescent materials, and the effect of the electrical bias in chemical degradation.

The goal of this work is fabrication of planar LEEC based on iTMCs. In this Mémoire, we investigate the effect of the processing conditions and quality of the substrate on the morphological properties of two component films. The films were made of the transition metal complex bis(2-phenylpyridine-C,N)(2,2′-bipyridine-N,N′)iridium(III) hexafluorophosphate $Ir(ppy)_2(bpy)^+PF_6^-$ as an active layer, and in some studies $Ir(ppy)_2(bpy)^+PF_6^-$ as an ionic liquid to improve device performance. We also include preliminary device performance measurements on LEECs based on such films.

1.2 Light Emitting Electrochemical Cells (LEECs)

The first reports on LEECs were published by the Heeger group [25]. These early LEECs were based on organic polymers as the light emitting material. According to the working mechanism proposed by Pei (electrochemical model (Figure 2)) [25], under the action of an applied electric field, the salt which is blended to the light emitting organic polymer dissociates to produce mobile cations and anions, which migrate toward the electrodes. The ions produce the electrochemical doping of the polymer, with a p-doped region forming in proximity of the anode and an n-doped region forming in proximity of the cathode.

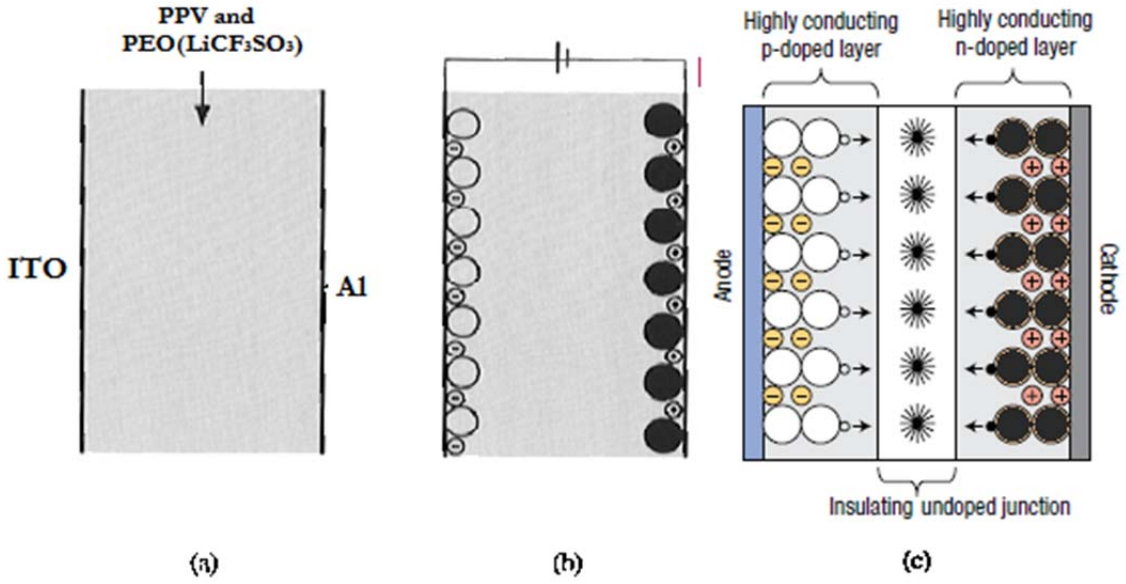

Figure 2: Electrochemical processes in LEECs, as proposed by Heeger. (a) Before the voltage is applied. (b) Immediately after the voltage is applied. (c) Light emission after voltage is applied. Large open and closed circles are oxidized and reduced molecules respectively, circled minus and plus are anions and cations, small open and closed circles are holes and electrons and asterisks are photons [25-27]

Because of electrochemical doping, the organic polymer film is conductive and the contacts at the organic polymer/metal electrode interface are ohmic. The charge carrier injection becomes independent of the work function of the metal electrodes. Following these initial publications, attempts were made to further explore the working mechanism of these devices by other groups [28-32]. A different operating mechanism for LEECs was proposed by Friend [33], excluding electrochemical doping. Upon application of an electrical bias, ions accumulate near the electrodes and an electric double layer at the semiconductor/electrode interface is formed. Due to the produced electric field, the charge injection barrier is reduced. As the electric fields near the interfaces increase, the electric field in the bulk of the emitter layer decreases. Thus, because of the charge concentration gradient, charge carrier diffusion occurs into the neutral bulk of the polymer (Figure 3). The Friend model (electrodynamic model) claims that any electrochemical doping present in LEECs under normal operation is unlikely.

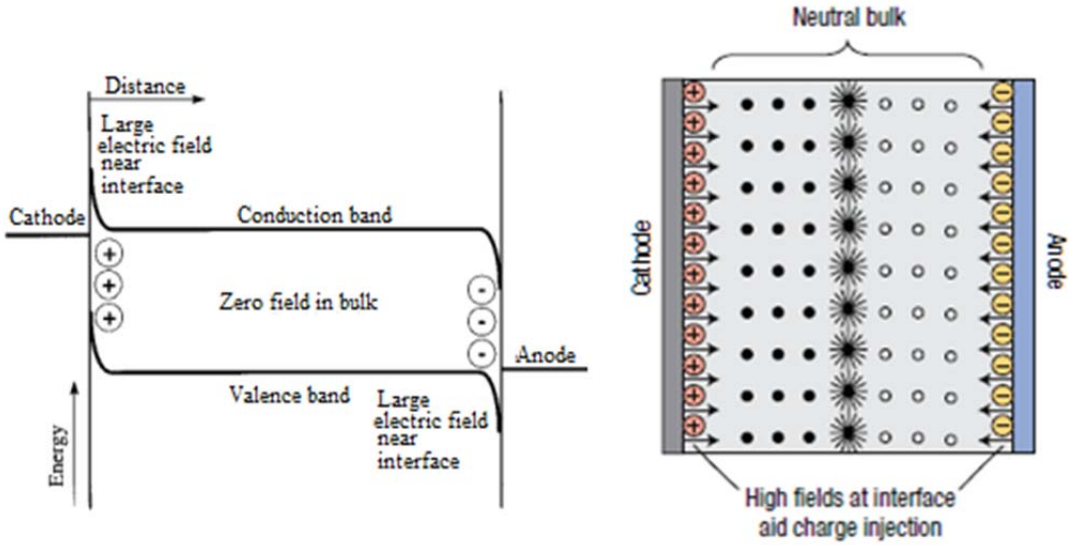

Figure 3: A schematic band diagram for a working LEEC in Friend's model [27, 33]. Circled minus and plus are anions and cations, small open and closed circles are holes and electrons and asterisks are photons.

In the electrochemical doping model the p-type and n-type regions are electrically conducting, so the electric field in these regions is zero. The light emission zone (also known as the exciton radiative recombination zone) is where the majority of the electric field exists. In the electrodynamic model, the electric field only exists near the electrodes, while in the light emission zone the electric field is nearly zero. The distribution of the electric field in both models is illustrated in Figure 4.

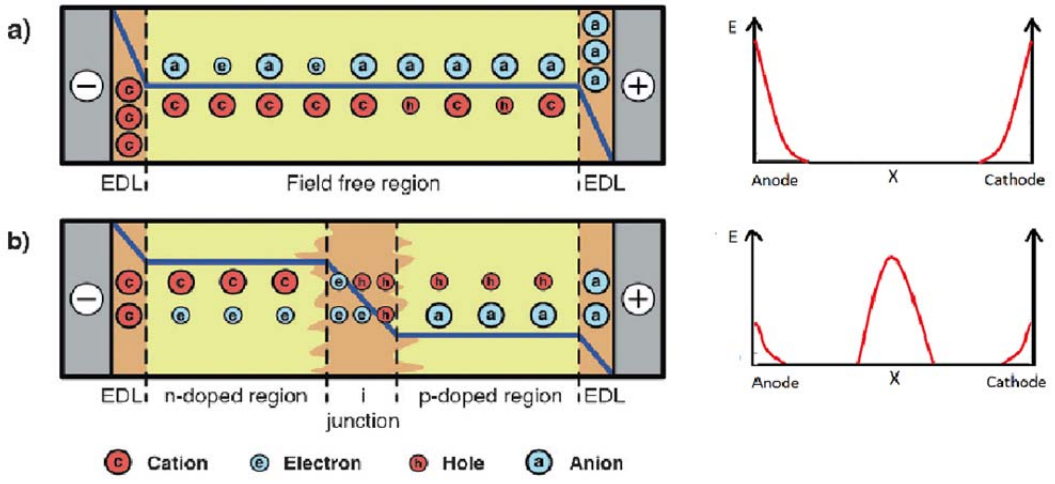

Figure 4: Distribution of the electric field within a LEEC, as described by the a) electrodynamic and b) electrochemical models [27, 34]

Subsequent studies reporting direct photoluminescence (PL) and electroluminescence (EL) imaging in LEECs with planar configuration showed a region of quenched PL that would indicate the presence of a doped polymer [35, 36]. These results suggest that the model presented by Pei is able to describe the working mechanism of LEECs. However, direct evidence to show this model is accurate and complete is still lacking.

Not only polymers but also iTMCs have been used as the light emitting materials in LEECs. iTMCs were used by Handy [37] to demonstrate LEECs with high brightness, high efficiency, and good stability. Bard [38] investigated the effect of the different TMC anions on the electroluminescence properties of LEECs, showing that the behaviour of LEECs also depends on the type and size of the counter anions in the film.

In 2005, Malliaras [39] used 1-butyl-3-methylimidazolium hexafluorophosphate $BMIM^{+}PF_6^{-}$ as the IL to improve the response time of LEECs based on iTMCs. ILs are of extreme interest for LEECs since they constitute a source of cations and anions and at the same time they facilitate ionic movement in the film [40]. After these initial experiments, different complexes with various metals and ligands were used to make LEECs with different emission colours and efficiencies [39, 41-43].

ILs are ionic compounds that are liquid at room temperature [44]. These compounds have a number of valuable physical and chemical properties such as high ionic conductivity [45], high thermal stability [46], non-flammability [47] , negligible vapour pressure [47], and stability in ambient air [48]. In some methods of LEEC fabrication, inorganic salts were used [5, 14-16, 49] while in most of them various kinds of ILs were preferred [13, 18, 45]. The advantages of ILs over inorganic salts are their solubility in most organic solvents, wide temperature range of the liquid phase, and non-volatility. The high viscosity that causes low conductivity can prevent their practical application as electrolytes [44]. Nevertheless, in the case of imidazolium salts, a high conductivity of 0.1 S/cm has been achieved [40]. Furthermore, the polarity and melting point of the imidazolium salts can be tuned by changing the substituents at the N atoms (1,3 positions) of the imidazole ring [50] (Figure 5).

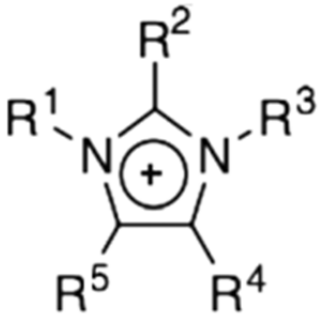

Figure 5: Molecular structure of an imidazolium cation with different substituents (R)

Generally, the cations of ILs used in LEECs are asymmetric with more than one heteroatom and the anions are weakly coordinating compounds. A result, ILs have high polarity but small interaction between counterions [48] [51].

1.3 Luminescent materials

The demand for novel and modern lighting technologies is paralleled by the development of (electro)luminescent materials. Electroluminescence (EL) is a phenomenon of non-thermal light generation under an applied electrical bias, with subsequent current generation, to a specific material. This event was first observed in 1936 [1] for an inorganic material (ZnS) sandwiched between two electrodes. After that, in 1960 the first generation of LEDs was fabricated using

GaAsP, for commercial use. Three years after this achievement [2], EL from organic crystals of anthracene was detected. The efficiency and lifetime of this material in comparison with inorganic materials was very small, so no effort was done to improve efficiency until the late 1980's when researchers introduced the new generation of LEDs made with organic fluorescent molecules. The method for fabricating these new LEDs, physical vapour deposition, was costly and time consuming. In 1990, Friend et al. [3] facilitated a deposition technique using the solution casting method for a conjugated polymer over a large surface area. In addition to large deposition areas, low cost fabrication and capability of making very thin films are other advantages of using organic materials in electroluminescent devices. Generally speaking the most important advantage of organic materials is their adjustable color, made possible changes by their molecular structures.

Nowadays the synthesis of different EL materials is understood and different colors are attainable [4-8].

1.3.1 Organic electronic molecules

In semiconductor compounds both electrons and holes can be transported. A high electron affinity (low ionization potential) is required for electron (hole) conduction in the semiconductor [52]. The ability of charge transfer at the electrode, charge transport within the material, and luminescence efficiency are major parameters for organic electroluminescent materials [53]. Formation of transparent and non-crystalline films is one of the requirements of EL materials. Another, that complexation with molecules in adjacent layers should not occur [52]. Anthracene in single crystalline form is one of the famous electroluminescent organic compounds [54-56]; however due to poor charge injection and transport, these devices need a high operating voltage of more than 100 V [54]. EL of other organic materials such as tetracene [57-60], naphthalene [61], anthracene [62], pyrene [63] and quinacridone [64] were also investigated by different groups. However, low charge injection from the electrodes and low fluorescence quantum efficiency prevent using these materials as an emissive layer in lighting devices.

Polymer molecules are another group of materials used in electroluminescence devices. These molecules can be synthesized for a variety of purposes including different colors. Luminescent or

photoabsorptive functional groups can be added to the polymer backbone to change the properties of the organic materials. The energy band gap and the redox potential of polymers are controllable by attaching electron-withdrawing groups, electron-donating groups, or side chains [65]. Electron-donating groups shift the luminescence to lower energy and electron-accepting groups shift the luminescence to higher energy (blue shift) [66]. Doping can also change the conduction and luminescence properties of some polymers because doping can insert different energy states in the energy band gap. For instance, doping can change the electronic properties of semiconducting polymers to make them insulators or conductors [67][68]. One of the most important polymers in light emitting devices is poly(p-phenylenevinylene) (PPV) (Figure 6a) [69]. Alkoxy functionalization groups in PPV decrease the band gap of this polymer and cause a color change from yellow green for PPV to red emission for poly[2-methoxy-5-(2'-ethylhexyloxy)-p-phenylenevinylene] (MEH-PPV) (Figure 6b) [21]. Adding long side chains causes the polymeric chains to separate from each other avoiding the non-radiative relaxation and leading to higher efficiency by comparison to analogous polymers [53][70].

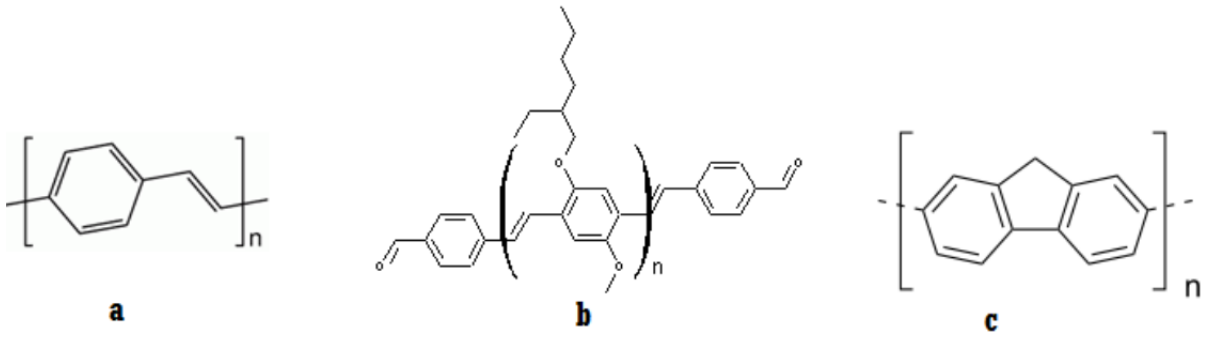

Figure 6: Molecular structures of EL compounds. a) PPV, b)MEH-PPV, c) Polyflurene

Polyfluorene (Figure 6c) [71] and its analogues are other polymers commonly used in OLEDs because of their remarkable solubility, solid-state fluorescence quantum efficiency, and their thermal and chemical stability [72, 73].

1.3.2 Ionic transition metal complexes (Electrophosphorescent materials)

Electrophosphorescent materials efficiently convert electrical energy to light. In a phosphorescence process, both singlet and triplet states are involved. Light emitting devices

made with phosphorescent materials can reach 100% internal quantum efficiency [74]; transition metal complexes are typical organometallic molecules that are used for this purpose. In these series of compounds, heavy metal atoms such as Os, Ru, Ir etc are located at the center of these complexes cause a strong spin-orbit coupling (SOC) that enables an intersystem crossing (ISC) between singlet and triplet states. When the spin of the excited electron and ground state electron are paired (unparallel) or unpaired (parallel), the molecular electronic state is called singlet and triplet state, respectively. The intersystem crossing process is a non-radiative process in which the transition occurs between two electronic states with different spins. In the spin-orbit coupling phenomenon, the electromagnetic interaction between the electron spin and the magnetic field of the nucleus causes a shift in the energy levels of the electron. When SOC is strong, it means that the energy of the electron is sufficient enough to overcome the spin forbidden transition from singlet to triplet and consequently the emission from triplet states can compete with non-radiative quenching which reduces the emission efficiency [75].

When a phosphorescent material is used in light emitting devices, due to the participation of both triplet and singlet excitons in the radiative process the quantum efficiency of the device increases [76]. An exciton is a neutral quasi-particle consisting of an electron and a hole. In addition to excited states localized on the ligands, the transfer of the electron from the metal to a ligand forms excited states and the metal atoms take part in these excited states. These states are known as a metal-ligand charge transfer (MLCT) excitons. In comparison with ligand excitons (excited states localized on the ligands), MLCT excitons have a higher overlap with the metal in the complex. As a result the spin orbit coupling is higher and therefore mixing between singlet and triplet MLCT states is greater (Figure 7).

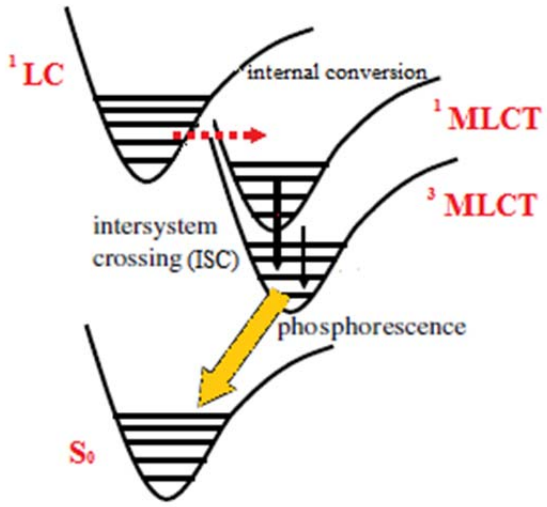

Figure 7: Emissive states in a transition metal complex; when the spin-orbit coupling is strong, the intersystem crossing (ISC) and internal conversion (a transition from a higher electronic state to a lower electronic state with same multiplicity) occur fast (in nano second range) [77]. The MLCT (triplet) usually has the lowest energy state and usually emission happens from this lowest state [78].

To have a high efficient electroluminescence it is necessary to block triplet states from reaching low energy states of surrounding molecules. By increasing the rate of triplet capture we can achieve this. One useful way to increase the rate of triplet capture is to add another molecule called a "guest", to the main host molecule, in low concentration (around 10%) [79] . Another approach is to use a special organic layer as a triplet blocking layer in device fabrication [80].

1.4 Mechanism of luminescence

If an electron is excited by light, the following radiative relaxation generates a photon with lower energy (longer wavelength) with respect to the exciting light and this phenomenon is known as photoluminescence. However in electroluminescence, the recombination of electrons and holes forms the excited electronic state of the molecular species. Similarly, if electron excitation occurs by a chemical reaction, it is termed chemiluminescence, which usually occurs only in gaseous or liquid phases.

1.4.1 Photoluminescence

The main three steps in photoluminescence are absorption, photochemical transition and emission. Photon absorption occurs in the range of femtosecond (10^{-15}), causing electron excitation from the ground state. It is followed by a photochemical transition between molecular orbitals with different configuration. Finally, there is a radiative or non-radiative decay to the lower energy ground state, generating photons or phonons, respectively. Regarding the life-time of the excited state, luminescent bands can be attributed to either fluorescence or phosphorescence.

In order to explain the concepts of fluorescence and phosphorescence, a brief explanation of electronic orbital configurations is needed. To have a better understanding of singlet and triplet electronic states it is better to imagine a system with two electrons. Electrons are electrically charged particles that generate a magnetic angular momentum by spinning around an arbitrary Z axis. In the ground state (S_0), electrons are paired (antiparallel), and the net electronic spin is zero. The electrons in excited singlet states are antiparallel and have a zero spin magnetic moment, shown as S_1, S_2. According to the electron orientation along the axis, an electron's spin magnetic moment can be UP and DOWN. However if two excited electrons do not follow Pauli's rule and adopt an unpaired configuration, a molecular beam of this configuration can be resolved in three different states, which is called triplet.

If spin up and down are shown as α and β, the three possibility of the triplet states could be defined as: $T_+ = \alpha_1 \alpha_2$, $T_- = \beta_1 \beta_2$ and $T_0 = \alpha_1 \beta_2$ for $M_s = 1$, -1, and 0, respectively [81]

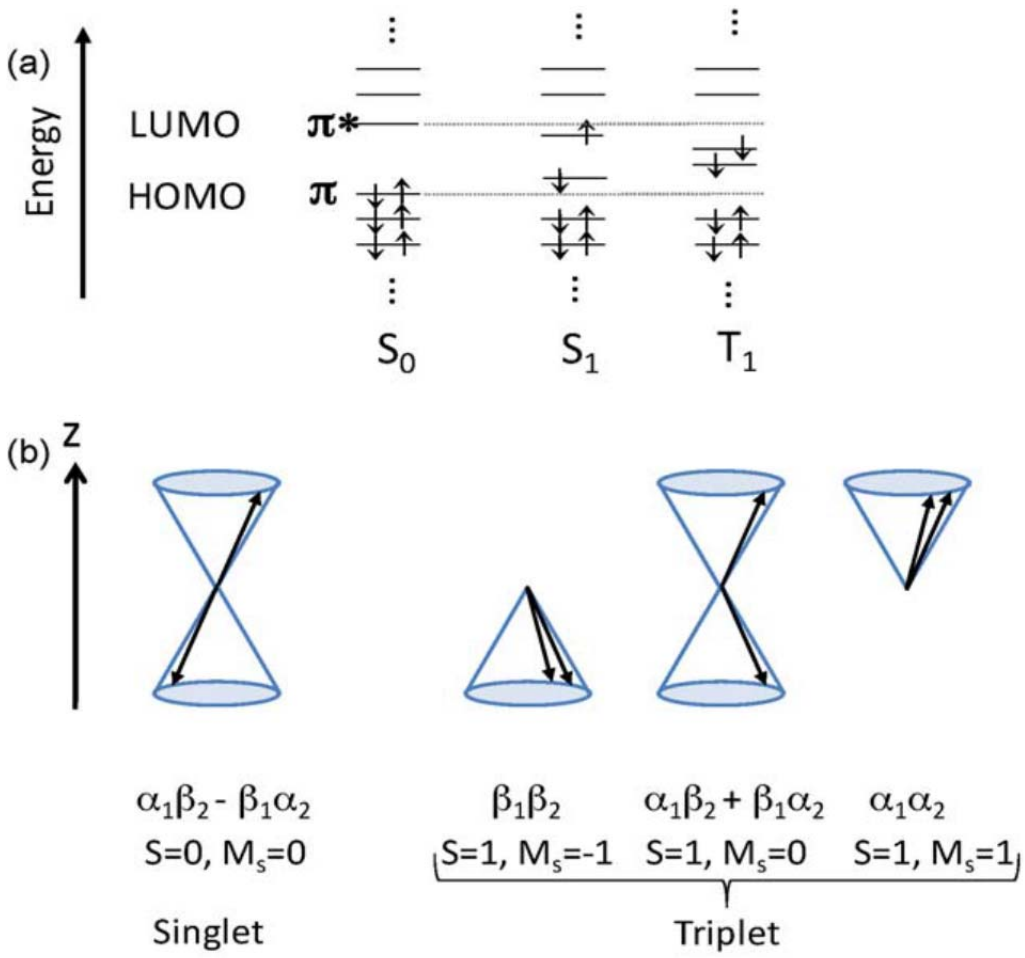

Figure 8: (a) Scheme of an orbital configuration in singlet and triplet states. Electron spins are shown by the arrows. For the triplet state, only one spin configuration is shown. (b) Vectorial representation of the singlet and three triplet states in a two-electron system. The two spins, indicated by arrows, orient around a local magnetic field in the z-direction. In the Ms = 0 state of the singlet configuration, the spin vectors are in opposite directions and 180^{o} out-of-phase while for a corresponding triplet state, the spin vectors are in-phase, and as a result, the magnetic momentum along the x-y plane is non-zero while the other three in phase configurations yield a triplet state.

In a Jablonski diagram, the various energy levels of electrons and intramolecular processes leading to radiative and non-radiative transitions are illustrated (Figure 9).

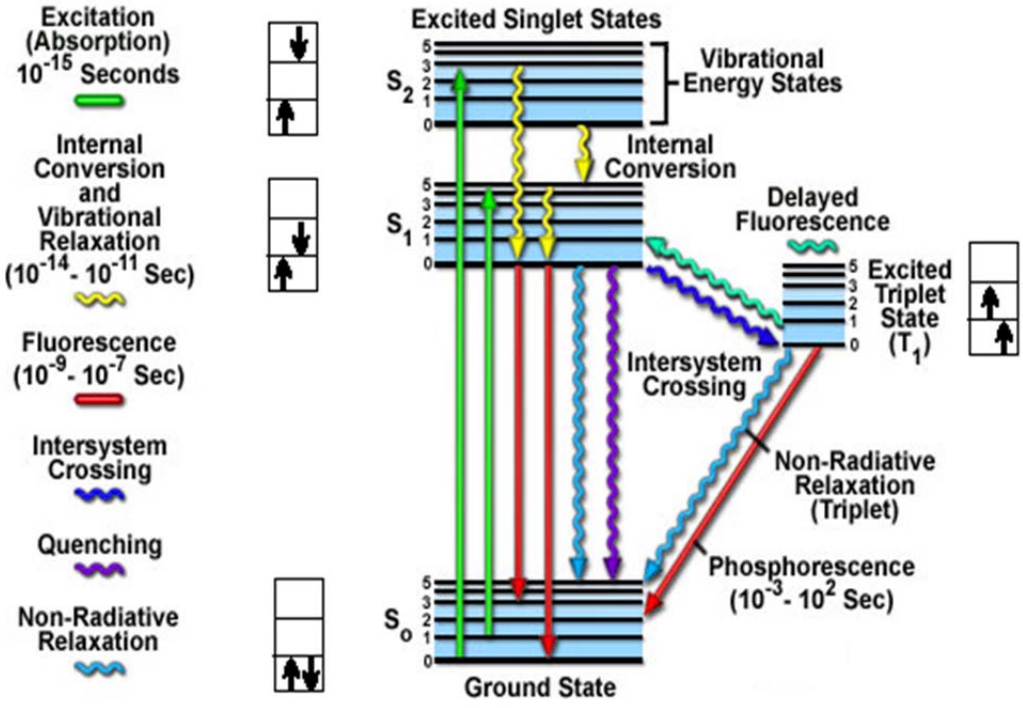

Figure 9: Jablonsky diagram depicts various energy levels and intramolecular transitions [82]

The arrows and boxes represent the electrons in the Molecular Orbitals (MOs). Energy absorption excites an electron from the Highest Occupied Molecular Orbital (HOMO) to the Lowest Unoccupied Molecular Orbital (LUMO), thus forming an excited singlet state, S_1. If the spin of electron is reversed, the lowest excited state will be T_1. As it is shown in Figure 9, radiative transition between two energy levels with the same multiplicity ($S_1 \rightarrow S_0$) and different multiplicity ($T_1 \rightarrow S_0$) is called fluorescence and phosphorescence, respectively. Due to the time needed for spin orientation of the electron from T_1 to S_0, phosphorescence is much slower than fluorescence (around 10^6 seconds) [81]. The study of the interaction between light and a molecule can provide useful information about the chemical system. For instance, the shape of the absorption and emission spectra are narrow and sharp in the case of atoms. Because their electronic states are defined by the valence electron's orbitals, a certain amount of energy is required for the electron to be excited. However, in molecules the excited state consists of multiple, unresolved vibrational states resulting in broadening of the absorption and emission spectra [81].

1.4.2 Electroluminescence

To describe electroluminescence, we can start with various types of processes that happen in the EL phenomenon. The three major components of the EL process are: the use of an electrical bias to accumulate charge carriers of opposite signs (electrons and holes) between two electrodes; the movement of the charge carriers through the electroluminescent material; and the recombination of the charge carriers to generate EL [83]. According to the type of excitation, the EL can be categorized in three different classes: *high-field EL*, *impact EL,* and *recombination EL*. In *high-field EL* light is generated by using a high electric field to directly excite the atomic or molecular states. The collision of high-energy electrons with the atoms of the emitter molecules causes some covalent bonds to break between atoms of the emissive material, resulting in the release of bound electrons into the conduction band [34]. A large number of minority charge carriers will be produced, resulting in an increase in the reverse current thus increasing the probability of tunneling from the valence band to the conduction band, preventing crystal breakdown. The major problem of this excitation is that the high applied field may breaksdown the crystal before electrons jump to the excited state. The field strength when breakdown occurs for most crystalline luminescent material is around 10^6 V/cm [83].

In *high impact EL,* after electron excitation the high–energy electrons collide inelastically with each other before recombination. The strength of the applied field and collision forces originating from the interaction of the electrons and the vibrational wave of the lattice results in sufficient energy for the electron to be ionized [34]. The required energy in high impact EL is about 2-3 eV. At room temperature, these materials do not follow this type of EL. The *recombination EL* (also referred to as injection EL) is defined as the emission of light produced from the combination of free charge carriers (electrons with holes) injected from the surface of the crystal or at a p-n junction of the semiconductor or at the electrodes after charge injection. For this process, the materials should be in direct contact with electrodes, the light is thus caused by recombination of majority and minority carriers in the band gap of the crystal [83].

In general, in EL processes, after the application of an electrical bias, the density of charge carriers is high near the electrodes. Subsequently, some of the mobile charge carriers diffuse or drift to a region with different energy states that can receive these charge carriers. After this step,

the electrons and holes recombine and release their excess energy in the form of light (and heat). Another possibility is the formation of excitons. This exciton moves through the material until it reaches the *luminescence center* and emits radiation. The luminescence center is the recombination centre in that the luminescence occurs [84]. During the movement of the excitons, the processes of excitation and de-excitation always take place.

It has been experimentally proved that the rate of exciton transfer is equal to the rate of electron transfer multiplied by the rate of hole transfer [85]. Therefore the principles of electron transfer can also be applied to exciton hopping.

Recombination is a process in which electrons and holes will annihilate finally. The energy of this stabilization is released in a radiative or non-radiative process. In radiative processes the energy is released as a photon and in non-radiative processes the energy is released as heat by various mechanisms. This process is divided into two major groups: direct and indirect recombination.

A direct band gap semiconductor has aligned conduction and valence bands (Figure 10a). If the energy and momentum of electrons in the valence band plus the energy and momentum of incident photons are equal to the empty state in the conduction band, the photon will be absorbed. This means that the momentum and energy of all particles are conserved. The momentum of photons is small in comparison with their energy. For each photon the momentum (p) is calculated by: $p=E/c$ $\mathrm{p} = \frac{\mathrm{E}}{\mathrm{c}}$ where c is the speed of light (3×10^8 m/s) and E is the energy of the optical photon (in the order of 10^{-19} Joule). When E is equal to the band gap energy; a phonon easily produces electron-hole pairs because electrons do not require much momentum from the photon.

Because of this, in both emission and absorption of the photon, the momentum is conserved without the collaboration of the phonon. When we talk about momentum conservation, it means that the transitions occur between electronic states of equal momentum. The emission of a photon is illustrated in Figure 10a by vertical arrows.

The indirect transition shown in Figure 10b is forbidden because of the large difference in momentum between the initial and final states. In indirect band gap semiconductors, light

absorption of light requires the help of a phonon which has low velocity (close to the speed of sound in solids). A low velocity phonon causes small energy and large momentum compared to a photon.

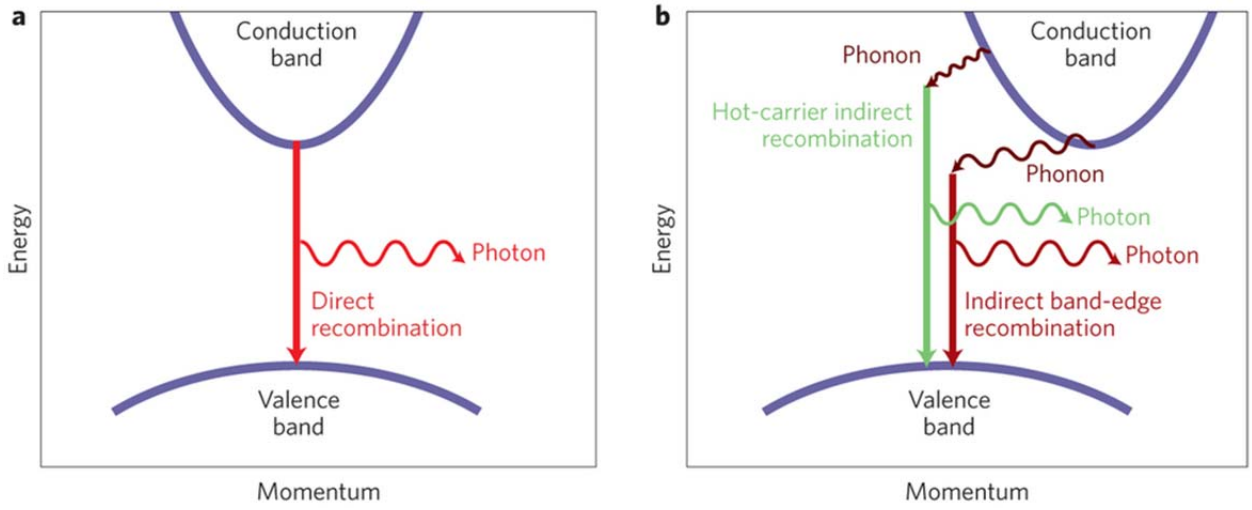

Figure 10: Schematic of the band diagram for: (a) direct band gap. The conduction band and the valence band are at the same momentum values. The momentum and energy are conserved in both photon absorption and emission (the electron-hole recombination processes) without the assistance of phonons, (b) Indirect band gap. The absorption of photon can be assisted with the simultaneous absorption of a phonon and emission of phonon. In the case of phonon absorption, the minimum energy of the photon which can be absorbed is a little below the energy band gap and a little above the band gap in phonon emission [86].

According to the conservation of momentum and energy, photon absorption occurs with the assistance of the phonon. In other words, an electron for recombination needs the energy to interact with either a photon to gain energy or a phonon (lattice vibration) to gain or lose momentum. In this process, the difference between the electron momentums is compensated by the emission of a photon, making the frequency of emitted light:

$$\varepsilon_1 - \varepsilon_2 - K\theta = h\omega$$

Here ε_1 and ε_2 are the energy of electron and hole respectively and $K\theta$ is the energy for phonon formation [87].

1.5 Objective of this work

The long term objective of this work is the development of a thin film formation procedure to improve charge transport and recombination in LEECs based on iTMCs.

It is known that changing the substrate impacts the growth and morphology/structure of organic films, and consequently the film functional properties (e.g., charge carrier transport and electroluminescence). In fact, the substrate surface energy together with the chemical composition of the film and the film processing conditions all play important roles in determining the film morphology and structure. Hence, our main objective consists in controlling film formation in the interelectrode region (channel) of LEECs.

This study consists in comparing thin film formation on different substrates used in planar and vertical LEEC configurations. The hypotheses underlying this work are the following:

- In addition to favoring ion redistribution in the thin film during electrical bias application, the IL molecules promote the formation of vertical structures (rods) of the complex. Such structures limit charge transport in planar devices. However these rod structures can provide micro LEECs if the voltage is applied to both ends of the rods.
- The presence of the IL molecules can affect the PL spectra of the films. Separation between complex molecules can reduce non-radiative path of relaxation and consequently PL intensity will increase in the presence of IL.

The investigation of the chemical composition of the film and surface morphology in different substrates used in LEECs enables an understanding of why previous attempts to make low voltage planar LEECs using iTMC as emissive films were not successful.

CHAPTER 2 EXPERIMENTAL SECTION

2.1 Device fabrication

We fabricated two different types of devices, with planar and vertical configurations. Electrodes in planar devices were of the same color (Au), fabricated by photolithography. In vertical (sandwiched) devices electrodes were of two-color type (ITO and thermally evaporated Al).

The fabrication route of LEECs is presented below.

2.1.1 Solution preparation

Ir $(ppy)_2(bpy)$, purchased from SolarisChem was used as the emissive material. The ionic liquid was $BMImPF_6$ from Iolitec (Ionic Liquid Technologies). Ionic liquid may contain residual water that affects the operation of the device. To purify the ionic liquid, it was heated at 70 ˚C for at least 12 hours under high vacuum condition (10^{-5} Torr).

Solutions of 10 mg/mL of the complex and 27 μl/mL of $BMImPF_6$ in acetonitrile were prepared separately. The solutions of the Ir complex were filtered using 0.1 μm pore size PTFE syringe filter.

Two component blends were prepared by two different approaches: in the first, solutions were mixed in a molar ratio of (Ir/IL) 1:1. In the second, $BMImPF_6$ is added directly in the solution of the Ir complex to obtain a second solution with (Ir/IL) 1:1 molar ratio. The blends are stirred on a magnetic plate at room temperature for at least 2 hours.

2.1.2 Planar device

The employed substrates were glass or highly doped (n-type) Si (100) wafers (resistivity of 0.002-0.003 Ω·cm) covered with either 100 nm or 200 nm-thick dry thermally grown SiO_2 dielectric (100 nm: 34.5 nF/cm^2 capacitance, 200 nm: 17.26 nF/cm^2 capacitance). Fabrication of patterned interdigitated gold electrodes on the SiO_2 surface was achieved with the following procedure (Figure 11):

1) Glass or SiO_2 wafer was heated for 20 minutes at 190 ˚C for removal of residual water.

2) Lift off resist LOR5A (microchem) was spun onto the substrate at 2000 rpm for 1 min. After soft baking (at 190 ˚C for 3 mins), the positive photoresist SPF 1813 (Shipley) was spin coated on LOR 1A and baked at 115 ˚C for 1 min.

3) Coated wafer was placed in the mask aligner (MA-4) and exposed to the UV lamp through a photo mask in a Karl Suss mask aligner. Hard contact in constant power mode was used for exposure.

4) Developer MF319 (Microchem) was used for 75 seconds to remove the photoresist in exposed area. The exposed regions of photoresist were dissolved in the developer leading at the same time to dissolution of the underlying lift off resist layer from the open windows.

5) Using e-beam evaporator first Ti (5 nm) was deposited to increase the adhesion of the gold to the glass or SiO_2, and then Au (40 nm) was evaporated on top.

6) Remover PG (Microchem) was used for half an hour at 70 ˚C to lift off the resist and provide the substrate with interdigitated electrodes

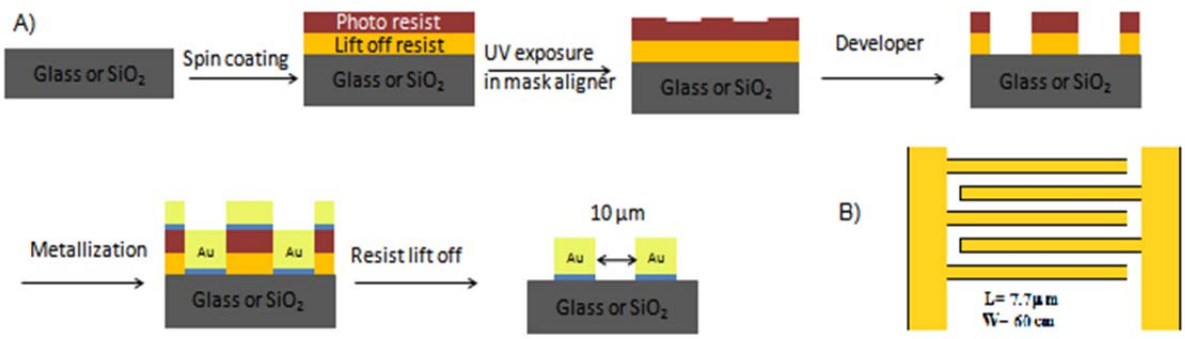

Figure 11: A) Microfabrication steps for interdigitated gold patterned substrate, (B) Top view of the substrate

To have a device with planar configuration (Figure 12), about 50 µL of the Ir solution/blend solution (depending on device with or without IL) was spin coated at 1000 rpm for 1 minute. The films were thereafter dried on a hot plate at 80 ˚C for at least 1 h. Prior to the solution deposition, the substrates were cleaned by subsequent ultrasonic treatment in isopropanol (10 minutes), acetone (15 minutes), and again isopropanol (10 minutes). In the last cleaning step the substrates were exposed to UV ozone for at least 10 minutes. The active surface area of the device was 4.3 mm^2. The thickness of the film is around 300 nm.

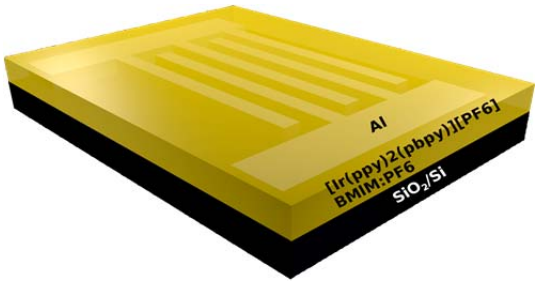

Figure 12: Illustration of the sample used in planar configuration

2.1.3 Vertical device

In order to fabricate the vertical device (Figure 13), first the patterned indium tin oxide (ITO) on glass was cleaned in Triton 100X detergent in DI water, DI-water, and isopropanol by sonication, followed by UV-ozone treatment for 20 minutes.

Before solution deposition, around 100 nm thick poly (3, 4-ethylenedioxythiophene): poly (styrene sulfonate) (PEDOT: PSS) (CLEVIOS PVP AI 4083) mixed with Dimethyl sulfoxide (DMSO) was spin coated on ITO at 4000 rpm for 40 sec and annealed at 170 °C for 20 minutes. DMSO was added in volume ratio PEDOT:PSS/DMSO 95:5 (v/v%) to increase the conductivity of the layer and improve the surface morphology. Before deposition, PEDOT:PSS solution was filtered using a hydrophilic syringe filter 0.45 µm pore size (Millex HV). Blends of Ir complex/ionic liquid were then deposited at 1000 rpm for 1 minute and the film was annealed for 2 hours at 80 °C. Finally, Al electrodes (80 nm) were thermally evaporated using a shadow mask

under vacuum conditions (10^{-5} Torr) using an evaporator placed in an inert atmosphere glovebox. The active surface area of the device was 12.6 mm^2. The thickness of the film is around 300 nm.

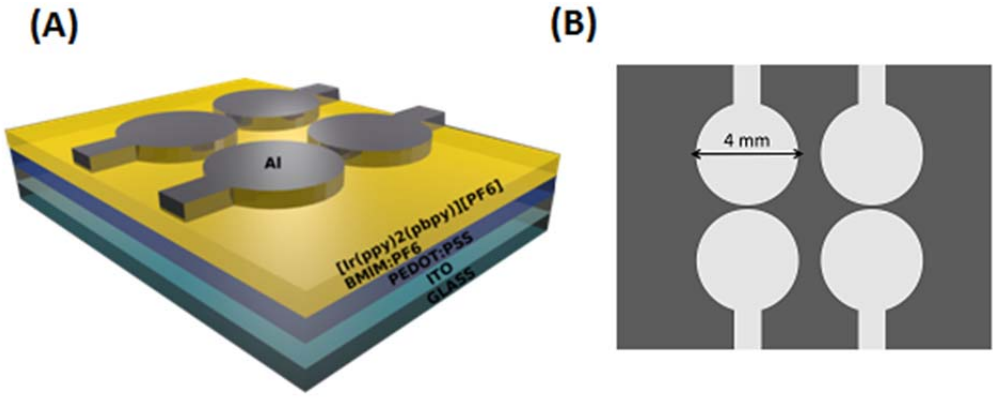

Figure 13: Structure of vertical device (A) and corresponding shadow mask geometry (B).

In both the planar and vertical devices, a Laurell spin coater (WS-400-6NPP) and a hot plate in the glove box were used for deposition and thermal treatment of the films.

2.2 Experimental techniques

In this section the experimental techniques employed for the characterization of the organometallic layers are described: (i) Fluorescence hyperspectral microscopy and (ii) Atomic Force Microscopy (AFM). The working principles underlying these methods will be explained in detail.

2.2.1 Fluorescence hyperspectral imaging

Fluorescence is a phenomenon due to the radiative relaxation of a sample, after light absorption [88]. Figure 14 illustrates the typical behavior of a fluorescence spectrum observed after absorption of light by the sample. The vibronic structure in the absorption vs fluorescence spectrum is visible. Energy loss by non radiative thermalization causes the fluorescence spectrum red shift with respect to the absorption spectrum [88].

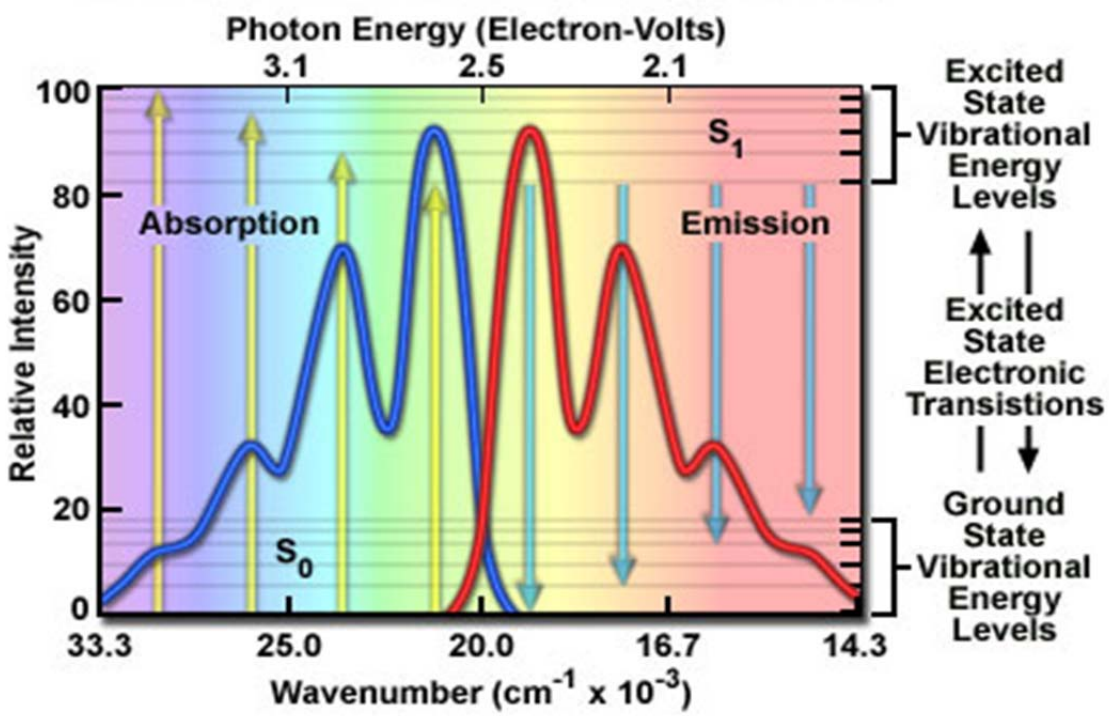

Figure 14: Electronic absorption and emission bands [89]. The space between vibrational energy level is similar for the ground and excited states, resulting in mirror images. The Stokes Shift is measured as the difference between the maximum wavelengths in the excitation and emission spectra of a fluorescent material

Fluorescence hyperspectral imaging was used to investigate the morphology of our films before and after blending with the ionic liquid as well as a function of the approach adopted to prepare the blend. The microscope has different important parts that have remarkable effects on sample imaging. The microscope is shown in Figure 15 [89].

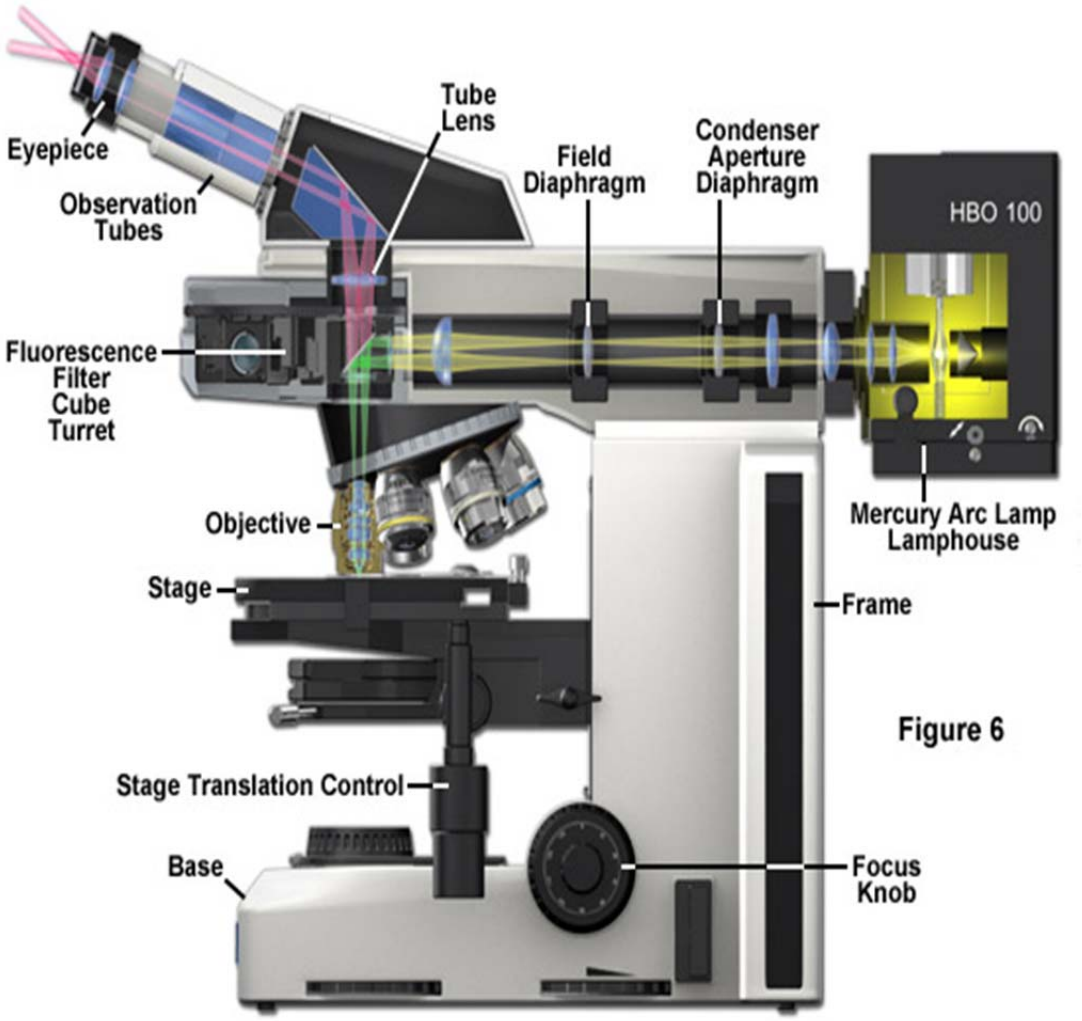

Figure 15: Anatomy of the fluorescence microscopy [89]

One of the important parts in fluorescence microscopy is the light source. As a function of the sensitivity of the detector, quantum yield and absorption spectrum of the investigated emissive material, a light source with appropriate spectral distribution should be chosen. The most common source in fluorescence microscopy is the mercury arc lamp. Its spectral profile is shown in Figure 16. Xenon arc lamps, metal-halide and LED are other light sources.

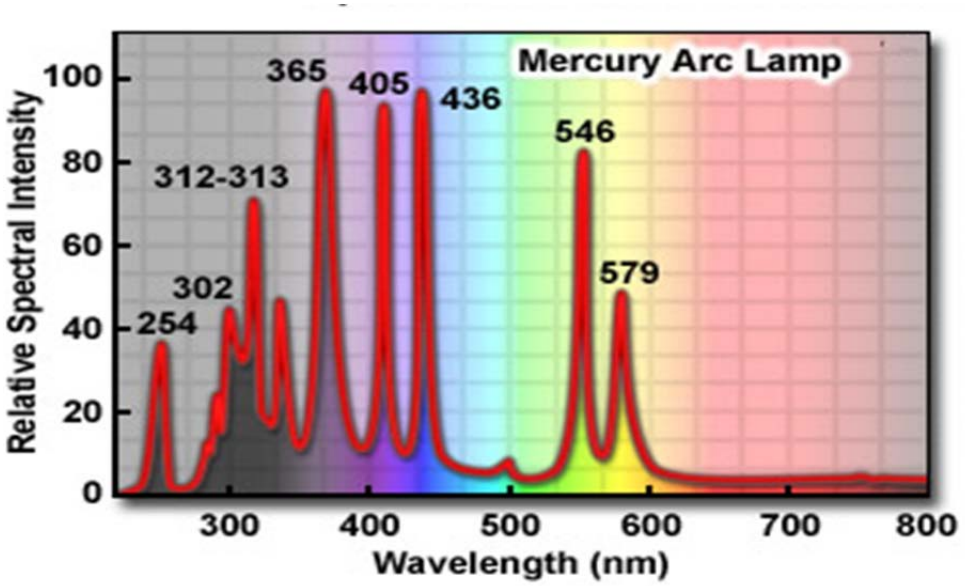

Figure 16: Spectral profile of the mercury lamp [89]

A filter block (cube) is also part of the instrument. The cube consists of the excitation filter, the emission filter, and the dichroic beamsplitter (Figure 17). The excitation filter (*exciter*) passes the wavelengths that excite the sample. The emission filter (*emitter*) just transmits any emitted fluorescence from the sample. The *dichromatic beamsplitter* is a thin piece of coated glass located to the optical path of the microscope at a 45 degree angle; it can reflect the excitation light but transmit the emitted fluorescence [90].

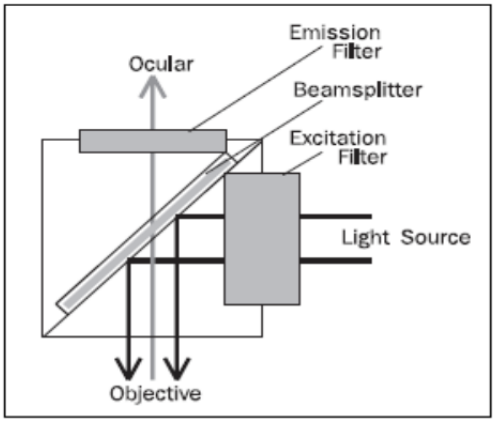

Figure 17: Scheme of filter block [90]

Common filter blocks are named after the type of excitation filter; for instance ultraviolet excitation is named as DAPI which is used in this study Figure 18.

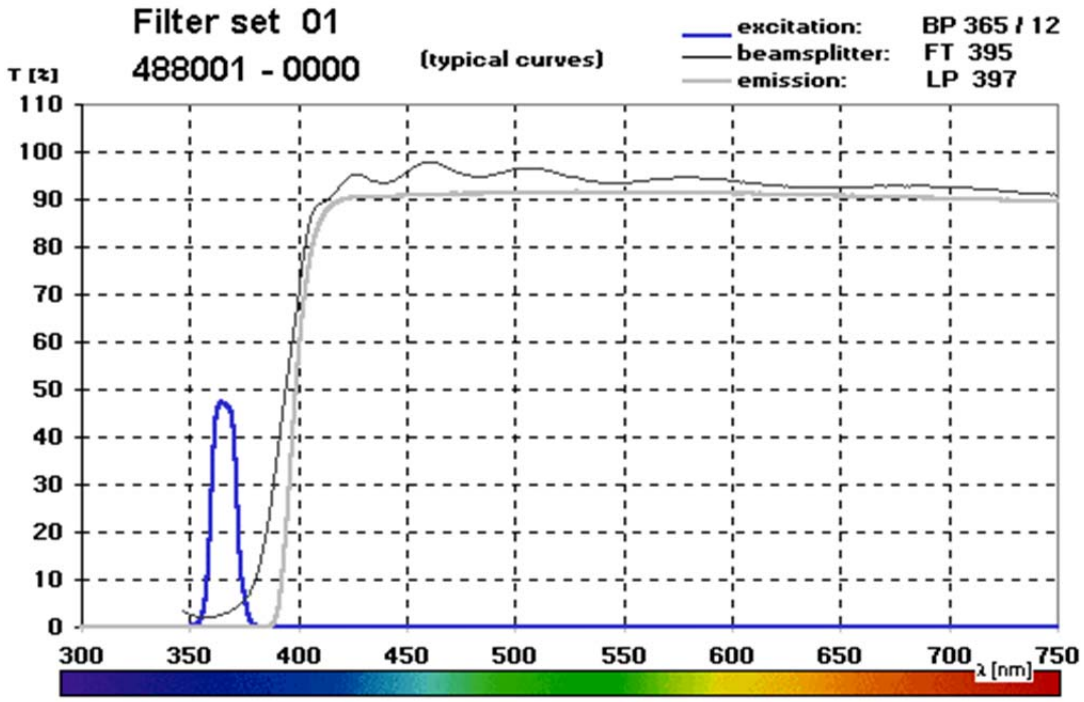

Figure 18: Illustration of the characteristics of UV excitation (DAPI) Filter [89]

In our experiment Fluorescence Hyperspectral Imaging was performed with PARISS (Prism And Reflector Imaging Spectroscopy System by LightForm Inc., Asheville, NC, USA), an imaging spectrometer coupled to a cooled scientific CCD camera to record the spectra. The hyperspectral images (spectral maps) were generated in the ‘‘push broom’’ mode by use of a wavelength-dispersive spectrometer collecting all wavelengths simultaneously at each location along the slit by translating the field of view (FOV) underneath the spectrometer on an automated translation stage connected to the microscope (Olympus BX-51) (Figure 19)

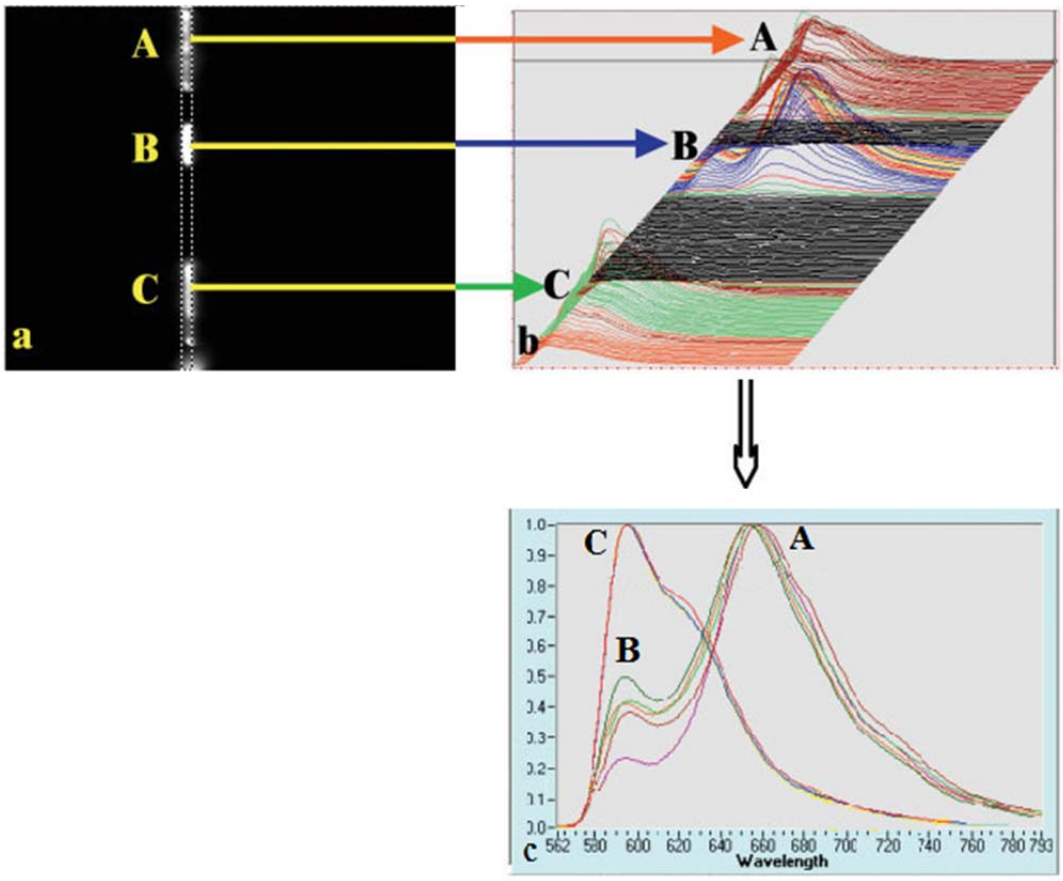

Figure 19: Spectral mapping of the fluorescence spectra of luminescent grain. (a) The PL image of the emissive material. Rectangular section of the FOV is allowed to pass through the entrance slit. (b) Spectra from points in the FOV. (c) The spectra in the FOV are sorted into a two-dimension plot [91] .

The information was collected with PARISS 8.0 software with a minimum correlation coefficient (min CC)>0.98, in real time. The image size and spatial resolution was calculated by dividing the slit height (5 mm) and slit width (25 μm) to the magnification of the objective lens of the microscope. All the spectra from the film were obtained in vacuum, at room temperature. Fluorescence images were collected from the films excited at 360 nm. Classes of spectra were given pseudocolor codes, which were correlated and painted onto the FOV in its associated pseudocolor, forming the classified image [92].

2.2.2 Atomic Force Microscopy (AFM)

AFM is a powerful tool for imaging the surface of the systems and provide the surface topography information, including surface roughness. AFM is widely used in the field of material science because of its high resolution in the nanometer range.

The working mechanism of AFM is based on the deflection of a cantilever. A scheme of a typical AFM is given in Figure 20.

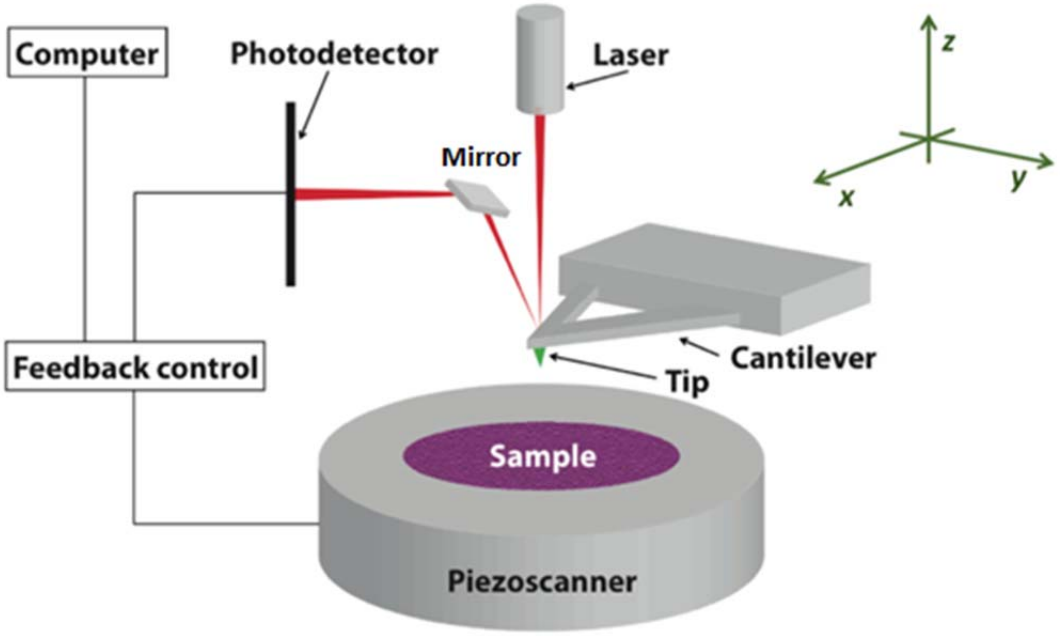

Figure 20: Scheme diagram of AFM [93]

To have a precise and fine positioning, piezoelectric actuators are used. The sample is interrogated by a tip that is connected to a cantilever. There are two main methods of AFM imaging: contact and tapping (intermittent contact) modes (Figure 21). The difference between these two modes is that in contact mode, the tip is always in contact with the sample however in tapping mode, the tip is oscillated and comes in contact with the sample intermittently.

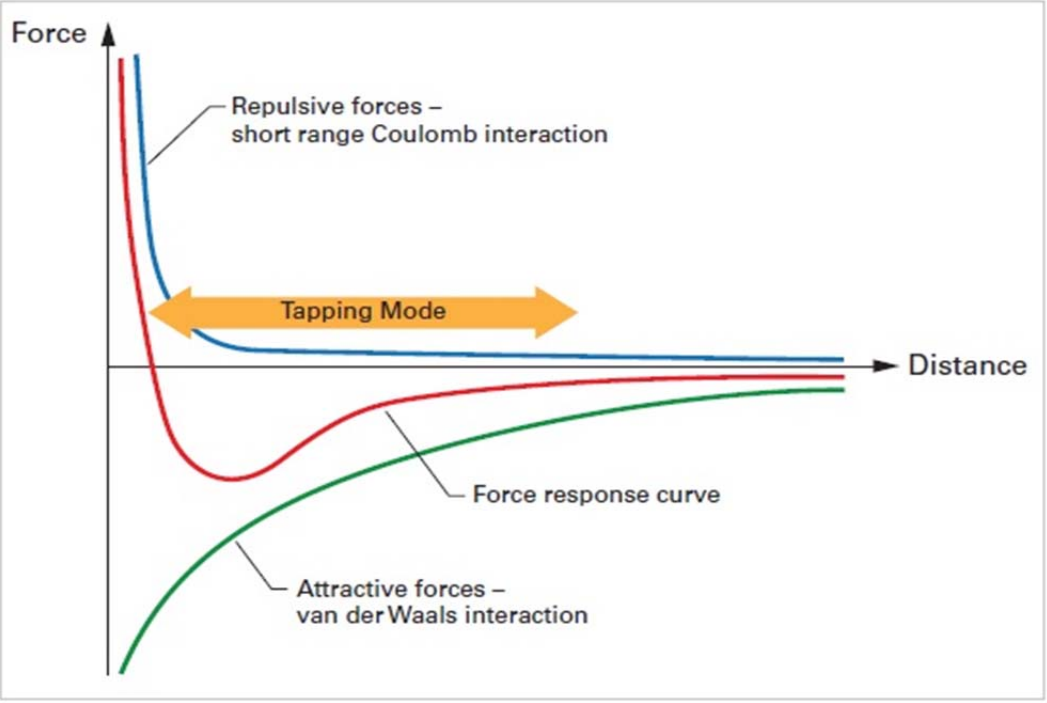

Figure 21: Force-distance curve between the AFM tip and a sample. When the atoms of the tip and sample are moved close together, first they weakly attract each other by van der Waals interaction. As the distance is decreased the attractive force increases until the electrons start electrostatically repelling each other so that the net force becomes repulsive and the atoms are in "contact". Figure adapted from [94].

In contact mode, the tip is in contact with the surface and the applied force is kept constant to a certain value which is the deflection setpoint. The cantilever deflection is adjusted to maintain as close as possible to the setpoint value by the instrument feedback loop (Figure 22). Changes in the cantilever deflection are attributable to changes in the surface topography [95].

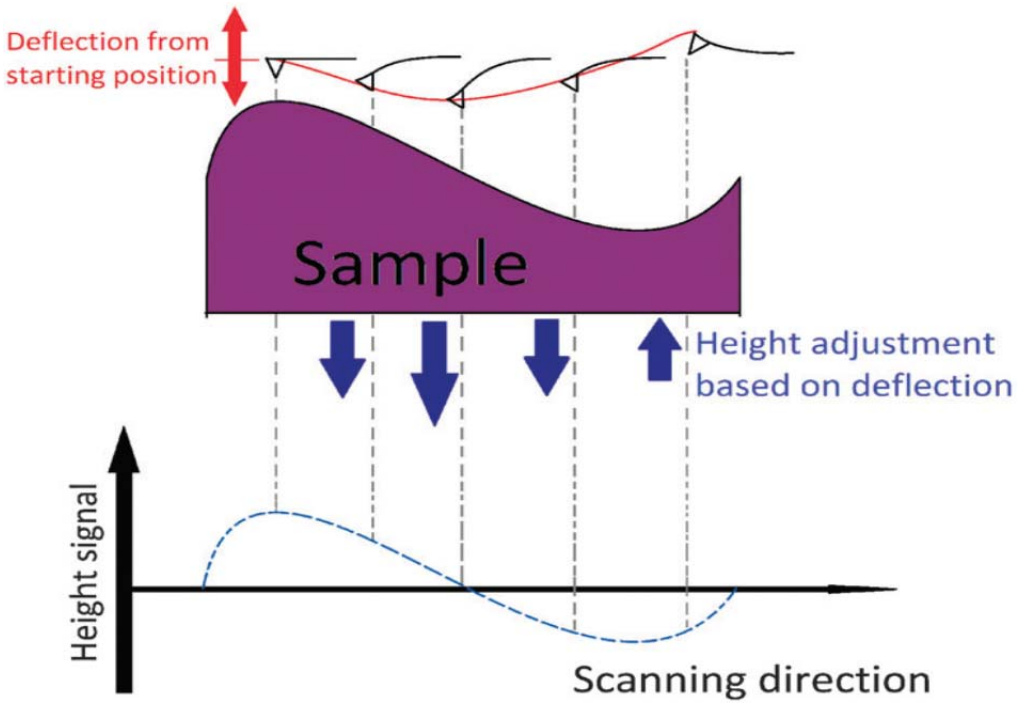

Figure 22: AFM contact mode with a constant cantilever deflection, whereby the deflection is used as feedback to adjust the tip-to-sample distance [95].

However contact mode has some disadvantages. First is that because organic materials are soft in contact with AFM tip they will be scratched or the bonds at the surface will be broken. Second drawback is the tip in contact with hard surface may be damaged. To reduce these disadvantages tapping mode is invented.

In all of our experiments, the only imaging method used was tapping mode. In this section, this imaging method will be discussed.

In tapping mode by applying the mechanical or magnetic force to the free end of the oscillating cantilever, the cantilever is adjusted near its resonance frequency. As the tip comes in proximity of the sample the free end amplitude decreases and energy is transferred from the oscillating tip to the sample. During scanning by changing the distance between probe and the sample, the system kept the certain amplitude value. This allows the tip to scan the surface at constant energy loss from the tip to the sample and making height images. Different physicochemical properties of the surface cause the phase difference between driving vibrations and the free end vibration producing phase images.

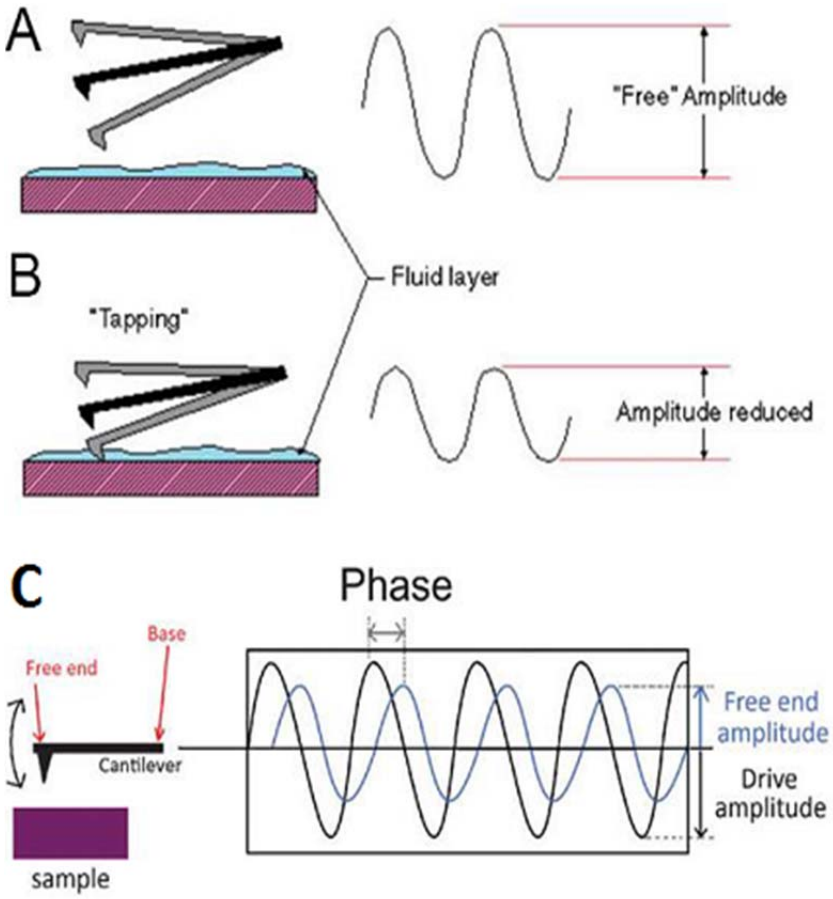

Figure 23: A) Tapping mode cantilever oscillation amplitude (A) when it is free and (B) during scanning. Adapted from the reference [96]. (C)Phase signals in the AFM tapping mode resulting from the phase difference between the driving vibration and the free end vibration. Adapted from the reference [95]

Any change in cantilever position usually causes displacement of the visible laser beam reflected off the back of the cantilever onto a photodiode (Figure 24).

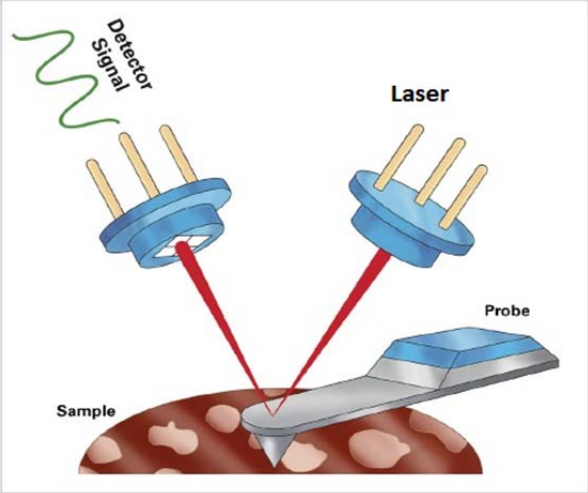

Figure 24: Schematic of the AFM detection system [94]

The photodetector is a split photodiode with high sensitivity to light intensity. Even a very small deflection of cantilever (0.1 nm) is amplified and detected by this system [97].

2.2.3 Charge transport characterization

The characterization of the planar LEECs was done under vacuum (10^{-5} Torr) in a Lake Shore Desert cryogenic electrical probe station connected to a semiconductor parameter analyzer (SPA, Agilent B1500A). Beryllium-Copper alloy (10 μm diameter) tips from Metal Specialty Co. were used.

The probe station designed for non-destructive electrical testing includes high-precision micro-manipulated probe stages surrounded by a thermal radiation shield. The station is equipped with a silicon photodiode (Hamamatsu S1337-33BQ) for light detection from the sample. The noise equivalent power of the photodiode is 8.1×10^{-15} W/Hz ^{½}. The sample is mounted on a removable sample holder (chuck). The probe station is directly connected through a transfer arm to the glove box providing N_2 environment for air sensitive materials and devices. The environment in the probe station can be varied depending on the requirements of the characterization ($P=10^{-6}$ Torr, N_2, etc). Most of measurements were done under vacuum condition. For each device, the current and photocurrent were measured at room temperature. The voltage applied to the planar devices was relatively high, i.e. maximum either 150 or 200 V, to have enough energy to overcome the resistivity of the emissive material deposited in the channel.

The current–voltage characteristics for vertical LEECs were done in an inert atmosphere via a computer-controlled Keithley 6202. A silicon photodiode (Hamamatsu S1337-16BR) was installed beneath the window under the glovebox. The measurement was done in nitrogen glovebox at room temperature.

CHAPTER 3 RESULTS AND DISCUSSION

3.1 Preparation of thin films for LEECs

In the past two decades, a lot of research on vertical LEECs based on iTMC has been carried out. Although the working principle of planar LEECs based on iTMCs is reported [98], the effect of film morphology on the performance of these kind of devices has not been investigated. Moreover, the impact of different ionic liquids (having the anion in common with the emissive complex) in operation of vertical devices is reported [45], but studies on their effect on film morphology are lacking.

In this MSc work, we explore the formation of thin emissive films on different substrates used in LEECs. Such an investigation is aimed at shedding light onto the working principle of planar LEECs. Beside the substrate effect, the effect of blending an ionic liquid to the complex on film formation and device performance has been investigated.

3.2 Thin film morphology characterization of LEECs based on $Ir(ppy)_2(bpy)^+PF_6^-$

Iridium complexes containing ortho-metallated ligands are attractive phosphorescent molecules because of the simplicity of synthesis and facility of purification. Both ionic and neutral Iridium complexes display useful spectroscopic properties such as high emission quantum yields and long excited state lifetimes. They have a vast application in LEDs [5], LEECs [5], sensors and luminescent biological probes [99], and protein staining [100].

In this section, the morphology of thin films of $Ir(ppy)_2(bpy)^+PF_6^-$ on different substrates used in LEEC fabrication is investigated by hyperspectral imaging and AFM.

3.2.1 Photoluminescence images and spectra

Fluorescence hyperspectral imaging is a technique to characterize fluorescent samples. The sample can consist of different components, with various spectral properties. By collecting spectral information in a field of view (FOV) and making a fluorescent spectral map of the

sample, its topography can be inferred. To shed light onto the morphological properties of the thin films at the micrometric scale, fluorescence hyperspectral imaging was used. It should be noted that different color tonality originates from different fluorescence intensities.

Patterned Au on SiO_2 substrate

The PL images of a thin film of $Ir(ppy)_2(bpy)^+PF_6^-$ on SiO_2 substrate pre-patterned with Au electrodes (referred to as planar $Ir(ppy)_2(bpy)PF_6$ LEEC) are shown in Figure 25.

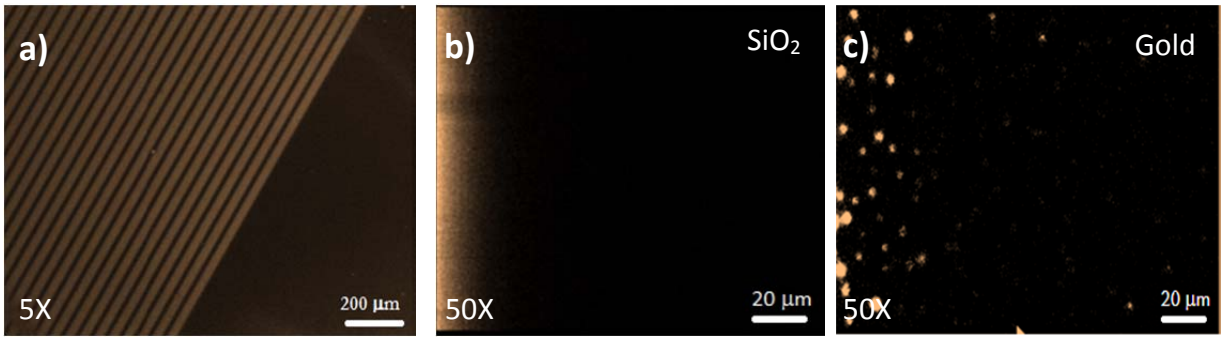

Figure 25: PL images of a thin film of $Ir(ppy)_2(bpy)^+PF_6^-$; a) On a pre-patterned Au on SiO_2 substrate (image was taken under vacuum), b) On SiO_2 (ambient air); c) On gold (ambient air). The microscope stage was moving during the acquisition. Since the absorption peak of the Ir complex is in the UV region (ca 260 nm in Figure 61), the used filter cube was DAPI, for excitation wavelength at 350-370 nm (Figure 18).

The absorption spectra (appendix Figure 61) of the complex show intense bands in the ultraviolet part of the spectrum between 200 nm and 320 nm. These bands are associated with ligand centered (LC) transitions of the ligands [101].

Figure 25a shows that emission from the Ir complex film on SiO_2 is of weaker intensity than on gold. One possible reason is that a portion of the excitation (emission) light is reflected from the gold electrode surface. Another possible reason is the different molecular organisation on gold with respect to SiO_2 leading to a more emissive material on gold (Figure 25 c).

Figure 25b and c (corresponding spectra in Figure 28**Error! Reference source not found.**) were taken in ambient air. The microscope stage was moving from right to left during light exposure. Therefore the right portion of the image was exposed to light for a longer time with respect to the

left portion. These images show that in addition to self-quenching, photobleaching has occurred. Photoluminescence was detected only for the first 30 seconds of acquisition, whereas the emission from the Ir complex film in vacuum conditions was almost constant for more than 30 minutes. Self-quenching is caused by intermolecular relaxation in non-radiative path [102]. Photobleaching is attributable to the water and oxygen molecules in the ambient air. Upon light-exposure, oxygen molecules can be excited to form a triplet state and react with the emissive material, thus causing bleaching [103] [104].

In order to study the PL spectra from the thin film of the complex, the origin of emission should be explained. The emission of $Ir(ppy)_2(bpy)^+PF_6^-$ comes from the cationic part. The structure of the ions in the complex is shown in Figure 26. As it is shown the cations are separated by a sheet of anions in the lattice.

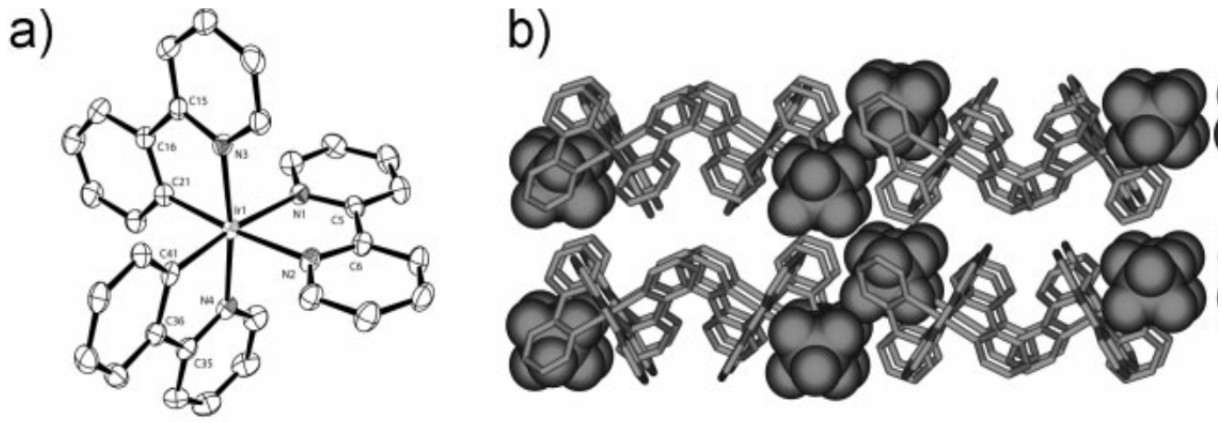

Figure 26: Structures of $Ir(ppy)_2(bpy)^+PF_6^-$. a) $Ir(ppy)_2(bpy)^+$ cation present in the complex. b) Packing of $Ir(ppy)_2(bpy)^+$ (stick illustration) and PF_6^- (space filling illustration) [105].

Costa *et al* [45] calculated the molecular and electronic structures of the $[Ir(ppy)_2(bpy)]$ cations using density functional theory (DFT). In their study, they showed the atomic orbital combination of the highest occupied and the lowest unoccupied molecular orbitals (HOMO and LUMO) of the complex. Their results are in agreement with the experimentally observed crystalline structure and photophysical properties of the complex [105]. In their study they found that the HOMO is a mixture of the Iridium *d* orbitals participating/contributing in the π bonding (d_π) and π orbitals of the phenyl group, distributed equally among the two ppy ligands. The

LUMO level is located on bpy ligand without any overlap with HOMO (Figure 27). Furthermore the LUMO level is well separated from LUMO+1 (0.87 eV).

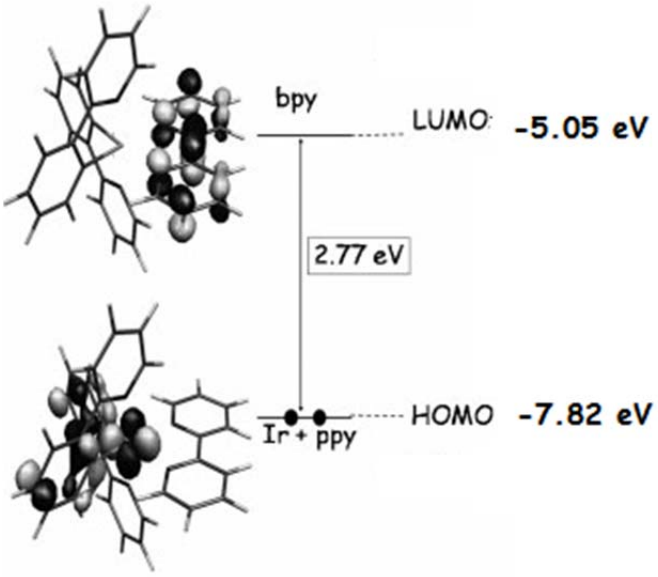

Figure 27: Schematic energy diagram of the molecular orbitals of $Ir(ppy)_2(bpy)^+$[105].

PL emission of the complex originates from metal-to-ligand charge transfer (MLCT) electronic transitions. The emission depends on the complex environment and the circumstances of excitation (photons or voltage). In this complex, the lowest triplet state (T_1) is a mixture of MLCT and ligand-to-ligand charge transfer (^{3}MLCT/^{3}LLCT). It means that the electron excitation can occur from the metal and/or phenyl ring of ppy (HOMO) to bpy ligand (LUMO). Due to this electron transfer the coordination sphere shows contraction [105].

PL spectra of the thin film of $Ir(ppy)_2(bpy)^+ PF_6^-$ deposited on gold patterned SiO_2 substrates (from both gold and SiO_2 parts) are shown in Figure 28.

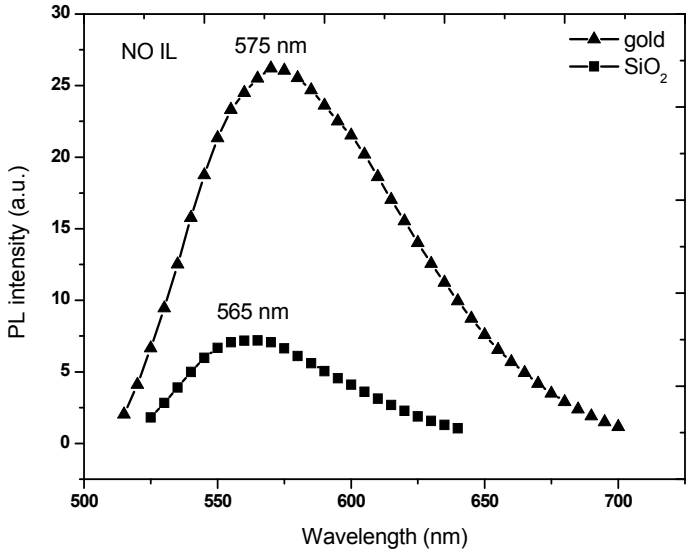

Figure 28: PL spectra of spin coated thin films of $Ir(ppy)_2(bpy)^+ PF_6^-$ on both SiO_2 and gold parts. DAPI used as a filter cube. The spectra were taken under vacuum.

In Figure 28 we can see the intensity of luminescence in gold is higher than SiO_2. The spectra of the emissive film on both SiO_2 and gold have almost the same broad shapes. This shows the negligible effect of substrate on excited state vibrational states that causes peak broadening. In this case, the spectrum of the film on SiO_2 is blue shifted in comparison with the film on gold. This difference might originate from the different morphologies of the film on different substrates, in turn attributable –among others– to the different surface energy of the two substrates [106]. Generally, adhesion of materials on rough substrates should be higher than on smoother ones because of higher surface area [107]. However, the lower wavelength emission from SiO_2 region results from stronger adhesion of the complex to the SiO_2 in comparison with gold. Stronger adhesion on the SiO_2 surface may come from van der Waals forces between the molecules of the complex and the SiO_2 surface [108].

Spin coating yields thin films with thickness between 100-200 nm. In order to have thicker films with a highly ordered molecular arrangement, the complex solution was drop-casted on SiO_2 substrate (Figure 29). In this method, solvent evaporation is slower in comparison with spin coating method, therefore the molecules have more time to orient with higher stability. This film

is thermodynamically more stable than the spin coated one. The fast drying time in spin coating method can affect the phenomena of self-assembly or crystalline formation [107].

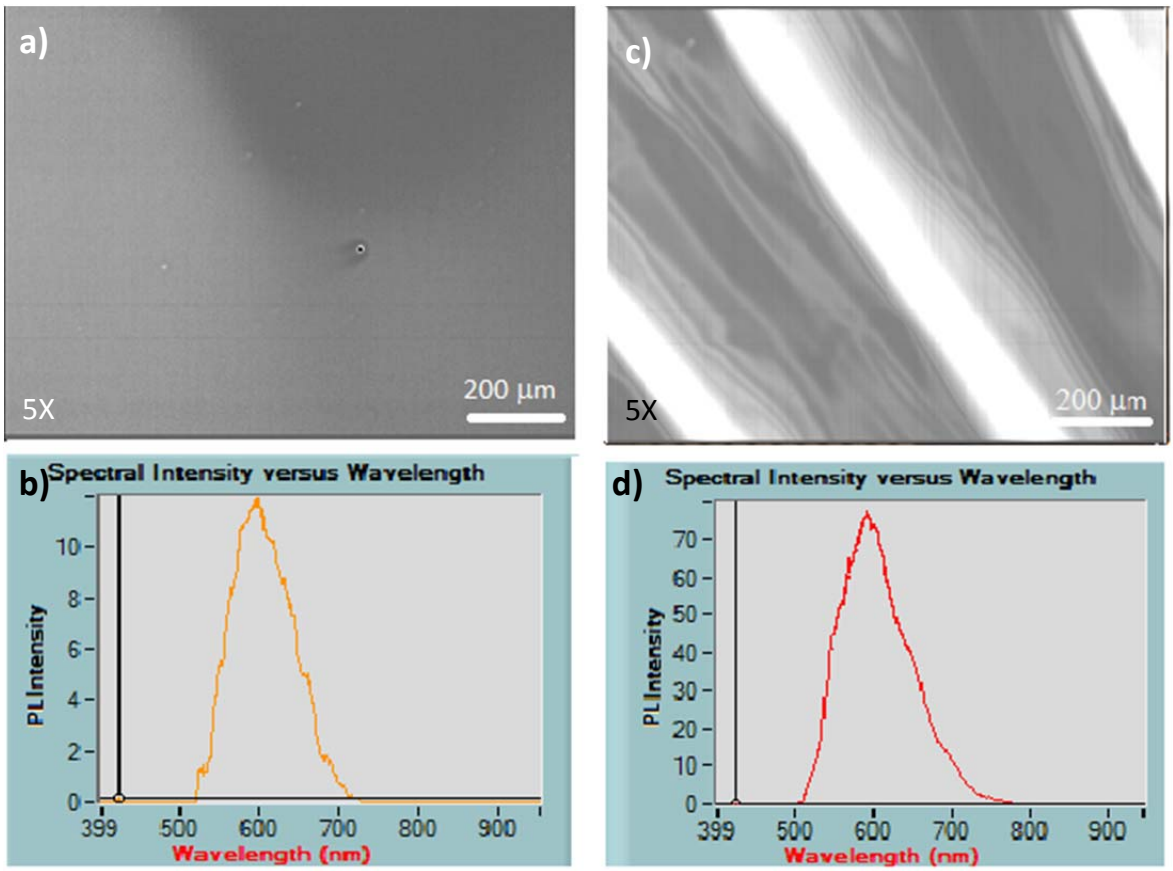

Figure 29: Thin film of $Ir(ppy)_2(bpy)^+PF_6^-$ drop cast on SiO_2 substrate. a) PL image and b) PL spectrum ($\lambda_{max,\ emission}$ ca 590 nm) from the central part of the drop; c) PL image and d) PL spectrum ($\lambda_{max,\ emission}$ ca 585 nm) from the area near the edges of the drop. Spectrum (d) is from brighter area in Figure c), with a higher concentration of emissive material. Darker area in image c) had the same spectrum as b). The images and spectra were taken under vacuum. DAPI filter cube was used.

In regions with higher thickness, light penetration depth consists of more emissive molecules in comparison with thinner region; thus it can excite more molecules to generate higher PL. According to the images and spectra, the center of the film is thin with lower PL intensity (Figure 29 a).

Drop cast films on SiO_2, with respect to spin coated ones, showed a red shift. This behavior can originate from different film structures with different stability.

Patterned Au on glass substrate

Another substrate used in LEEC fabrication is glass. Transparent substrates prevent any current leakage from the bottom when they have been used as substrates in electrical devices. Different molecular orientation in the channel causes different electrical behaviour. Thus to choose the best substrate for LEEC, electrical characterization is needed. For the investigation of film formation on glass, the solution was spin coated and drops cast on top of the glass substrate patterned with gold.

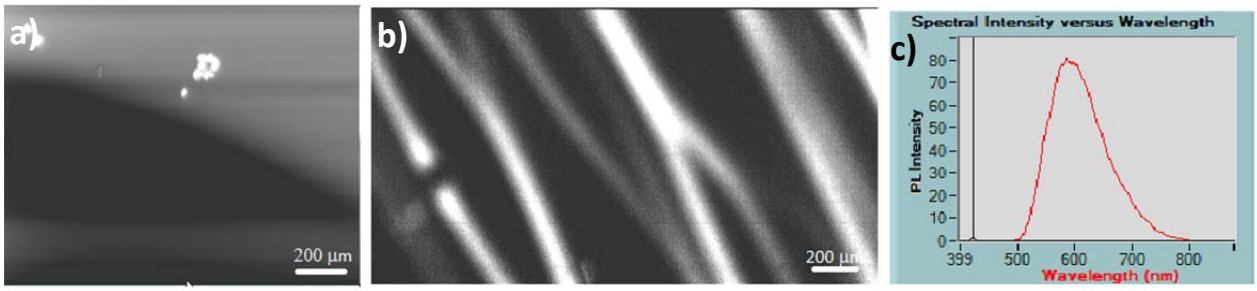

Figure 30: Thin film of $Ir(ppy)_2(bpy)^+ PF_6^-$ on glass substrate. a) Spin coated film, b) Drop cast film, c) PL spectrum of drop casted film ($\lambda_{max,\ emission}$ ca 580 nm). Images and spectrum were taken under vacuum. DAPI filter cube was used.

The spin coated film was uniform (Figure 30 a) over a scale of about 1.5 mm^2 and when its emission reached a certain intensity around 80 (Figure 30 c) the quenching was very slow even in ambient air. Complex cations can orient so that they limit the penetration of oxygen and water molecules, resulting in limited quenching. Drop cast film on glass (Figure 30b) showed almost the same structure as drop cast film on SiO_2, i.e., regions with different thickness of emissive thin film.

In this case, the PL intensity from the film on the gold area is less than on the glass region (Figure 31). Moreover, the spectrum from the gold region shows blue shift in comparison with the glass part. The reason can be higher adhesion of the complex on gold than glass. Higher roughness of the gold (gained from AFM) surface causes higher adhesion of the complex.

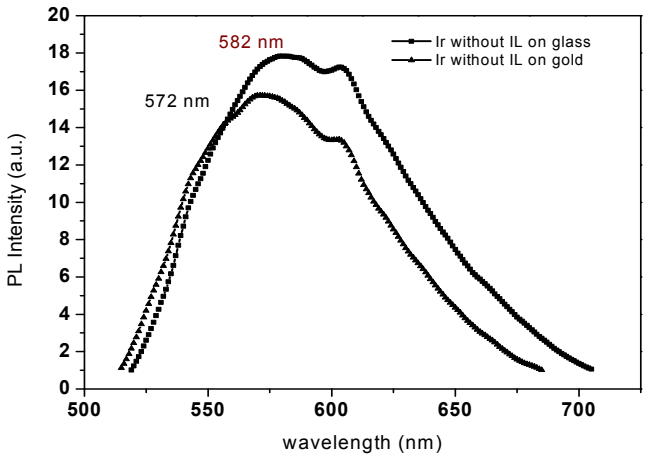

Figure 31: PL spectra of thin films of $Ir(ppy)_2(bpy)^+PF_6^-$ deposited on Au patterned glass substrate. DAPI filter was used. The spectra were taken under vacuum.

ITO on glass

ITO on glass is a common substrate used in vertical LEECs as an anode. It is quite transparent in the visible portion of the solar spectrum and conductive (around 10^4 S/cm). ITO has a disordered and rough structure [109]. The complex is deposited on ITO using both spin coating and drop casting methods. The maximum peak of emission from the film spin coated on ITO was 580 nm which has been reported in [110]. The spectra on both glass and ITO are the same. This can be attributed to the similar structures of these substrates that cause similar morphology and adhesion of the film.

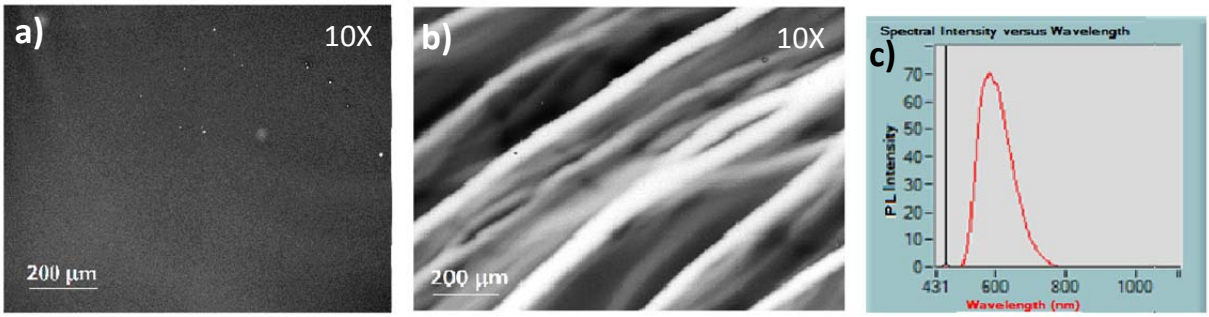

Figure 32: Thin film of $Ir(ppy)_2(bpy)^+PF_6^-$ on ITO substrate a) Spin coated film, b) Drop casted film, c) PL spectrum of the film ($\lambda_{max,\ emission}$ ca 580 nm). DAPI filter cube was used. Spectrum was taken under vacuum.

ITO covered with PEDOT:PSS

In vertical LEECs most of the time PEDOT:PSS has been used to reduce ITO roughness to provide smoother surfaces which are necessary for charge transport in electronic devices. In addition, smooth surface reduces adhesion of the film to the substrate and increases PL. In other words smooth surface increases the crystalline structure of the film [111]. Therefore the film formation on ITO covered by PEDOT:PSS should be investigated as well. Figure 33 shows the image and spectrum of the film deposited on ITO covered with PEDOT:PSS.

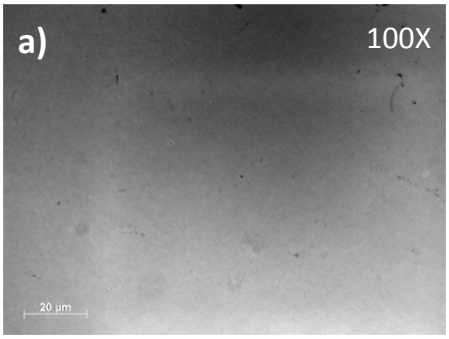

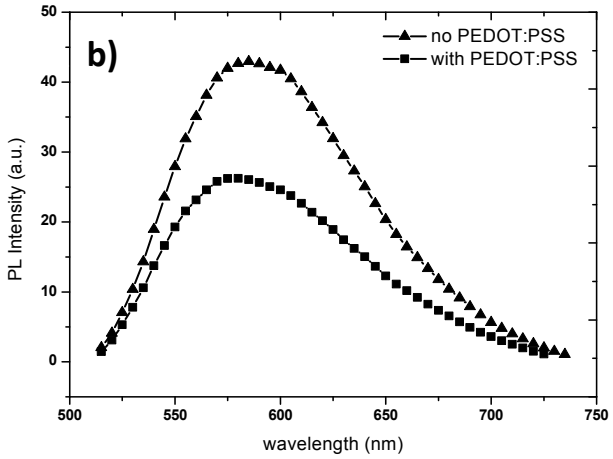

Figure 33: Spin coated thin film of $Ir(ppy)_2(bpy)^+PF_6^-$ a) PL image on PEDOT:PSS-covered ITO. b) PL spectra of the films on both ITO substrate and PEDOT:PSS-covered ITO. $\lambda_{max,\ emission}$ ca 580 nm. DAPI filter cube was used. The spectrum was taken in ambient air as soon as the film was exposed to light.

The number of aggregates on ITO/ PEDOT:PSS substrate is lower than ITO substrate . (AFM images also prove); however the spectra show that although the presence of PEDOT:PSS between ITO and emissive film reduces the roughness of the film, it can reduce the intensity of emitted light. This behavior can be attributed to the penetration of anions into the PEDOT:PSS layer that provides basic environment. In this basic region PEDOT:PSS can have a small absorption at 570 nm and reduce the emission intensity [112, 113]. However in the case of an electronic device, the application of a PEDOT:PSS layer plays an important role in device performance. The PEDOT:PSS layer provides a well-defined work function higher than that of ITO and also avoids indium and oxygen penetration into the active layer, providing longer device lifetime [111]

3.2.2 AFM images

The morphology of the thin films of $Ir(ppy)_2(bpy)^+PF_6^-$ deposited on various substrates used in LEEC fabrication is investigated. The objective of this investigation is to recognize the final structure of the thin film and its effect on photo- and electroluminescence.

Patterned Au on SiO_2 substrate

AFM images of a film of $Ir(ppy)_2(bpy)^+PF_6^-$ on both gold and SiO_2 regions of Au patterned SiO_2 substrate are shown in Figure 34. The surface roughness of this film is different on the gold and glass portions. Furthermore the image obtained from gold shows the formation of *spikes* with an average height of 100 nm (Figure 35).

These spikes were brighter in PL images. Therefore we can attribute these bright spots to the bulky aggregation of the complex on gold. However these spikes do not appear on SiO_2 surface and no phase separation was observed on the film (Figure 34 b). Thus complex deposition makes SiO_2 surface very smooth (even smoother than bare SiO_2 (RMS= 0.8 nm)). It means that the complex adhered very well to this surface. This adhesion causes lower emission intensity (Figure 25). Moreover the holes (voids) on the surface make vast region for oxygen and water penetration that cause photobleaching. Since in this device the channel is SiO_2, thus it cannot be good candidate to be used in planar devices.

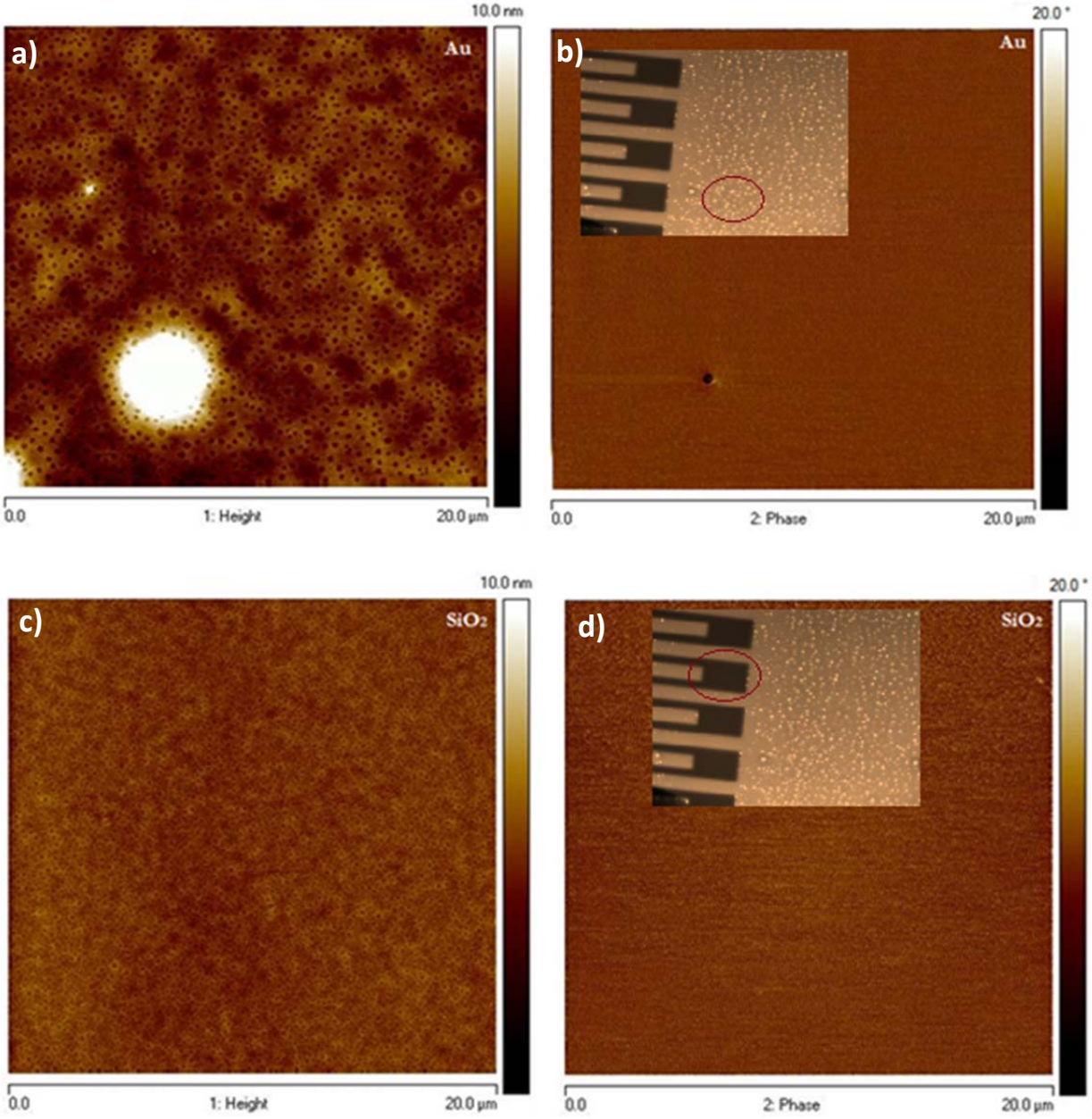

Figure 34: 20 µm × 20 µm AFM images of spin coated thin films of $Ir(ppy)_2(bpy)^+PF_6^-$ on gold/ SiO_2 substrate. a) Height image on gold, RMS= 4.28 nm, b) Phase image on gold, c) Height image on SiO_2, RMS= 0.46 nm and d) Phase image on SiO_2. Insets are the PL images of the film on interdigitated Au patterned on SiO_2, the circles shows the regions that AFM images were taken.

The profile section of these regions (Figure 36 and Figure 37) showed that the depth of holes in the film on both gold and SiO_2 are between 1-2 nm. Solvent evaporation during annealing step causes these damples. But due to the more adhesion of the complex on SiO_2, the surface areas of the holes on gold are larger than on SiO_2.

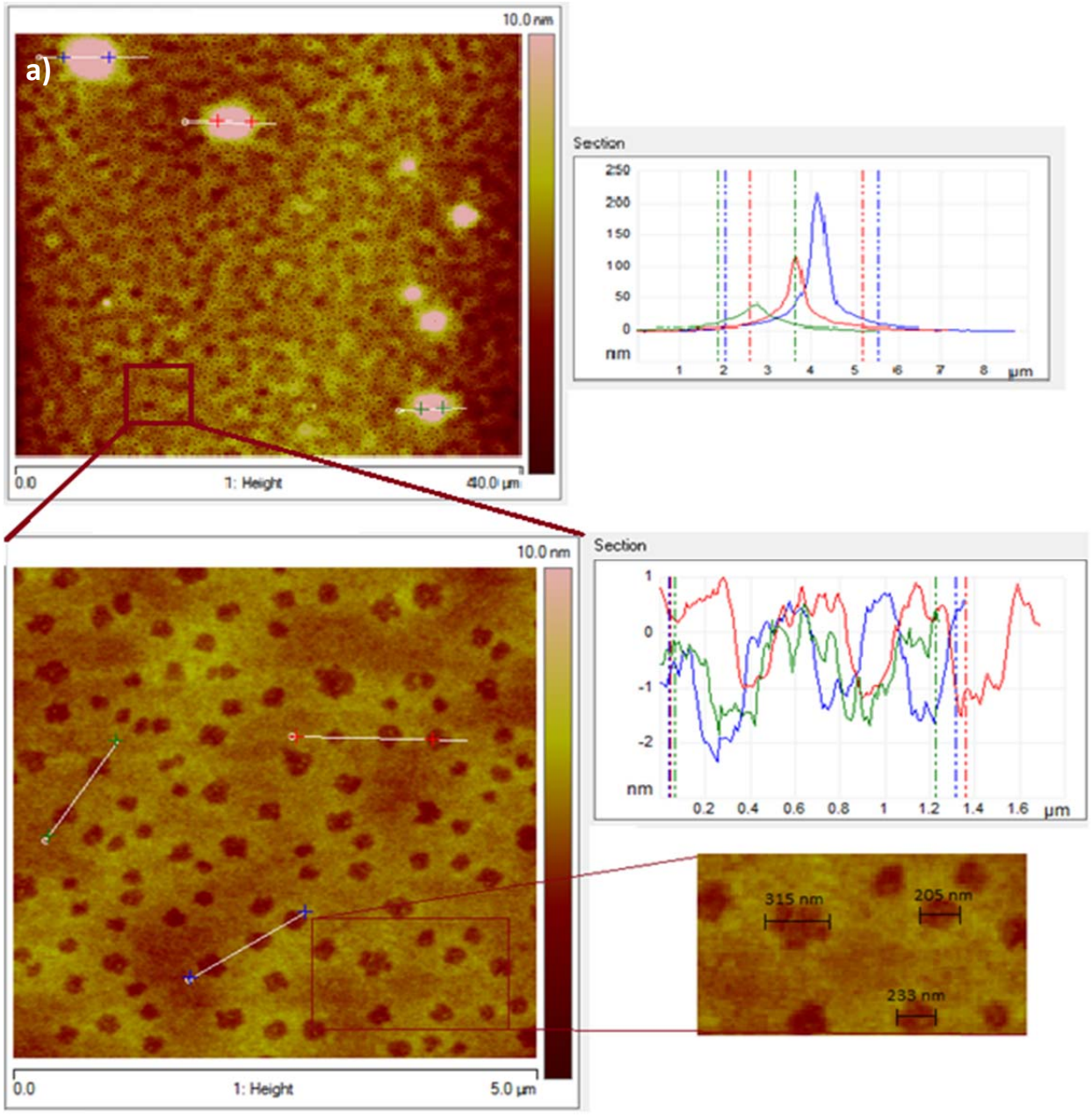

Figure 35: AFM section profile of spin coated thin films of $Ir(ppy)_2(bpy)^+PF_6^-$ on Au patterned on SiO_2 substrate on gold region.

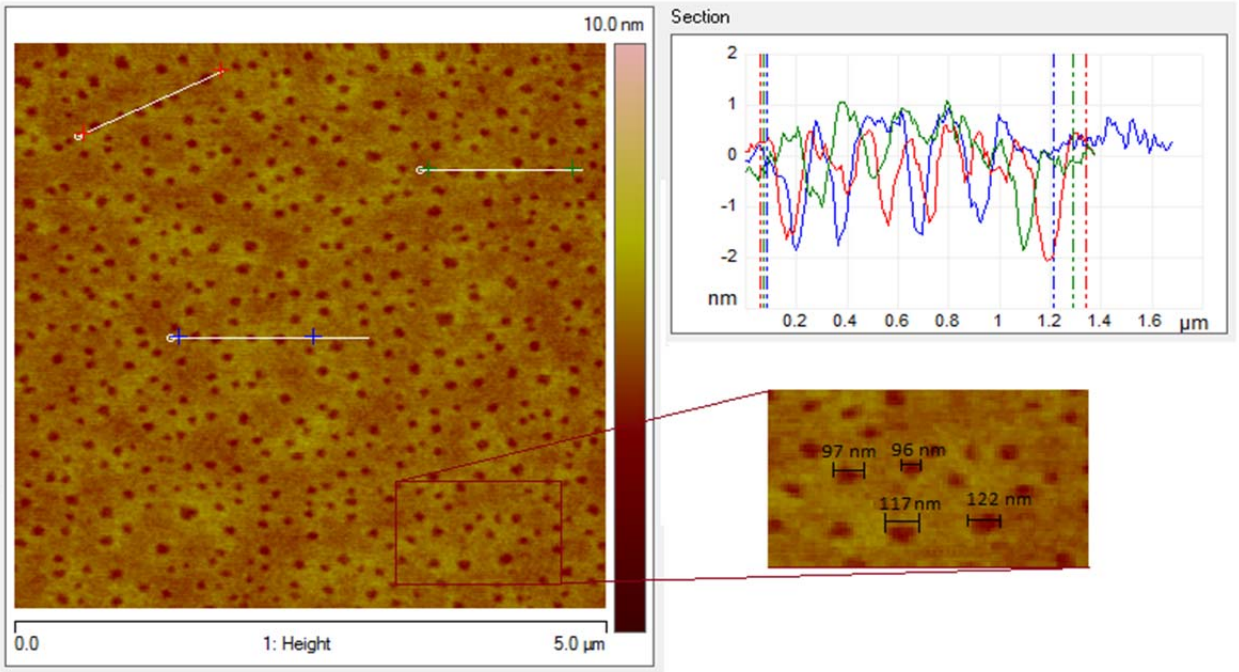

Figure 36: AFM section profile of spin coated thin films of $Ir(ppy)_2(bpy)^+PF_6^-$ on Au patterned on SiO_2 substrate on SiO_2 region.

ITO substrate

To compare the roughness of the substrates after film formation the AFM images of the bare substrates of ITO and PEDOT:PSS covered ITO are shown in Figure 37 and Figure 38.

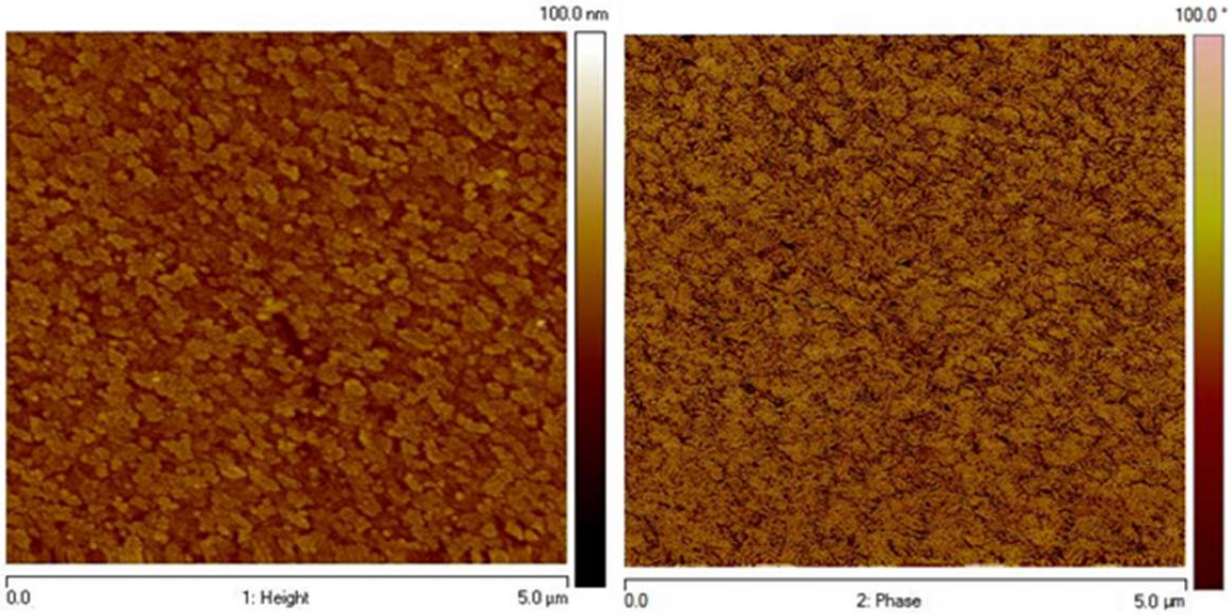

Figure 37: AFM image of bare ITO substrate rms=4.9 nm.

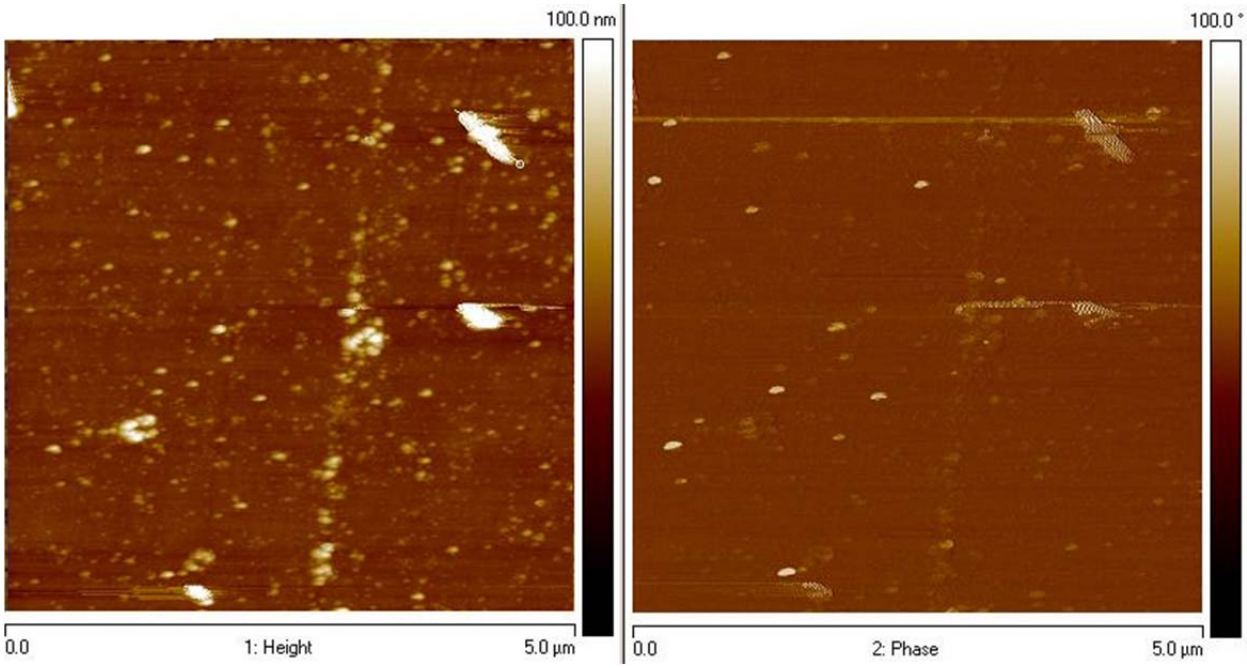

Figure 38: AFM image of ITO covered with PEDOT:PSS. rms=1.8nm.

In this step, the film formation on top of ITO is investigated. In vertical LEECs (ITO as a substrate), the operation voltage is low, ca 3-4 V. It means that the device has good charge injection and transport [105, 114]. Having smooth thin films plays an important role in these

phenomena. AFM images of the films on ITO show the formation of homogenous and smooth films. Thickness of the film is around 200 nm. The roughness of bare ITO is 4.9 nm (appendix **Error! Reference source not found.**) while for ITO covered with the complex is 1.16 nm. Phase images show no phase separation on ITO (Figure 39).

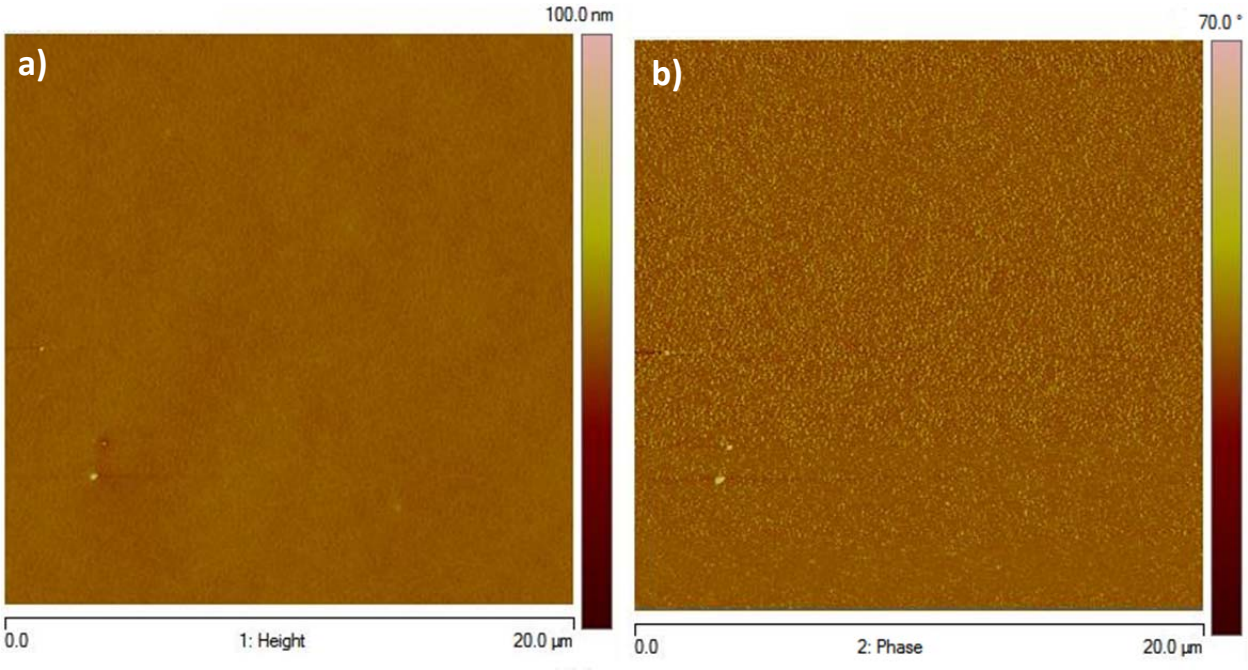

Figure 39: 20 µm × 20 µm AFM images of spin coated thin films of $Ir(ppy)_2(bpy)^+PF_6^-$ on ITO. RMS= 1.16 nm. a) Height image, b) Phase image.

ITO covered with PEDOT:PSS

PEDOT:PSS is a polymer that can trap electrons near the anode and provide high field strength in that region leading to the improved balance of injection rates for electrons and holes and consequently higher device efficiencies [115]. In addition, PEDOT:PSS smoothes the ITO surface to provide good path for charge injection and transport. AFM images of the film formed on ITO/PEDOT:PSS prove this (Figure 40). The roughness of the film changed to 0.49 nm in the presence of PEDOT:PSS. The phase image shows a homogenous film with no phase separation. So far ITO/PEDOT:PSS is the best substrate to be used in LEECs. However in addition to complexity of patterning ITO to have the channel smaller than 100 microns, PEDOT:PSS deposition on one electrode in the planar configuration needs further investigation.

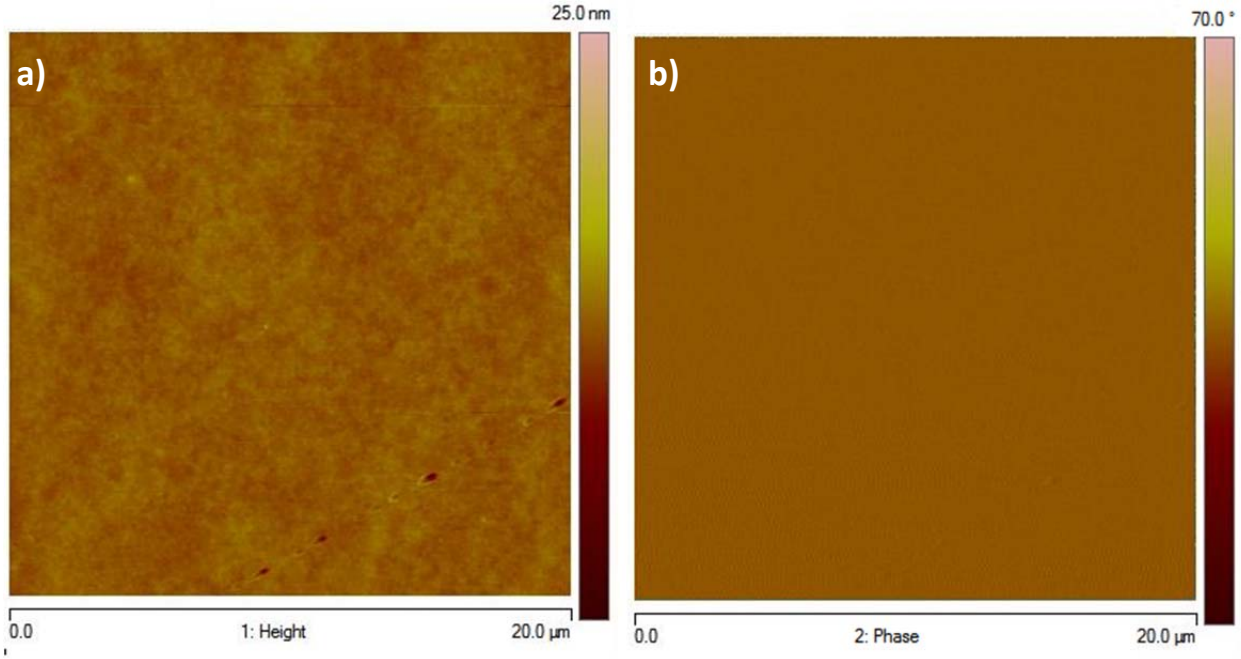

Figure 40: 20 µm × 20 µm AFM images of spin coated thin films of $Ir(ppy)_2(bpy)^+PF_6^-$ on PEDOT:PSS-covered ITO. RMS= 0.49 nm. a) Height image, b) Phase image.

3.3 Thin film morphology characterization of LEECs based on $Ir(ppy)_2(bpy)^+PF_6^-$ blended with $BMIm^+PF_6^-$

In general, films of emissive materials are responsible for generating light in LEECs. In these films, interactions between closely packed molecules usually cause quenching of exited states. Therefore, providing steric hindrance to limit self-quenching can increase the light intensity in these devices [116]. In addition, the working principle of LEECs is based on ion redistribution and ion mobility during device operation. Therefore the low ionic conductivity in the solid state causes long turn-on times (t_{on}), defined as the time required to reach a maximum luminance. Most approaches to improve t_{on} reduce device stability [13, 19, 20, 39, 117, 118]. However the most promising approach to reduce t_{on} is the addition of an ionic liquid (IL) [39]. ILs are used to increase the mobile ion density in the thin film. They can also be placed among iTMC molecules; therefore self-quenching will decrease.

Ionic liquids, molten salts at room temperature, are substances containing only ions with the melting point below 100˚C. Commonly used ILs are quaternary ammonium salts or cyclic amines that can be aromatic (e.g., pyridium, imidazolium) or saturated (e.g., piperidinium, pyrrolidinium) [40]. The cations of ILs employed in LEECs are generally bulky and asymmetric and the anions of ILs are weakly coordinating compounds. Therefore, the resulting IL is a highly polar but non-coordinating solvent [48].

The ionic conductivity of ILs at room temperature ranges between 0.1 and 10 $mScm^{-1}$. The conductivity of ILs is due to the movement of ions between two electrodes. It is inversely proportional to the medium viscosity which is defined by ion size, polarizability, van der Waals interaction and hydrogen bonding [119]. In ionic liquids, stable ionic aggregation may be formed by ion–ion interactions that avoid ionic conductivity. Therefore choosing compatible IL and material is very important.

In our study we used $BMIm^+PF_6^-$ whose anions (PF_6^-) are the same as our ionic TM compound.

There are two different strategies in blending IL to the complex solution (explained in chapter 2): i) Direct addition of IL droplet to the complex solution (approach A), ii) Mixing of two solutions of IL and complex (approach B). However in both cases we have same molar ratio (Ir complex: IL, 1:1 molar ratio). Films with different morphology were formed due to the circumstances of blending, so we expected to see different electrical behavior. In approach B, addition of the solvent decreases the viscosity of IL and makes it a well-behaved reversible redox couple in comparison with pure $BMIm^+PF_6^-$ [120].

In general, ILs are excellent solvents for spectroscopic studies because they have low absorption over large wavelength ranges in typical spectroscopic instrumental methods.

Acetonitrile is a typical polar aprotic solvent that does not solvate anions [121]. This property can increase the mobility of the ions and as a result the ion conductivity. On the other hand $BMIm^+PF_6^-$ is a protic IL. It means that it can participate in hydrogen bonding by its cationic part, thus PF_6^- can move freely in solution [122]. In approach B, the cations ($BMIm^+$ and $Ir(ppy)_2(bpy)^+$) of both solutions are solvated by acetonitrile so there are more space between the cations in comparison with approach A. Then we expected to see more space between aggregates in second approach.

3.3.1 Photoluminescence images and spectra

In this section the morphology and photoluminescence of the thin film of $Ir(ppy)_2(bpy)^+PF_6^-$ blended with $BMIm^+PF_6^-$ on top of different substrates is investigated.

Patterned Au on SiO_2 substrate

In Figure 41 the PL images of the film prepared with first strategy (approach A) are shown.

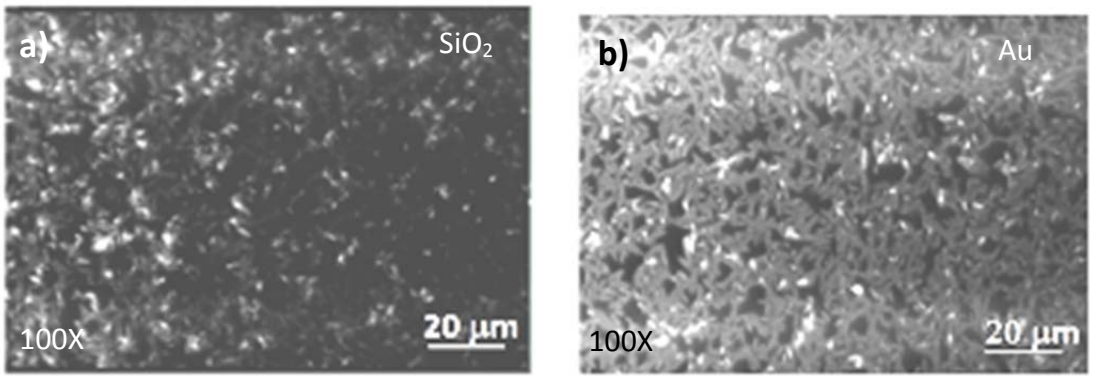

Figure 41: PL images of thin films of $Ir(ppy)_2(bpy)^+PF_6^-$ mixed with $BMIm^+PF_6^-$ (approach A) on SiO_2 substrate with interdigitated Au electrodes: a) 100 × magnification on SiO_2, b) 100 × magnification on the gold electrode.

The PL spectra of the films show that the light intensity emitted from the complex on gold is much higher than on SiO_2 (Figure 42) due to higher concentration of the complex on gold. However blue shift of the spectrum on SiO_2 in comparison with gold comes from higher IL concentration on SiO_2. It seems that although SiO_2 is smoother than gold, the adhesion of IL on SiO_2 is higher than gold; It means that this IL has tendency to stay more on SiO_2 than gold. SiO_2 is hydrophilic polar surface i.e. the surface with electric dipole or multipole moment. Therefore polar molecules have tendency to this polar surface [123]. $BMIm^+ PF_6^-$ is a polar IL. Its polarity is higher than that of acetonitrile [124]. Thus that has higher tendency to stay over SiO_2 polar surface than complex dissolved in acetonitrile. Hence IL molecules can reduce the interference of the energy levels of the SiO_2 surface and the complex that consequently causes a blue shift to occur in the SiO_2 spectrum (Figure 42).

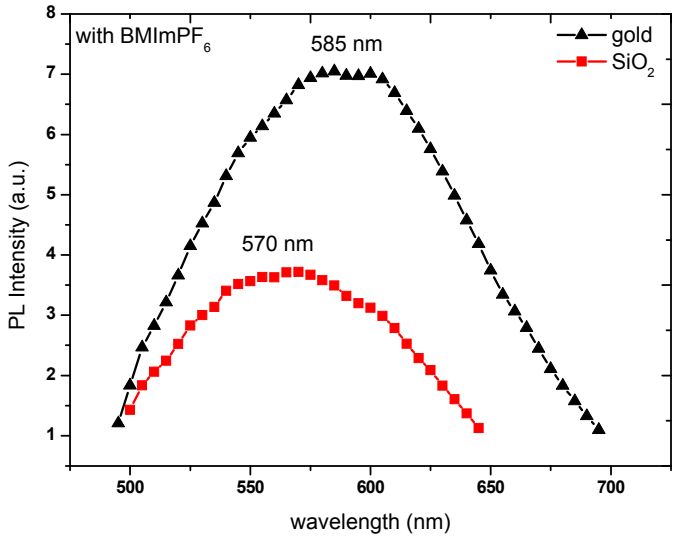

Figure 42: PL spectra of thin films of $Ir(ppy)_2(bpy)^+PF_6^-$ mixed with $BMIm^+PF_6^-$ (approach A) on Au patterned SiO_2 substrates, on SiO_2 and gold electrode portions. DAPI filter cube was used. Spectra were taken in air as soon as the film was exposed to the light.

After the LEEC was made with the blend, a voltage was applied to the device for a long time (around 10 hours) and afterwards PL images were taken. In this condition the accumulation of cations of both complex and IL on the negative electrode formed bright areas with black spots (Figure 43). The black spots can be attributed to $BMIm^+$ and also a small number of PF_6^- with no emission. The images also show that $Ir(ppy)_2(bpy)^+$ were located on the negative electrode and made this electrode much brighter than the positive one (polarization on electrodes). Different brightness in two electrodes is due to the different thickness and concentration of emitter material. However more studies are needed. Bright field images have higher resolution (Figure 43 a,b). Number of black spots on negative electrode is higher than positive electrode.

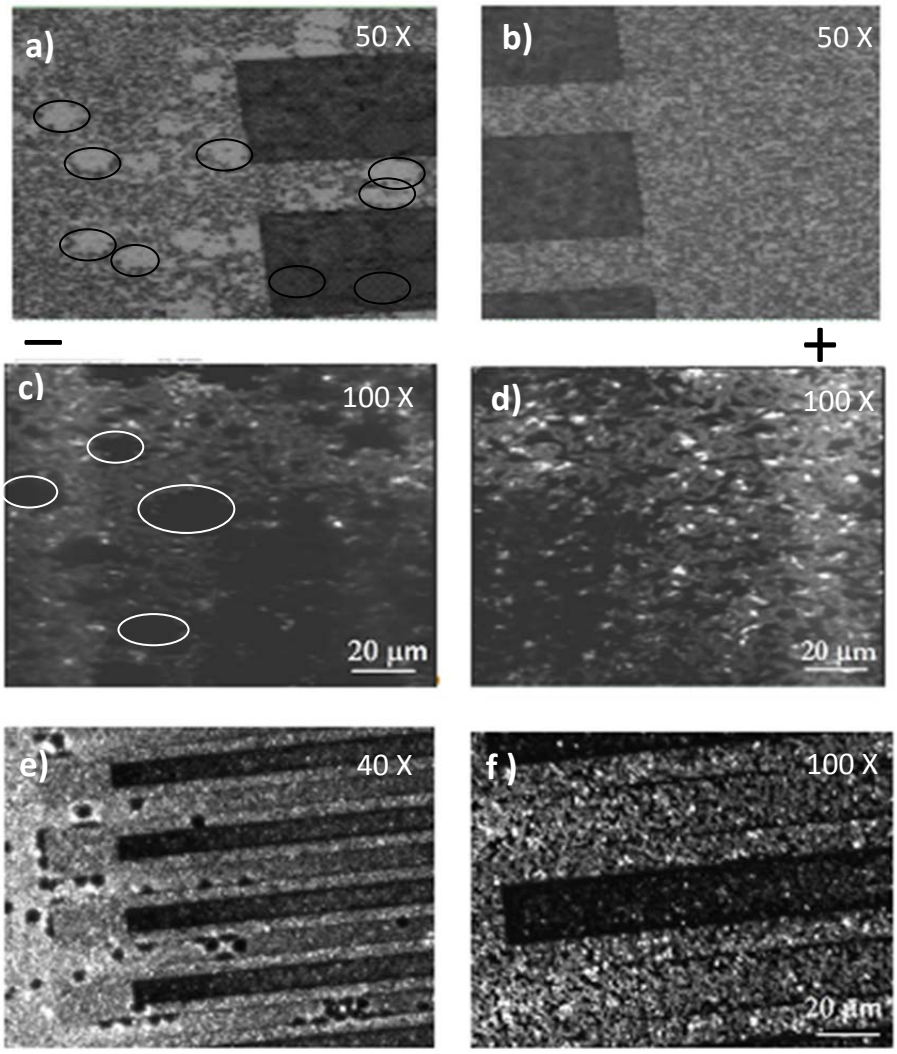

Figure 43: PL images of spin coated thin films of $Ir(ppy)_2(bpy)^+PF_6^-$ mixed with $BMIm^+PF_6^-$ (approach A) on interdigitated gold patterned SiO_2 substrates. a) Bright field image of the film after application of a negative bias to the Au electrode (the Au electrode corresponds to the clear portion of the substrate). The aggregates of $BMIm^+$ are depicted by black empty circles. b) Bright field image of the film after application of a positive bias to the Au electrode (the Au electrode corresponds to the clear portion of the substrate), with lower ion aggregation. c) PL image of the film on a) with DAPI filter; white circles suggest $BMIm^+$ aggregates with no PL. d) PL image of the film in b) with DAPI filter. e) PL image of the whole interdigitated electrode region: the negatively biased electrode area is brighter and full of aggregates if compared to the positively biased electrode region. f) PL image as in e), with a higher magnification.

In another study, the device was fabricated with the solution blend made with approach B. In this case the complex and the IL were dissolved in acetonitrile separately and afterwards they mixed with 1:1 molar ratio. The structure of the film is different from the film made with approach A (Figure 41.)

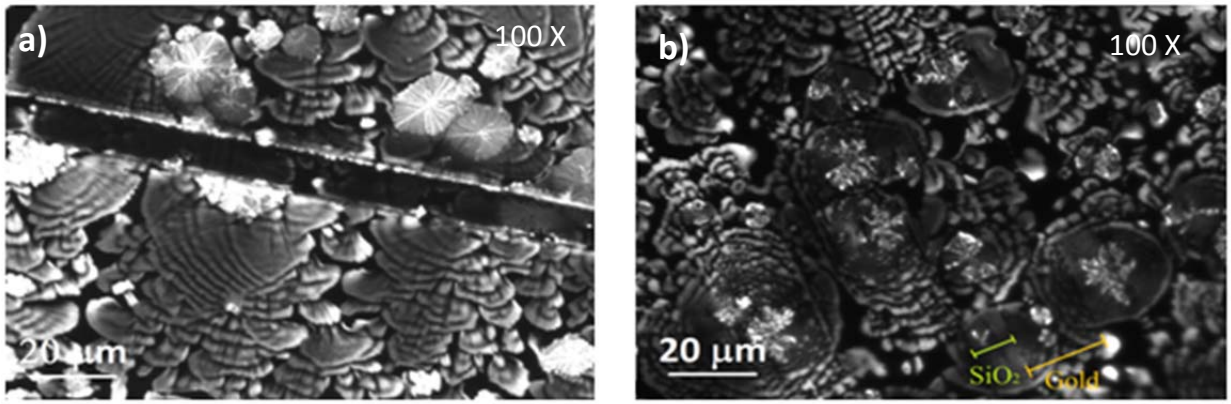

Figure 44: PL image of a thin film of spin coated $Ir(ppy)_2(bpy)^+PF_6^-$ mixed with $BMIm^+PF_6^-$ (approach B) on Au electrode patterned SiO_2. a) Single channel substrate. The channel is partly covered by the complex. b) Interdigitated substrate.

As mentioned, emission is from the cationic part. Therefore in Figure 44, the bright star parts are the accumulation of $Ir(ppy)_2(bpy)^+$. π-π stacking among the cations can form these structures that seem vertically formed. However this was not observable in the thin film of complex without IL on top of the same substrate, so the star shape is due to the presence of IL.

There is a discontinuity in the film formation, i.e. the circular structures are partly connected to each other. This can possibly reduce charge transport and, as a result, the device current. Hydrogen bonding between $BMIm^+$ and ligands of the complex can be a reason for the formation of these separated structures.

Drop casting of the complex solution on SiO_2 substrate showed the region with high concentration of the complex (as a background in Figure 45) and Ir complex islands in IL regions. These images may show thermodynamically stable structure of Ir complex/IL blending. It seems that the compatibility of this ionic Ir complex and $BMIm^+PF_6^-$ (because of possibility of making hydrogen bonds) is not good enough to form homogenous film on SiO_2 substrate.

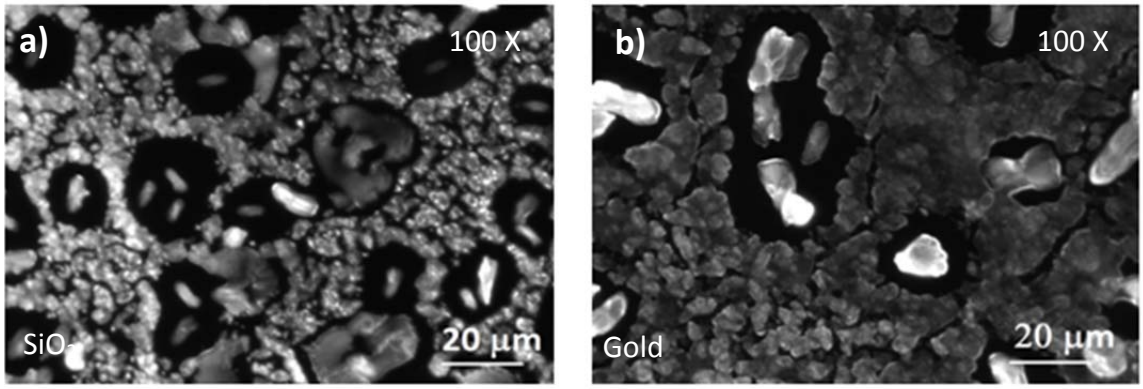

Figure 45: PL images of the drop cast thin film of $Ir(ppy)_2(bpy)^+PF_6^-$ mixed with $BMIm^+PF_6^-$ (approach A) on a) SiO_2 substrate and b) gold electrode. DAPI filter cube was used. The structure on gold is more condensed than its structure on SiO_2.

In this case after voltage application on electrodes, we saw the same behavior as what was observed on spin coated films. Cations accumulated on negative electrode and formed emissive aggregates. Positive electrodes are dark while the negative electrodes and the channel are bright (Figure 46).

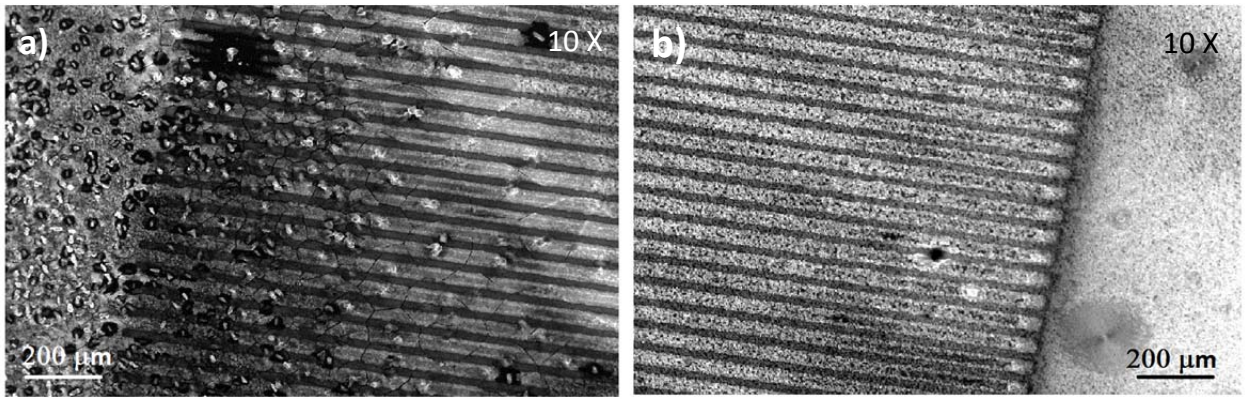

Figure 46: PL images of drop cast thin films of $Ir(ppy)_2(bpy)^+PF_6^-$ mixed with $BMIm^+PF_6^-$ (approach A) on interdigitated gold patterned SiO_2 substrate. The images were taken after application of an electrical bias: a) negative electrode, b) positive electrode. DAPI filter cube was used.

Patterned Au on glass substrate

Investigation of the thin film of $Ir(ppy)_2(bpy)^+ PF_6^-$ / $BMIm^+PF_6^-$ on Au patterned glass substrate showed interesting structures. In spin coated film, although film formation on gold and glass was different, the micro aggregates were distributed homogenously (Figure 47). Sizes of aggregates are different on glass and gold. However they are separated from each other and formed discontinuous films. For instance in the channel (Figure 47 a) the aggregates were observed like individual spots, so we could not expect detecting any electroluminescence unless the applied electrical power makes some changes in the channel. AFM phase images can show that the black parts can be IL or bare substrate.

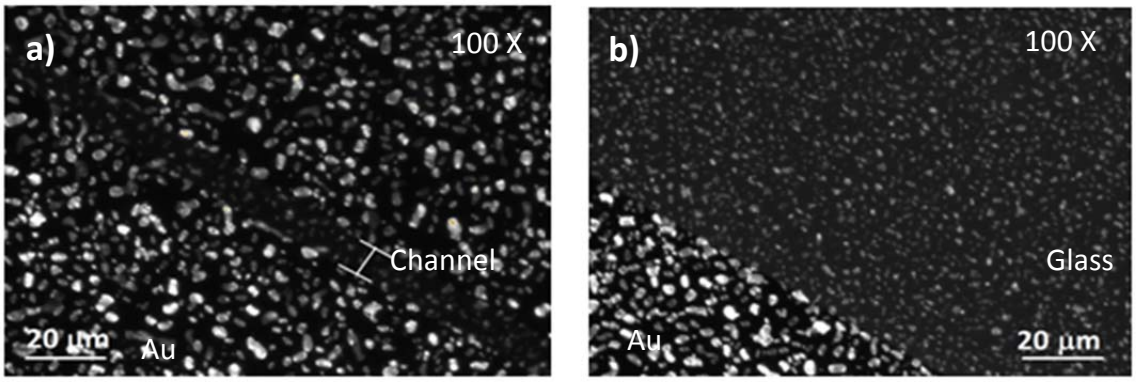

Figure 47: PL images of spin coated thin films of $Ir(ppy)_2(bpy)^+ PF_6^-$ mixed with $BMIm^+PF_6^-$ (approach B) on gold patterned glass substrate. a) Channel of the device between two gold electrodes; b) Different film morphologies on gold and glass. DAPI cube filter was used.

Film formation by drop casting method on gold/ glass substrate was investigated. The results were unexpected. The film showed different structure in various parts (Figure 48).

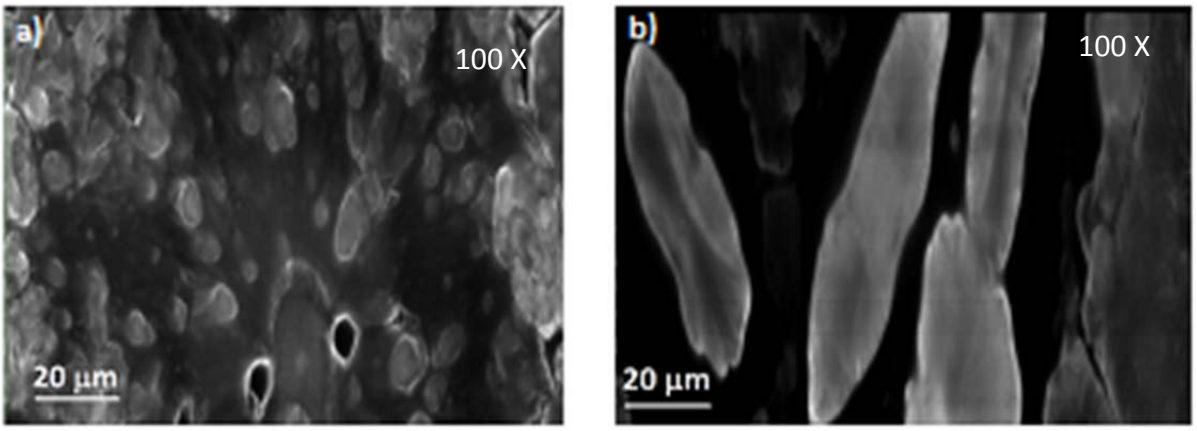

Figure 48: PL images of drop cast films of $Ir(ppy)_2(bpy)^+PF_6^-$ mixed with $BMIm^+PF_6^-$ (approach B) on gold electrode. The film formed different morphologies: a) relatively continuous, with dark spots of ionic liquid; b) micro-rods islands, possibly spaced by ionic liquid regions. DAPI filter was used.

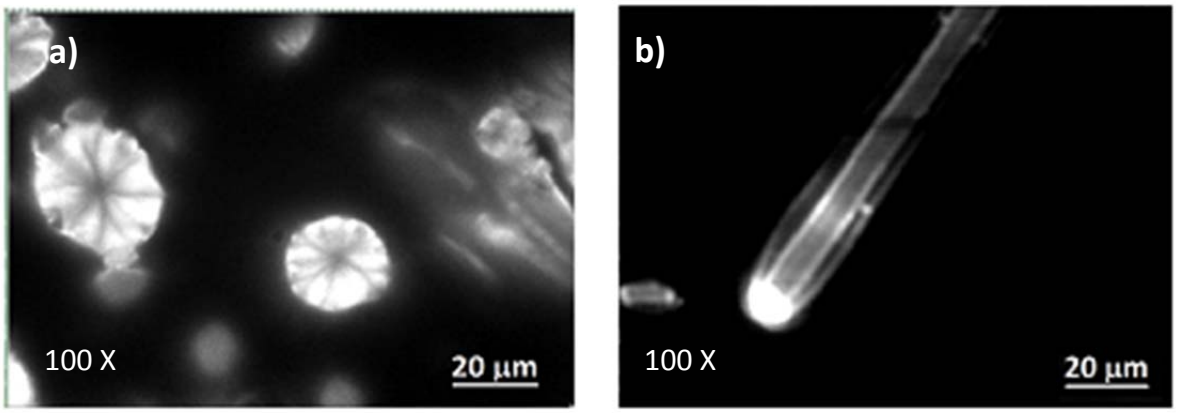

Figure 49: PL images of drop cast films of $Ir(ppy)_2(bpy)^+PF_6^-$ mixed with $BMIm^+PF_6^-$ (approach B) on Au patterned substrate: a) Rods often formed vertically on the glass portion of the substrate, not connected one to another ; b) Occasionally rods were longer, with bright centers. DAPI filter cube was used.

As it is shown in Figure 49, the rods on glass are completely separated from each other. The bright center of the rods can be attributed to the interaction between the emissive components of the complex ($Ir(ppy)_2(bpy)^+$) so that the cations are in the middle and the anions (PF_6^-) around

them. They are so packed that the ions of IL cannot penetrate among them otherwise the layer would be formed like spin coated film (shown in Figure 47). These structures can be caused by π-π stacking between the ligands of the complex.

These vertical rod-structures were similar with what were formed in the channel. Therefore the discontinuity is not suitable for EL generation. We tried to control the rod formation in the channel to have continuous path for charge transfer (recombination). However just a small portion of the channel could be covered by continuous film. Moreover the films mainly formed on top of the channel, not between two electrodes; therefore the positions of the tips during voltage application are very important. They should be put at the region with continuous structure.

The spectra of the thin films made with the complex solution and the solution blend show that the presence of IL in the layer caused a red shift (Figure 50). The reason for this behavior was discussed before.

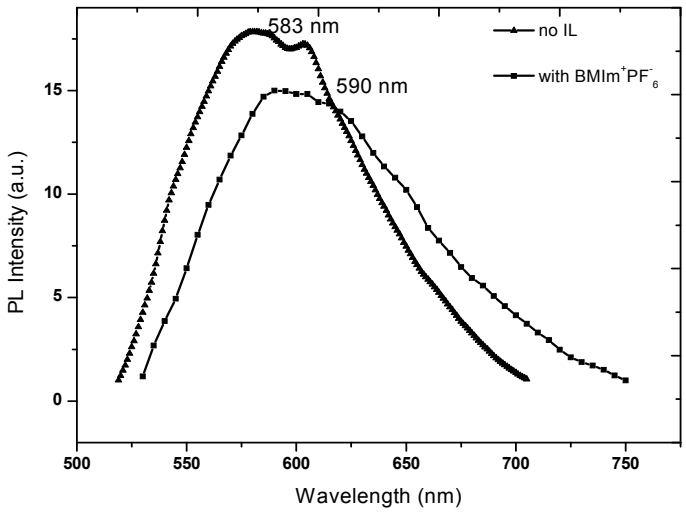

Figure 50: PL spectra of spin coated thin films of $Ir(ppy)_2(bpy)^+PF_6^-$ with and without the ionic liquid (IL) $BMIm^+PF_6^-$, deposited on a glass substrate patterned with gold electrodes. The PL peak in presence of IL shows red shift. DAPI filter cube was used. The spectra were taken under vacuum.

ITO substrate

Final investigation is assigned to the thin film of blend solution on top of ITO substrate. This substrate was investigated due to its importance in vertical devices. Both spin coated and drop casted films showed inhomogeneity in the emissive thin film. The spin coated film (Figure 51) shows very small aggregates. It is normal that the aggregates in drop-casted film are bigger.

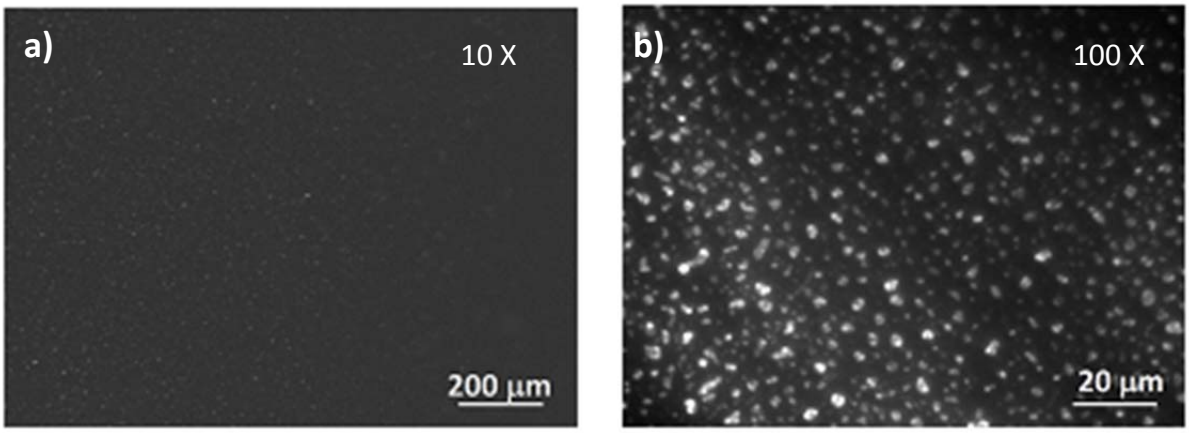

Figure 51: PL images at different magnification of spin coated thin films of $Ir(ppy)_2(bpy)^+PF_6^-$ mixed with $BMIm^+PF_6^-$ (approach B) on ITO substrate. a) 10× magnification, b) 100× magnification. DAPI filter was used.

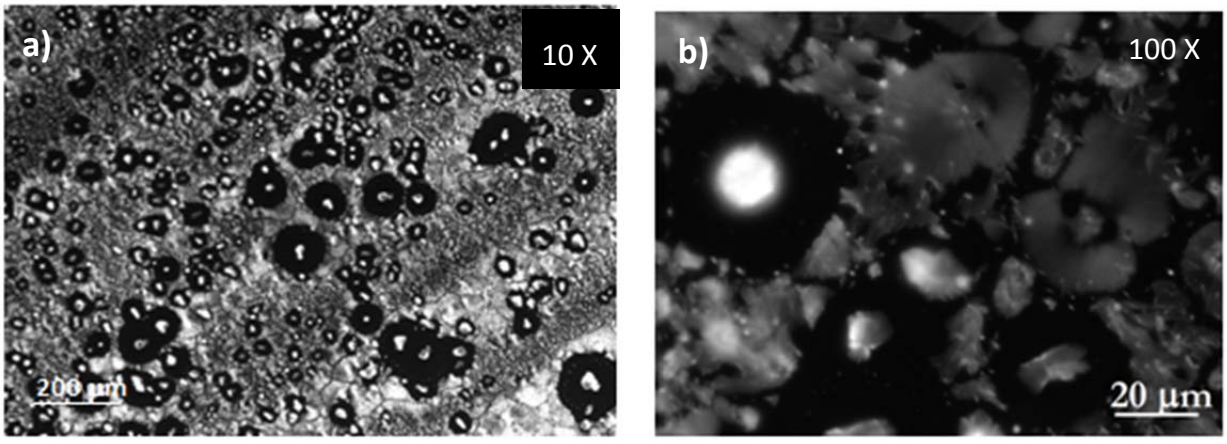

Figure 52: PL images of drop cast thin films of $Ir(ppy)_2(bpy)^+PF_6^-$ mixed with $BMIm^+PF_6^-$ (approach B) on ITO substrate. a) 10× magnification, b) 100× magnification. DAPI filter was used.

Since in several studies a hole blocker layer is used near anode, it is very important to check the film formation on ITO covered with PEDOT:PSS as a hole blocker.

ITO covered by PEDOT:PSS

So far we understand that the smallest aggregates are formed on ITO. In LEEC fabrication when ITO is covered with PEDOT:PSS, the device shows better performance due to providing smoother surface by PEDOT:PSS layer and the hole blocking property of this layer.

In Figure 53 the PL images of the film on top of the ITO covered by PEDOT:PSS are shown.

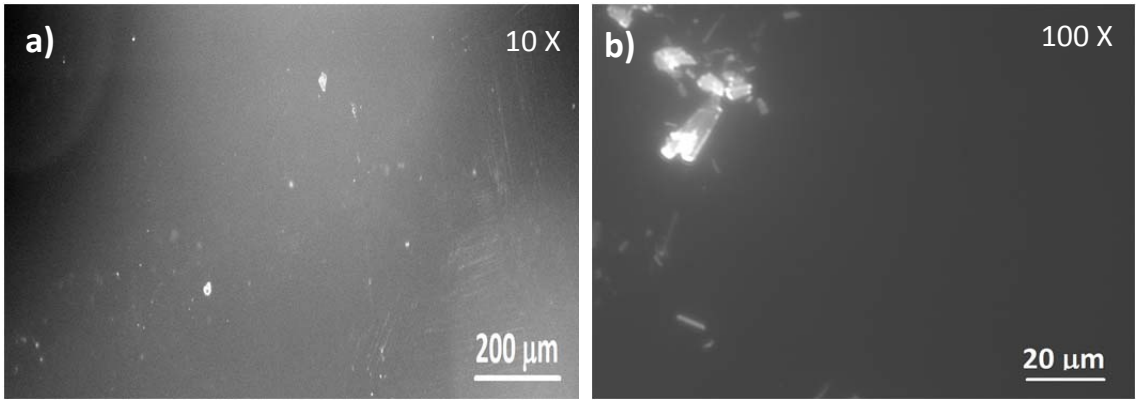

Figure 53: PL images of the spin coated thin film of $Ir(ppy)_2(bpy)^+ PF_6^-$ mixed with $BMIm^+PF_6^-$ (approach B) on ITO substrate covered with PEDOT:PSS.

Comparison between PL spectra of the film on ITO substrate and PEDOT:PSS covered ITO (Figure 54) shows that the presence of PEDOT:PSS does not have remarkable effect on peak position (energy levels of the complex) but in light intensity. As explained before, anion penetration causes light absorption in PEDOT:PSS at around 570 nm. Here in addition to anions of the complex we have anion from IL; thus we can see more reduction in light intensity [112] . However the presence of ionic liquid in the film can change the structure of PEDOT:PSS layer resulting in red shift in PL spectra in comparison with the spectra from thin film without IL.

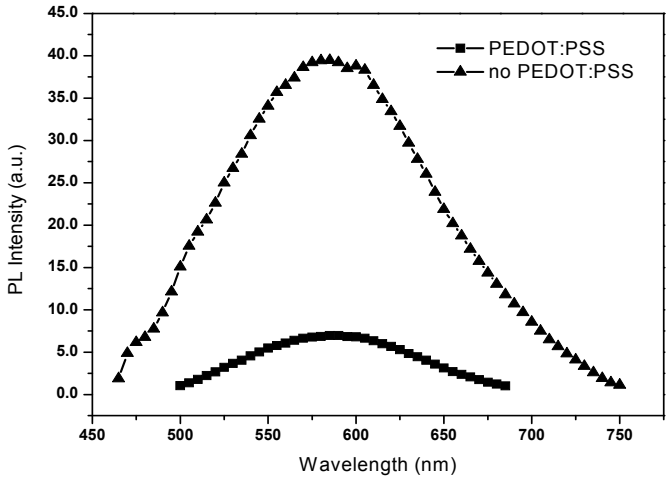

Figure 54: Comparison between spin coated thin films of $Ir(ppy)_2(bpy)^+PF_6^-$ mixed with the ionic liquid $BMIm^+PF_6$ (approach B) on bare ITO substrate and on ITO covered with PEDOT:PSS. $\lambda_{max,\ emission}$ ca 585 nm. The spectra were taken in air as soon as the film was exposed to light.

3.3.2 AFM images

In order to study the effect of $BMIM^+PF_6^-$ on thin-film morphology of the complex, AFM measurements were performed. AFM images of films made with the blend of complex and $BMIM^+PF_6^-$ coated on SiO_2, Au, ITO and ITO covered with PEDOT:PSS are shown. IL molecules cause aggregation and phase separation in the film, because they increase the intermolecular separation of the complex molecules. In addition they can make hydrogen bonds with ligands. Therefore uniform thin film could not be obtained.

Patterned Au on SiO2 substrate

AFM images of the thin film of $Ir(ppy)_2(bpy)^+PF_6^-$ mixed with $BMIm^+PF_6$ deposited on SiO_2 substrate are shown in Figure 55. The images prove that the film on top of gold is more condensed than SiO_2. However the phase images show two different phases in the film.

Generally phase images are monitored due to different chemical and viscoelastic properties of the different materials across the surface [125]. From these images we can recognize than there are two different phases in the film. On gold electrode the phase of vertical structures (flower

shapes) (Figure 55a) are different from other bumps. However this difference can originate from the different chemical interaction of the Si tip and the complex in addition to various viscoelasticity. Therefore we cannot recognize IL distribution. But looking at the PL images that show PL from all over the surface, it seems that IL molecules do not have a tendency to stay on gold the surface.

On SiO_2 (Figure 55b) the brown areas are the complex and the yellow parts are ionic liquid. The section profile shows spikes with an average height of 100 nm in brown areas (appendix Figure 63), thus these regions are the complex aggregates. It can be concluded that the ionic complex and $BMIm^+PF_6^-$ do not have good compatibility to be used in LEECs as an emissive film. Formation of vertical structures surrounded by IL does not provide a continuous film for charge transport in LEEC.

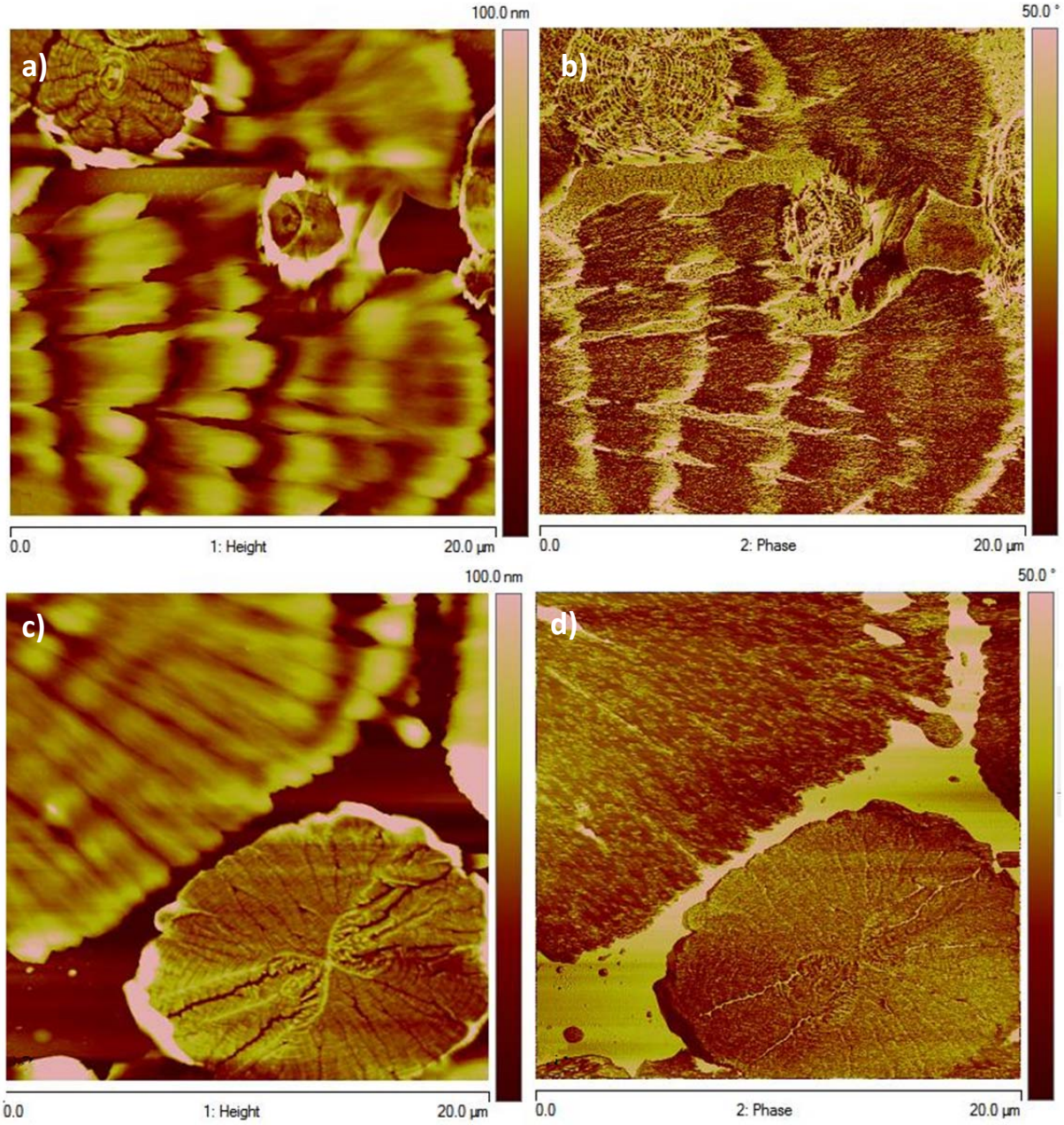

Figure 55: 20 µm × 20 µm AFM images of thin films spin coated $Ir(ppy)_2(bpy)^+PF_6^-$ mixed with $BMIm^+PF_6^-$ (approach B) on gold/SiO_2. a) Height image on gold, b) Phase image on gold, c) Height image on SiO_2, d) Phase image on SiO_2.

ITO substrate

AFM images of the film on ITO are shown in Figure 56. The film surface is full of aggregates in presence of IL. Some aggregates are bigger than 400 nm (appendix Figure 64). Phase separation is shown in Figure 56b. However presence of such big bumps in the surface decreases the resolution of the image. AFM image in lower scale shows that the background is ITO (appendix Figure 65). IL ions may entangle inside the complex lattice.

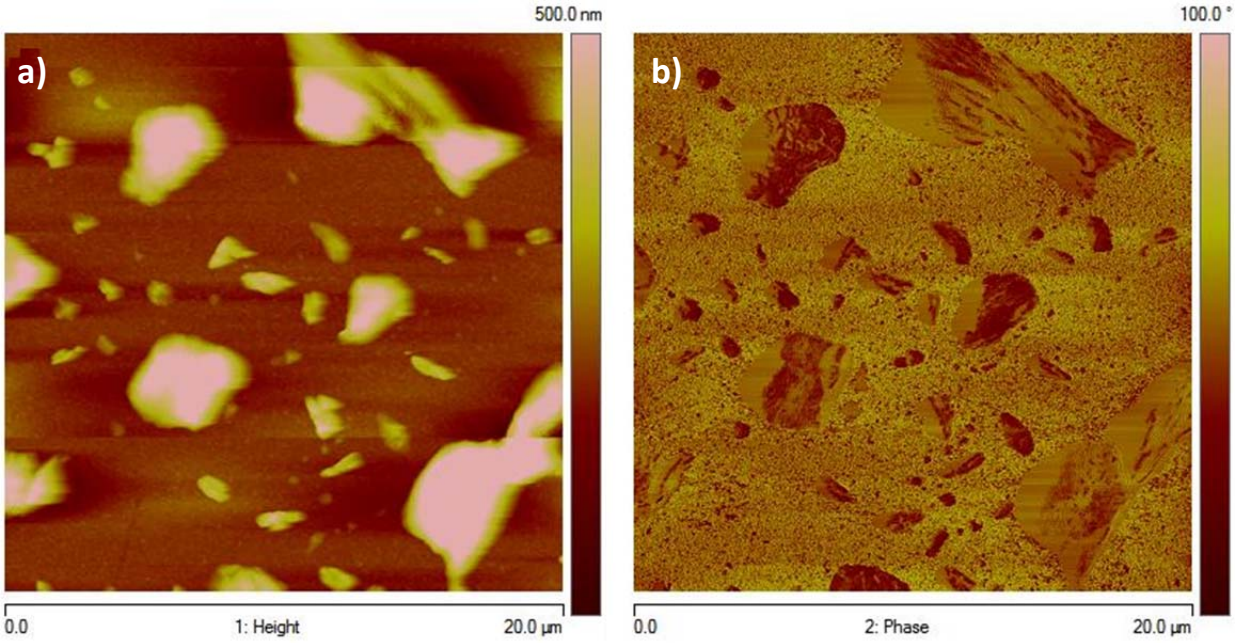

Figure 56: 20 µm × 20 µm AFM images of thin film spin coated from $Ir(ppy)_2(bpy)^+PF_6^-$ mixed with $BMIm^+PF_6^-$ (approach B) on ITO substrate. a) Height image b) Phase image.

ITO covered with PEDOT:PSS

In this last study, the morphology of the film on ITO covered with PEDOT:PSS is investigated. Although this polymer is being used to improve the morphology of the film, it seems that in presence of IL it cannot play its role properly. IL molecules can penetrate to PEDOT:PSS layer and cause the layer to swell [126]. This phenomenon can give an inhomogeneous surface that avoids uniform spreading of the solution and as a consequence forms a very rough film. This film is full of individual (discontinuous) aggregates that are not suitable for LEEC operation.

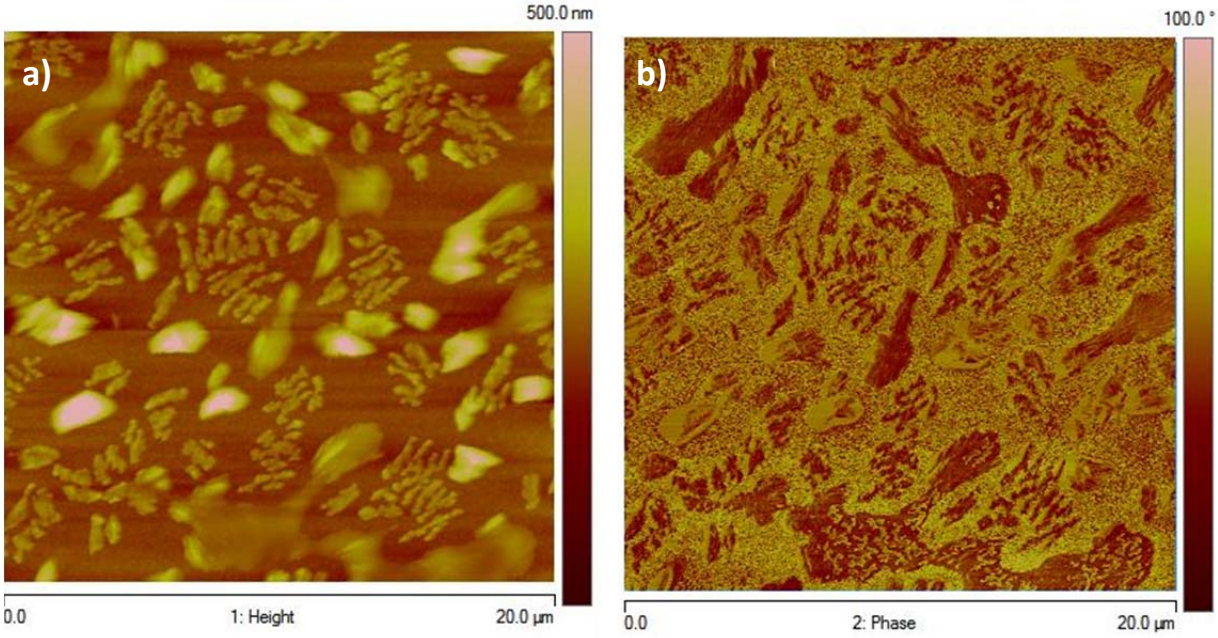

Figure 57: 20 µm × 20 µm AFM images of thin films spin coated from $Ir(ppy)_2(bpy)^+PF_6^-$ mixed with $BMIm^+PF_6^-$ (approach B) on ITO substrate covered with PEDOT:PSS. a) Height image. b) Phase image.

Nevertheless several research groups reported high efficient vertical LEECs using the blend of $Ir(ppy)_2(bpy)^+PF_6^-$ and $BMIm^+PF_6^-$ as an emissive layer [24, 105, 114].

Regarding to this work it seems that the light from their device came from the vertical aggregates individually. Metal evaporation on top of the film might make several separate micro LEECs that can generate light.

If this hypothesis is true, then by application of voltage on separate micro-rods (appendix Figure 62) we can produce light along the rod structure. This can give us the ability to use the complex in flexible lighting manufacturing in a very simple way.

The results of the investigations of the thin film morphologies are summarized in Table 2.

Table 2: Morphological and photophysical properties of Ir complex thin films with different chemical compositions investigated in this work.

Substrate	Thin film	Deposition method	Region	Morphology/ structure	Max PL
Au patterned electrode on SiO_2	No IL	Spin coat	SiO_2	Smooth surface Rms = 0.46 nm	565 nm
			Au	Rough surface Rms = 4.28 nm	575 nm
		Drop cast	SiO_2	Different regions with various complex concentrations and thicknesses	585 nm
			Au		
	$Ir(ppy)_2(bpy)+PF_6^-$: $BMIMPF_6$/1:1 molar ratio	Spin coat	SiO_2	Vertical micro-rods spaced by IL	570 nm
			Au	Condensed circular and rod-shape structures of the complex	585 nm
		Drop cast	SiO_2	Vertical micro-rod islands spaced by IL	
			Au	Condensed texture of the complex and micro-rods with different orientation	
Au patterned on glass	No IL	Spin coat	Glass	Smooth film in the center and different thickness near edge of drop	582 nm
			Au		572 nm
		Drop cast	Glass	Film with different thickness	580 nm
			Au		
	$Ir(ppy)_2(bpy)+PF_6^-$: $BMIMPF_6$/1:1 molar ratio	Spin coat	Glass	Small non continuous spots	590 nm
			Au	Spots larger than on glass	
		Drop cast	Glass	Micro-rods spaced by IL, usually vertical	590 nm
			Au	Compact rods	
ITO	No IL	Spin coat	ITO	Homogenous thin film rms =1.16 nm	580 nm
			PEDOT:PSS on ITO	Very smooth thin film Rms = 0.49 nm	580 nm
	$Ir(ppy)_2(bpy)+PF_6^-$: $BMIMPF_6$/1:1 molar ratio	Spin coat	ITO	Very rough film with aggregates about 100 nm high	585 nm
			PEDOT:PSS on ITO	Very rough surface	585 nm

3.4 Preliminary results on electrical characterization

In order to explore the possibility to employ the two-component films deposited on different substrates in LEEC applications we performed electrical and optical characterizations, simultaneously.

In thin films of Ir complexes we expected thet the redistribution of anions (PF_6^-) leads to the formation of a region of IrIV/IrIII complexs (p-type) near the anode and a region of IrIII/IrII complexs (n-type) near the cathode. When p- and n-type regions are formed near the electrodes, carrier injection is enhanced, leading to increment in device current and emission intensity. However addition of IL with same anion, to provide additional PF_6^-, can accelerate the formation of the p- and n-doped regions in the emissive layer, but the entanglement of bulky cations can possibly impede their migration. Smaller counter ions can accumulate near the electrodes with greater density and produce higher electric fields at the electrodes that help charge injection more efficiently. Besides, more ion accumulation near an electrode can generate very high electric field causing local electrochemical breakdown of the device [98].

Slinker *et al* [98] measured the electric filed distribution in LEEC based on Ru complex. They proved that the accumulation and depletion of mobile ions near the electrodes can build high electric fields in interfaces of emissive film and electrodes. However they did not report the effect of film morphology on device performance. In vertical devices [127] the operating voltage to generate light is around 4V while in planar devices [98] is around 120 V. It may result from the vertical rod formation in emissive thin film. These vertical structures can confine the path of charge transport and as a result improve charge recombination. Nevertheless in our study the planar LEEC based on Ir complex mixed with IL showed emissive spots in SiO_2 channel.

Patterned Au SiO_2 substrate

LEECs are generally characterized by applying different voltages and monitoring the current and photocurrent over time (Figure 58). Increasing voltages of 5, 10, 20 V were applied, with emission detected at 20 V (orange emission as observed by eye).

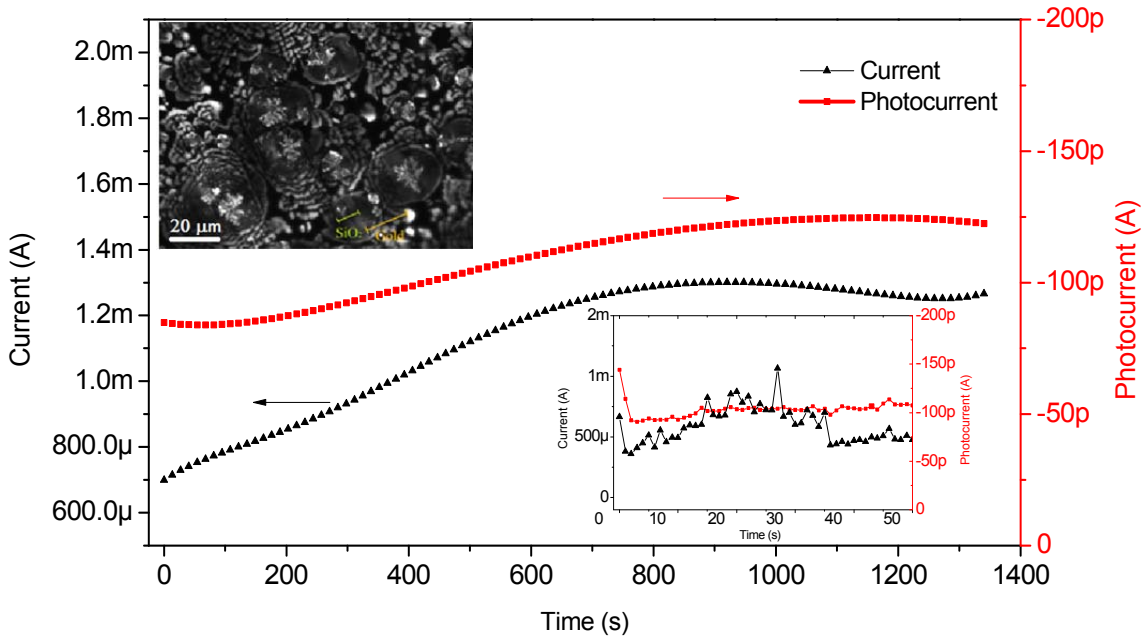

Figure 58: Current and photocurrent versus time for a thin film of $Ir(ppy)_2(bpy)^+PF_6^-$/$BMIm^+PF_6^-$ (Approach B) on Au patterned SiO_2 substrate (channel length is10 microns and width is 5 mm). Applied voltage is 20 V. The inset plot concerns the first 50 seconds of device operation.

After several hours there was a decrease in photocurrent. This emission could not be fully recovered in next measurements even in same condition. This is associated with the degradation of the emissive material during the LEEC operation, which is commonly seen in LEEC devices [128]. In our case we added IL. The electrochemical window of the IL used is around 4.5 Volts. It means that higher than this voltage, the IL will decompose and react with electrodes and other components of the film and increase the aggregation caused by these reactions. Moreover IL causes phase separation as a result of discrepancies in polarity. Therefore more reduction in brightness is not unexpected.

Several irreversible oxidations and subsequent decompositions under a high electric field have been proposed as mechanisms for degradation of LEECs based on cationic iridium complexes [114, 129].

During the electrical measurements, we faced an important issue that is the possibility to achieve the breakdown of the SiO_2 substrate after a certain voltage applied. Indeed SiO_2 is deposited over a doped silicon substrate such that when a voltage is applied between the two electrodes there is an electric field between the doped silicon substrate and each of the two gold patterned electrodes. The current from the bottom substrate (doped silicon), indicated from now on as leakage, shows a high correlation with device current for sufficiently high voltages (60 V for 200 nm thick SiO_2) shown in appendix Figure 66. In this electrical measurement the values of current and leakage are almost the same but with different signs. It means that all the current from the positive electrode vertically passed the dielectric and reached the conductive silicon. Another possibility is the ion penetration from thin film to the Si layer.

After current and/ or photocurrent were detected, the device was observed under fluorescence microscope again. Changes in morphology with respect to the applied voltage showed interesting structures on the surface (Figure 59).

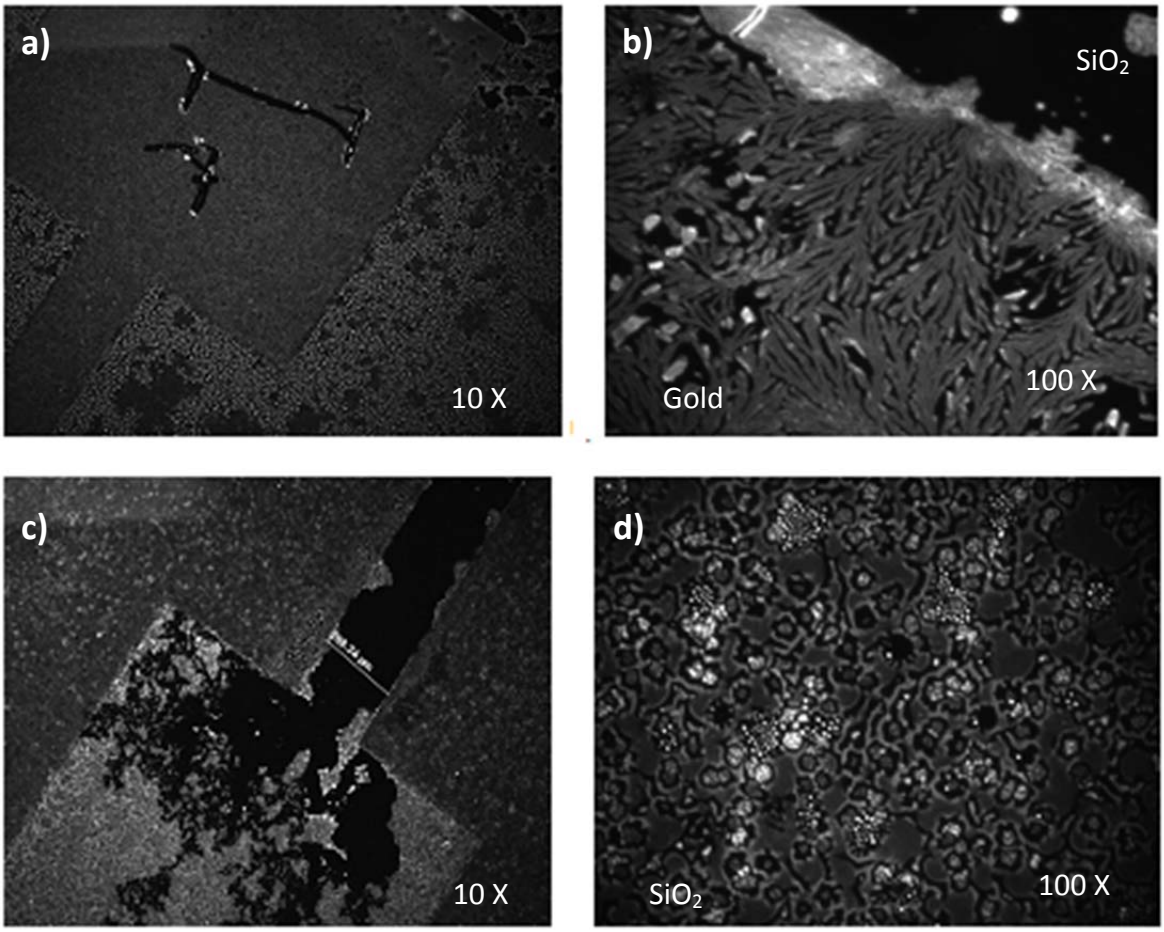

Figure 59: PL images of spin coated thin film of $Ir(ppy)_2(bpy)^+ PF_6^-$ mixed with $BMIm^+PF_6^-$ (approach B) on SiO_2 substrate after 150 V bias. a,b) negative electrode. c,d) positive electrode. DAPI filter cube was used.

In these figures we can see that after application of 120 V, bright spots formed on SiO_2 in the vicinity of the negative electrode while these spots are not observed in proximity of positive electrode. On the other hand, the positive electrode showed a large dark area which can be attributed to the accumulation of PF_6.

Patterned Au on glass substrate

In next step, we used the glass substrate to avoid leakage current. Same gold electrode geometry was used on glass substrate and measurement was done (

Figure 60).

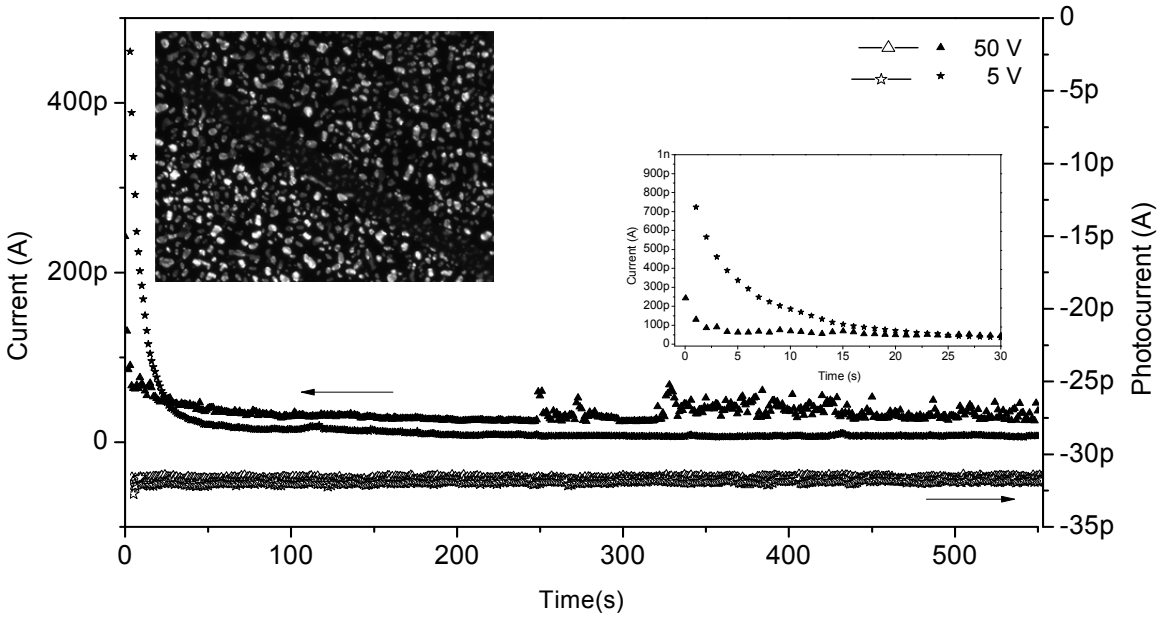

Figure 60: Current and photocurrent observed from thin films of $Ir(ppy)_2(bpy)^+PF_6^-$ mixed with $BMIm^+PF_6^-$ (approach B) on Au patterned glass substrate. Channel length is 10 microns and width is 4 mm. The inset plot includes data collected during first 30 seconds. PL image of the device is shown as inset.

The device had single channel geometry, thus the probability of having emissive material in the channel is much lower than interdigitated device. Devices with glass substrate did not show remarkable change when the voltage is increased. Furthermore low current may originate from the robust and vertical aggregates (rods) formed in the channel that cannot be reoriented even in high voltage. Therefore the glass cannot be a good candidate as a substrate to be used in planar LEECs.

CHAPTER 4 CONCLUSIONS AND PERSPECTIVES

In the field of novel light sources, OLEDs are currently the most developed devices in terms of efficiency, color quality, and operation lifetime. However, their complex and expensive manufacturing methods have motivated the researchers to find alternative device like LEECs. One of the advantages of LEECs over OLEDs is the smaller number of layers to be assembled. In LEECs based on iTMCs, the ionic nature of the phosphorescent complex used as the emissive material is one of the parameters that can reduce the operating voltage and increase device efficiency. Nevertheless, there are notable drawbacks for LEECs. In particular they have a long turn-on times. These can be improved by adding ILs to the emissive material. In turn, adding ILs reduces the life time of the device. Therefore, the fabrication of LEECs with high efficiency, fast turn-on, and long stability needs more investigation. Moreover, further efforts are needed to understand the mechanism of operation of the device and the processes of chemical degradation of the luminescent centers under operating condition.

Conventional LEECs based on iTMC are usually fabricated in vertical configuration. In this configuration the emissive layer is sandwiched between two electrodes such that detecting the luminescence region and charge accumulation regions is very difficult. Therefore to have a better understanding of the mechanism of operation of the device, LEECs with planar configuration are needed.

In this work we investigated the effect of ionic liquids (ILs) and substrates on formation/ structure of thin films for application in LEECs. The results showed that the fabrication of planar LEECs based on $Ir(ppy)_2(bpy)^+PF_6^-$ operating at low voltage is not easily achievable.

Thin films of $Ir(ppy)_2(bpy)^+PF_6^-$ and $Ir(ppy)_2(bpy)^+PF_6^-$/$BMIM^+PF_6^-$ were made on different substrates including Au-patterned SiO_2, Au-patterned glass, ITO, and PEDOT:PSS-covered ITO.

Au-patterned electrodes on both SiO_2 and glass substrates were used in planar devices and ITO and PEDOT:PSS covered ITO substrates were used in vertical LEECs, for comparative studies. We have found that the complex formed smooth films on SiO_2 and on ITO substrate covered with PEDOT:PSS.

We investigated the effect of ionic liquids on film formation. We found that presence of ILs causes inhomogeneous and discontinuous film morphologies, not favorable for charge transport between electrodes. On the other hand, in vertical devices it has been reported that the addition of ILs can increase the device efficiency [45, 114]. This improvement in device performance can be attributed to the complex structures that are formed vertically in addition to ion accumulation in proximity of the electrodes.

The results of this MSc work demonstrate that vertical structures of the complex (islands) form in presence of IL. If the voltage could selectively applied to these vertical structures, charge transport could occur and light could be generated.

In Au patterned SiO_2 substrates, the circular and vertical discontinuous structures spaced by ionic liquid regions were not stable (fixed): they could reorient toward electrodes by voltage application. In drop cast films, long rod-shaped structures, were formed. PL and AFM images of the films on both ITO and PEDOT:PSS covered ITO substrates showed very rough surfaces with huge and sporadic aggregates (around 200 nm) which are not suitable for charge transport in the channel of planar devices. Nevertheless in vertical devices made with the blend of complex/IL (on ITO and PEDOT:PSS covered ITO as substrates) generally after formation of vertical rods, another electrode is deposited on top; therefore each vertical structures (rod) can be an individual micro LEEC that generates light when a voltage is applied. The growth and morphology of the Ir complex films were found to depend significantly on the substrates and the composition of the emissive films.

A number of possible progresses for this MSc work are foreseen:

1) To understand the compatibility of the complex and IL by calorimetry techniques to find the heat associated with chemical and physical changes in the two component system.

2) To understand the mechanism of LEECs operation (to be compared with vertical devices) we can use parylene patterned interdigitated substrates. Interdigitated substrates provide for large channel areas to increase the possibility of continuous structure in the channel; in addition parylene patterning can limit ion accumulation/penetration at electrodes.

3) To fabricate LEECs in micro scale (in rod shape). We could use different approaches such as using polar solvents to control the rod growth and applying voltage on both ends of the rods. If these rods emit, it could be a new method to produce micro lighting devices.

4) To investigate the effect of ILs with different ions and chemical properties on film morphology and device performance.

REFERENCES

[1] C.J. Humphreys, *MRS Bull*, 33 (2008) 459-470.

[2] S. Reineke, F. Lindner, G. Schwartz, N. Seidler, K. Walzer, B. Lüssem, K. Leo, *Nature*, 459 (2009) 234-238.

[3] A.R. Duggal, D.F. Foust, W.F. Nealon, C.M. Heller, OLEDs for lighting: New approaches, in: Optical Science and Technology, SPIE's 48th Annual Meeting, *International Society for Optics and Photonics*,(2004) 241-247.

[4] Y.-P. Jhang, H.-F. Chen, H.-B. Wu, Y.-S. Yeh, H.-C. Su, K.-T. Wong, *Organic Electronics*, 14 (2013) 2424-2430.

[5] R.D. Costa, E. Ortí, H.J. Bolink, F. Monti, G. Accorsi, N. Armaroli, *Angewandte Chemie International Edition*, 51 (2012) 8178-8211.

[6] N. Li, S. Oida, G.S. Tulevski, S.-J. Han, J.B. Hannon, D.K. Sadana, T.-C. Chen, *Nature communications*, 4 (2013).

[7] R.B. Pode, C.J. Lee, D.G. Moon, J.I. Han, *Applied Physics Letters*, 84 (2004) 4614-4616.

[8] B.W. D'Andrade, R.J. Holmes, S.R. Forrest, *Advanced Materials*, 16 (2004) 624-628.

[9] S.J. Su, E. Gonmori, H. Sasabe, J. Kido, *Advanced Materials*, 20 (2008) 4189-4194.

[10] Z.Z. You, J.Y. Dong, *Applied Surface Science*, 253 (2006) 2102-2107.

[11] S.R. Forrest, *Nature*, 428 (2004) 911-918.

[12] J.M. Fernandez-Hernandez, S. Ladouceur, Y. Shen, A. Iordache, X. Wang, L. Donato, S. Gallagher-Duval, M. de Anda Villa, J.D. Slinker, L. De Cola, E. Zysman-Colman, *Journal of Materials Chemistry C*, 1 (2013) 7440-7452.

[13] M. Mydlak, C. Bizzarri, D. Hartmann, W. Sarfert, G. Schmid, L. De Cola, *Advanced Functional Materials*, 20 (2010) 1812-1820.

[14] S. Tang, J. Pan, H.A. Buchholz, L. Edman, *Journal of the American Chemical Society*, 135 (2013) 3647-3652.

[15] J. Fang, P. Matyba, N.D. Robinson, L. Edman, *Journal of the American Chemical Society*, 130 (2008) 4562-4568.

[16] T. Wågberg, P.R. Hania, N.D. Robinson, J.H. Shin, P. Matyba, L. Edman, *Advanced Materials*, 20 (2008) 1744-1749.

[17] Y. Hu, J. Gao, *Journal of the American Chemical Society*, 131 (2009) 18236-18237.

[18] L. He, L. Duan, J. Qiao, R. Wang, P. Wei, L. Wang, Y. Qiu, *Advanced Functional Materials*, 18 (2008) 2123-2131.

[19] H.J. Bolink, E. Coronado, R.D. Costa, E. Ortí, M. Sessolo, S. Graber, K. Doyle, M. Neuburger, C.E. Housecroft, E.C. Constable, *Advanced Materials*, 20 (2008) 3910-3913.

[20] M. Lenes, G. Garcia-Belmonte, D. Tordera, A. Pertegás, J. Bisquert, H.J. Bolink, *Advanced Functional Materials*, 21 (2011) 1581-1586.

[21] K.N. Swanick, S. Ladouceur, E. Zysman-Colman, Z. Ding, *Chemical Communications*, 48 (2012) 3179-3181.

[22] J.M. Fernández-Hernández, S. Ladouceur, Y. Shen, A. Iordache, X. Wang, L. Donato, S. Gallagher-Duval, M. de Anda Villa, J.D. Slinker, L. De Cola, *Journal of Materials Chemistry C*, 1 (2013) 7440-7452.

[23] N.M. Shavaleev, R. Scopelliti, M. Grätzel, M.K. Nazeeruddin, A. Pertegás, C. Roldán-Carmona, D. Tordera, H.J. Bolink, *Journal of Materials Chemistry C*, 1 (2013) 2241-2248.

[24] H.C. Su, F.C. Fang, T.Y. Hwu, H.H. Hsieh, H.F. Chen, G.H. Lee, S.M. Peng, K.T. Wong, C.C. Wu, *Advanced Functional Materials*, 17 (2007) 1019-1027.

[25] Q. Pei, G. Yu, C. Zhang, Y. Yang, A.J. Heeger, *Science*, 269 (1995) 1086-1088.

[26] Q. Pei, Yang, G. Yu, C. Zhang, A.J. Heeger, *Journal of the American Chemical Society,* 118 (1996) 3922-3929.

[27] J.C. Demello, *Nature materials*, 6 (2007) 796.

[28] I. Riess, D. Cahen, *Journal of applied physics*, 82 (1997) 3147-3151.

[29] Q. Pei, Y. Yang, G. Yu, C. Zhang, A.J. Heeger, *Journal of the American Chemical Society*, 118 (1996) 3922-3929.

[30] L. Holzer, F. Wenzl, S. Tasch, G. Leising, B. Winkler, L. Dai, A. Mau, *Applied Physics Letters*, 75 (1999) 2014-2016.

[31] F.P. Wenzl, P. Pachler, C. Suess, A. Haase, E.J. List, P. Poelt, D. Somitsch, P. Knoll, U. Scherf, G. Leising, *Advanced Functional Materials*, 14 (2004) 441-450.

[32] L. Holzer, B. Winkler, F. Wenzl, S. Tasch, L. Dai, A. Mau, G. Leising, *Synthetic metals*, 100 (1999) 71-77.

[33] N. Tessler, S. Graham, R. Friend, *Physical Review B*, 57 (1998) 12951.

[34] S. van Reenen, P. Matyba, A. Dzwilewski, R.A.J. Janssen, L. Edman, M. Kemerink, *Journal of the American Chemical Society*, 132 (2010) 13776-13781.

[35] J. Gao, J. Dane, *Applied Physics Letters,* 84 (2004) 2778-2780.

[36] J. Gao, J. Dane, *Applied Physics Letters*, 83 (2003) 3027-3029.

[37] E.S. Handy, A.J. Pal, M.F. Rubner, *Journal of the American Chemical Society*, 121 (1999) 3525-3528.

[38] M. Buda, G. Kalyuzhny, A.J. Bard, *Journal of the American Chemical Society*, 124 (2002) 6090-6098.

[39] J.D. Slinker, C.Y. Koh, G.G. Malliaras, M.S. Lowry, S. Bernhard, *Applied Physics Letters*, 86 (2005)173506-173503.

[40] J. Sayago, S. Bayatpour, F. Cicoira, C. Santato, *Toward Electrolyte-Gated Organic Light-Emitting Transistors: Advances and Challenges*, Wiley-VCH Verlag GmbH & Co. KGaA, 2013, pp. 215-232.

[41] B. Chen, Y. Li, W. Yang, W. Luo, H. Wu, *Organic Electronics*, 12 (2011) 766-773.

[42] C.-H. Yang, J. Beltran, V. Lemaur, J. Cornil, D. Hartmann, W. Sarfert, R. Fröhlich, C. Bizzarri, L. De Cola, *Inorganic chemistry*, 49 (2010) 9891-9901.

[43] M.S. Lowry, S. Bernhard, *Chemistry-A European Journal*, 12 (2006) 7970-7977.

[44] H. Ohno, *Electrochemical aspects of ionic liquids,* John Wiley & Sons, (2011).

[45] R.D. Costa, A. Pertegás, E. Ortí, H.J. Bolink, *Chemistry of Materials*, 22 (2010) 1288-1290.

[46] H. Ohtani, S. Ishimura, M. Kumai, *Analytical Sciences*, 24 (2008) 1335-1340.

[47] M.J. Earle, J.M. Esperança, M.A. Gilea, J.N.C. Lopes, L.P. Rebelo, J.W. Magee, K.R. Seddon, J.A. Widegren, *Nature,* 439 (2006) 831-834.

[48] B. Clare, A. Sirwardana, D.R. MacFarlane, *Synthesis, purification and characterization of ionic liquids, in: Ionic Liquids*, Springer, (2010), pp. 1-40.

[49] J. Fang, P. Matyba, L. Edman, *Advanced Functional Materials*, 19 (2009) 2671-2676.

[50] T. Welton, *Chemical reviews*, 99 (1999) 2071-2084.

[51] F.S. Oliveira, A.B. Pereiro, J.M. Araújo, C.E. Bernardes, J.N.C. Lopes, S. Todorovic, G. Feio, P.L. Almeida, L.P. Rebelo, I.M. Marrucho, *Physical Chemistry Chemical Physics,* 15 (2013) 18138-18147.

[52] A. Kukhto, *Journal of Applied Spectroscopy*, 70 (2003) 165-194.

[53] U. Mitschke, P. Bäuerle, *Journal of Materials Chemistry,* 10 (2000) 1471-1507.

[54] M. Pope, H. Kallmann, P. Magnante, *The Journal of Chemical Physics*, 38 (1963) 2042-2043.

[55] W. Helfrich, W. Schneider, *Physical Review Letters,* 14 (1965) 229.

[56] P.S. Vincett, W.A. Barlow, R.A. Hann, G.G. Roberts, *Thin Solid Films*, 94 (1982) 171-183.

[57] F. Cicoira, C. Santato, F. Dinelli, M. Murgia, M.A. Loi, F. Biscarini, R. Zamboni, P. Heremans, M. Muccini, *Advanced Functional Materials,* 15 (2005) 375-380.

[58] J. Wunsche, G. Tarabella, S. Bertolazzi, M. Bocoum, N. Coppede, L. Barba, G. Arrighetti, L. Lutterotti, S. Iannotta, F. Cicoira, C. Santato, *Journal of Materials Chemistry C,* 1 (2013) 967-976.

[59] A. Hepp, H. Heil, W. Weise, M. Ahles, R. Schmechel, H. von Seggern, *Physical Review Letters*, 91 (2003) 157406.

[60] C. Santato, I. Manunza, A. Bonfiglio, F. Cicoira, P. Cosseddu, R. Zamboni, M. Muccini, *Applied Physics Letters*, 86 (2005) 141106-141106-141103.

[61] F. Lohmann, W. Mehl, *The Journal of Chemical Physics*, 50 (1969) 500-506.

[62] J. Kalinowski, J. Godlewski, R. Signerski, *Applied Physics A*, 31 (1983) 215-220.

[63] J.G. Basurto, Z. Burshtein, *Molecular Crystals and Liquid Crystals*, 31 (1975) 211-217.

[64] S.E. Shaheen, B. Kippelen, N. Peyghambarian, J.-F. Wang, J.D. Anderson, E.A. Mash, P.A. Lee, N.R. Armstrong, Y. Kawabe, *Journal of applied physics,* 85 (1999) 7939-7945.

[65] J. Cornil, D. Beljonne, D. Dos Santos, J. Brédas, *Synthetic metals*, 76 (1996) 101-104.

[66] H. Schoo, R. Demandt, *Philips journal of research*, 51 (1998) 527-533.

[67] A.J. Heeger, S. Kivelson, J. Schrieffer, W.-P. Su, *Reviews of Modern Physics*, 60 (1988) 781.

[68] V. Maiorano, A. Bramanti, S. Carallo, R. Cingolani, G. Gigli, *Applied Physics Letters*, 96 (2010)133305.

[69] J. Burroughes, D. Bradley, A. Brown, R. Marks, K. Mackay, R. Friend, P. Burns, A. Holmes, *Nature*, 347 (1990) 539-541.

[70] H. Spreitzer, H. Becker, E. Kluge, W. Kreuder, H. Schenk, R. Demandt, H. Schoo, *Advanced Materials*, 10 (1998) 1340-1343.

[71] E. Sawicki, *Analytical Chemistry*, 24 (1952) 1204-1205.

[72] V. Bliznyuk, S. Carter, J. Scott, G. Klärner, R. Miller, D. Miller, *Macromolecules*, 32 (1999) 361-369.

[73] G. Klärner, J.I. Lee, M.H. Davey, R.D. Miller, *Advanced Materials*, 11 (1999) 115-119.

[74] C. Adachi, M.A. Baldo, M.E. Thompson, S.R. Forrest, *Journal of applied physics,* 90 (2001) 5048-5051.

[75] W. Zhu, Y. Mo, M. Yuan, W. Yang, Y. Cao, *Applied Physics Letters,* 80 (2002) 2045-2047.

[76] X. Yang, D. Neher, D. Hertel, T.K. Däubler, *Advanced Materials*, 16 (2004) 161-166.

[77] R.F. Rodrigues, P. Ferreira da Silva, K. Shimizu, A.A. Freitas, S.A. Kovalenko, N.P. Ernsting, F.H. Quina, A. Maçanita, *Chemistry-A European Journal,* 15 (2009) 1397-1402.

[78] K.-C. Tang, K.L. Liu, I. Chen, *Chemical physics letters*, 386 (2004) 437-441.

[79] H.-C. Su, C.-C. Wu, F.-C. Fang, K.-T. Wong, *Applied Physics Letters*, 89 (2006) 261118-261118-261113.

[80] S.J. Lee, J.H. Seo, J. Sea, G.Y. Kim, Y.Y. Jin, Y.K. Kim, *Journal of nanoscience and nanotechnology*, 9 (2009) 7044-7047.

[81] N.J. Turro, *Modern molecular photochemistry*, University Science Books, 1991.

[82] I.D.J.a.M.W. Davidson, Fluorescence Microscopy Interactive Java Tutorials Jablonski Energy Diagram, in, National High Magnetic Field Laboratory, Florida, 2006 http://micro.magnet.fsu.edu/primer/java/jablonski/jabintro/.

[83] Z.H. Kafafi, ed. *Organic electroluminescence*, CRC Press, 2005.

[84] V.A. Montes, R. Pohl, J. Shinar, P. Anzenbacher, *Chemistry-A European Journal,* 12 (2006) 4523-4535.

[85] G.L. Closs, M.D. Johnson, J.R. Miller, P. Piotrowiak, *Journal of the American Chemical Society,* 111 (1989) 3751-3753.

[86] M. Fujita, *Nature Photonics*, 7 (2013) 264-265.

[87] H. Henisch, *Reports on Progress in Physics*, 27 (1964) 369.

[88] J.R. Lakowicz,ed. *Principles of fluorescence spectroscopy*, Springer, 2007.

[89] E.E.W. Rudi Rottenfusser, Michael W. Davidson, Education in Microscopy and Digital Imaging, The Florida State University, Tallahassee, Florida, from http://zeiss-campus.magnet.fsu.edu/articles/basics/fluorescence.html.

[90] Reichman, Jay, *Handbook of optical filters for fluorescence microscopy*, Chroma Technology Corporation (2000).

[91] J.M. Lerner, *Cytometry Part A,* 69 (2006) 712-734.

[92] D. Işık, C. Santato, S. Barik, W. Skene, *Organic Electronics*, 13 (2012) 3022-3031.

[93] Amyhallr, An introduction to Atomic Force Microscopy, London, 2013 from http://amyhallr.wordpress.com/2013/03/15/atomic-force-microscopy/.

[94] AZoNano, Fundamentals of Contact Mode and TappingMode Atomic Force Microscopy, 2014 from http://www.azonano.com/article.aspx?ArticleID=3010.

[95] E.H. Chow, D.-K. Bučar, W. Jones, *Chemical Communications,* 48 (2012) 9210-9226.

[96] Vecco, (2013) from http://www.azom.com/article.aspx?ArticleID=3279.

[97] Atomic Force Microscopy for biological applications- interactive tutorial, in: N.S. Foundation (Ed.), 2014, from http://medicine.tamhsc.edu/basic-sciences/sbtm/afm/copyright.php.

[98] J.D. Slinker, J.A. DeFranco, M.J. Jaquith, W.R. Silveira, Y.-W. Zhong, J.M. Moran-Mirabal, H.G. Craighead, H.D. Abruna, J.A. Marohn, G.G. Malliaras, *Nature materials,* 6 (2007) 894-899.

[99] K.K.-W. Lo, S.P.-Y. Li, K.Y. Zhang, *New Journal of Chemistry*, 35 (2011) 265-287.

[100] P. Wu, E.L.M. Wong, D.L. Ma, G.S.M. Tong, K.M. Ng, C.M. Che, *Chemistry-A European Journal,* 15 (2009) 3652-3656.

[101] M.S. Lowry, J.I. Goldsmith, J.D. Slinker, R. Rohl, R.A. Pascal, G.G. Malliaras, S. Bernhard, *Chemistry of Materials,* 17 (2005) 5712-5719.

[102] Y. Kawamura, J. Brooks, J.J. Brown, H. Sasabe, C. Adachi, *Physical Review Letters*, 96 (2006) 017404.

[103] K.-C. Tang, K.L. Liu, I.C. Chen, *Chemical physics letters*, 386 (2004) 437-441.

[104] I. Georgakoudi, T.H. Foster, *Photochemistry and Photobiology*, 67 (1998) 612-625.

[105] R.D. Costa, E. Ortí, H.J. Bolink, S. Graber, S. Schaffner, M. Neuburger, C.E. Housecroft, E.C. Constable, *Advanced Functional Materials*, 19 (2009) 3456-3463.

[106] D.E. Packham, *International Journal of Adhesion and Adhesives*, 23 (2003) 437-448.

[107] M.A. Uddin, W.F. Ho, C.K. Chow, H.P. Chan, *Journal of Elec Materi,* 35 (2006) 1558-1565.

[108] Matt, Surface Energy — Its Relation to Contact Angle Analysis and Its Importance to your Business, (2010) from http://www.astp.com/archives/1138.

[109] M. Pope, C.E. Swenberg, *Electronic processes in organic crystals*, Clarendon Press Oxford, 1982.

[110] J.D. Slinker, A.A. Gorodetsky, M.S. Lowry, J. Wang, S. Parker, R. Rohl, S. Bernhard, G.G. Malliaras, *Journal of the American Chemical Society,* 126 (2004) 2763-2767.

[111] B. Friedel, P.E. Keivanidis, T.J.K. Brenner, A. Abrusci, C.R. McNeill, R.H. Friend, N.C. Greenham, *Macromolecules*, 42 (2009) 6741-6747.

[112] B. Winther-Jensen, K. West, *Reactive and Functional Polymers*, 66 (2006) 479-483.

[113] L.A.A. Pettersson, S. Ghosh, O. Inganäs, *Organic Electronics*, 3 (2002) 143-148.

[114] S.T. Parker, J.D. Slinker, M.S. Lowry, M.P. Cox, S. Bernhard, G.G. Malliaras, *Chemistry of Materials*, 17 (2005) 3187-3190.

[115] P.J. Brewer, P.A. Lane, J. Huang, D.D. Bradley, *Physical Review B*, 71 (2005) 205209.

[116] H.C. Su, F.C. Fang, T.Y. Hwu, H.H. Hsieh, H.F. Chen, G.H. Lee, S.M. Peng, K.T. Wong, C.C. Wu, *Advanced Functional Materials,* 17 (2007) 1019-1027.

[117] E. Zysman-Colman, J.D. Slinker, J.B. Parker, G.G. Malliaras, S. Bernhard, *Chemistry of Materials*, 20 (2007) 388-396.

[118] H. Rudmann, S. Shimada, M.F. Rubner, *Journal of the American Chemical Society*, 124 (2002) 4918-4921.

[119] Amulya KN. *Modern Electrochemistry 1: Ionics*. Vol. 1. Springer, 1998..

[120] A.M. Rizzuto, R.L. Pennington, K.D. Sienerth, *Electrochimica Acta*, 56 (2011) 5003-5009.

[121] T.W.G. Solomons, C.B. Fryhle, *Organic chemistry*, 9th ed, Wiley India Pvt. Limited, 2008.

[122] P. Attri, S.-H. Lee, S.W. Hwang, J.I. Kim, S.W. Lee, G.-C. Kwon, E.H. Choi, I.T. Kim, *PloS one*, 8 (2013) 68970.

[123] J. Drelich, E. Chibowski, D.D. Meng, K. Terpilowski, *Soft Matter,* 7 (2011) 9804-9828.

[124] S.N.V.K. Aki, J.F. Brennecke, A. Samanta, *Chemical Communications*, (2001) 413-414.

[125] W.W. Scott, B. Bhushan, *Ultramicroscopy,* 97 (2003) 151-169.

[126] V. Armel, J. Rivnay, G. Malliaras, B. Winther-Jensen, *Journal of the American Chemical Society*, 135 (2013) 11309-11313.

[127] A.A. Gorodetsky, S. Parker, J.D. Slinker, D.A. Bernards, M.H. Wong, G.G. Malliaras, S. Flores-Torres, H.D. Abruña, *Applied Physics Letters,* 84 (2004) 807-809.

[128] G. Kalyuzhny, M. Buda, J. McNeill, P. Barbara, A.J. Bard, *Journal of the American Chemical Society*, 125 (2003) 6272-6283.

[129] Y. Ohsawa, S. Sprouse, K. King, M. DeArmond, K. Hanck, R. Watts, *Journal of Physical Chemistry*, 91 (1987) 1047-1054.

[130] B. Beyer, C. Ulbricht, D. Escudero, C. Friebe, A. Winter, L. González, U.S. Schubert, *Organometallics*, 28 (2009) 5478-5488.

APPENDIX

Absorption spectrum

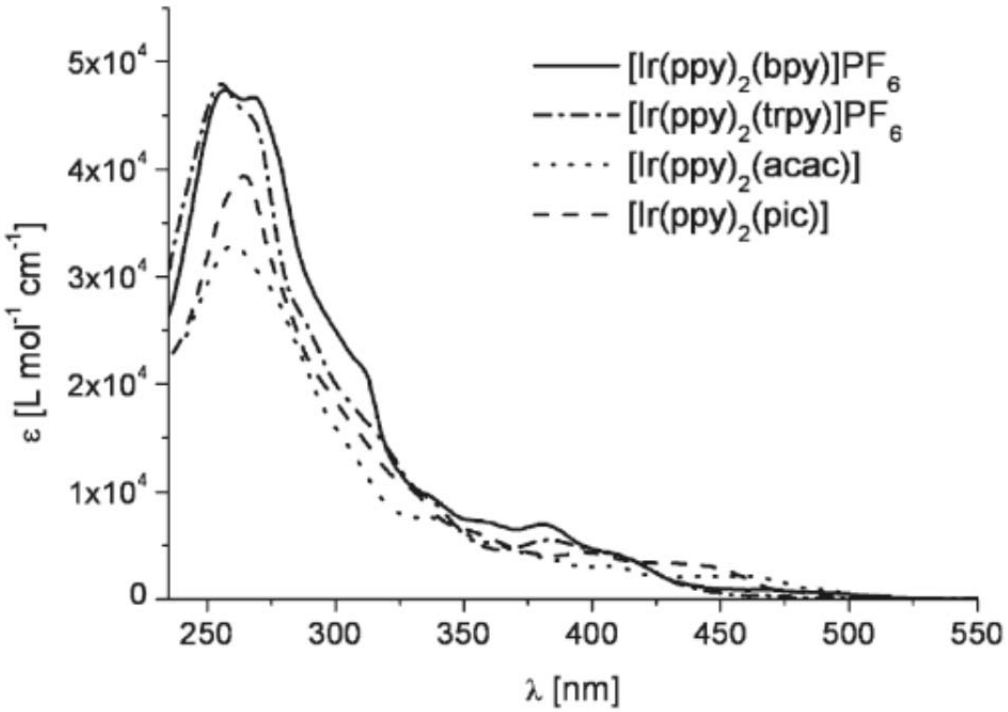

Figure 61: Absorption spectra of the thin film of $Ir(ppy)_2(bpy)^+PF_6^-$ [130].

PL images

One suggested approach to control the rod formation was preparation of rods in the solution and afterward the deposition of them in the channel.

For this purpose a polar solvent were used (ethanol). Ethanol was added to the blend solution. The vial was kept at room temperature and after 15 hours the solution was full of rods.

The rods were drop casted on the channel and put for annealing for 1 hour at 80 ^oC.

a)

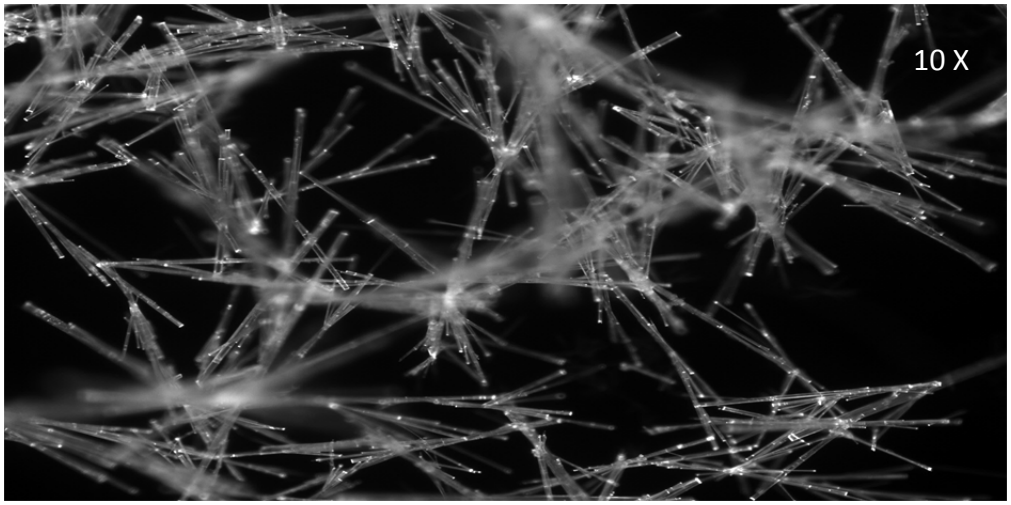

b)

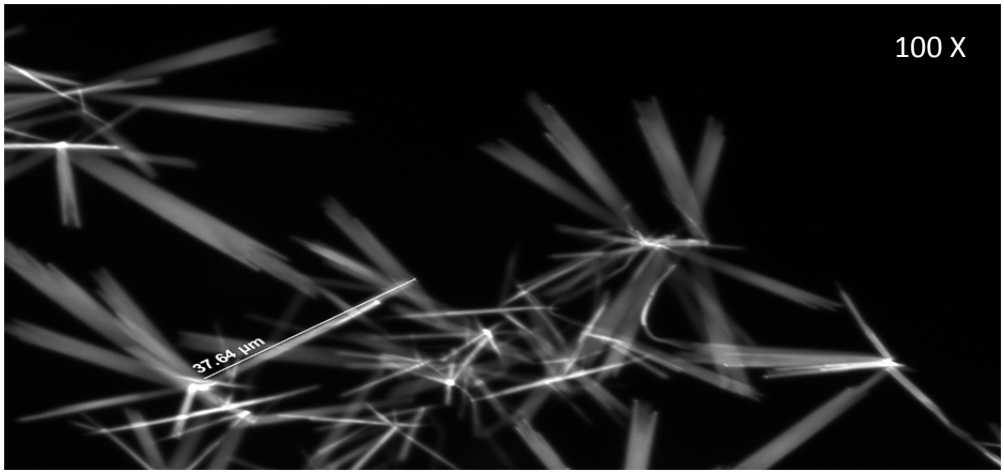

Figure 62: PL images of the drop casted thin film of $Ir(ppy)_2(bpy)^+PF_6^-$ mixed with $BMIm^+PF_6^-$ (approach B) adding polar solvent (ethanol) to increase the rod formation. Ethanol was added in ambient air. a) 10× b) 100×. DAPI filter was used.

Polar solvent increase both cations and anions movements and provide narrower and longer rods in comparison with aprotic solvent!

AFM images

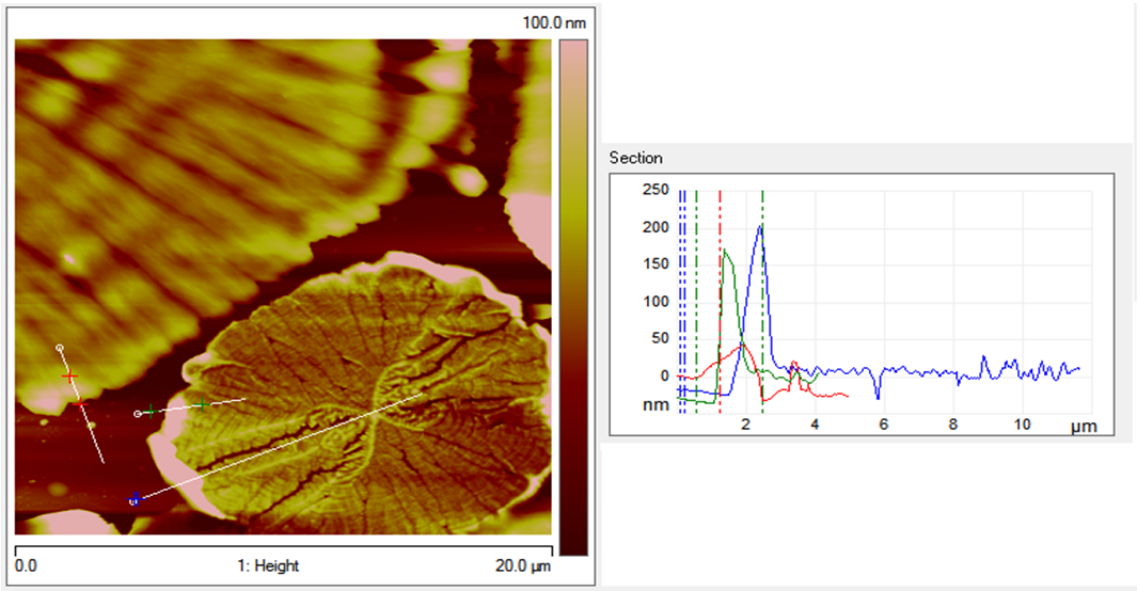

Figure 63: AFM Section profile of the thin film of $Ir(ppy)_2(bpy)^+PF_6^-$ mixed with $BMIm^+PF_6^-$ (approach B) on SiO_2 substrate

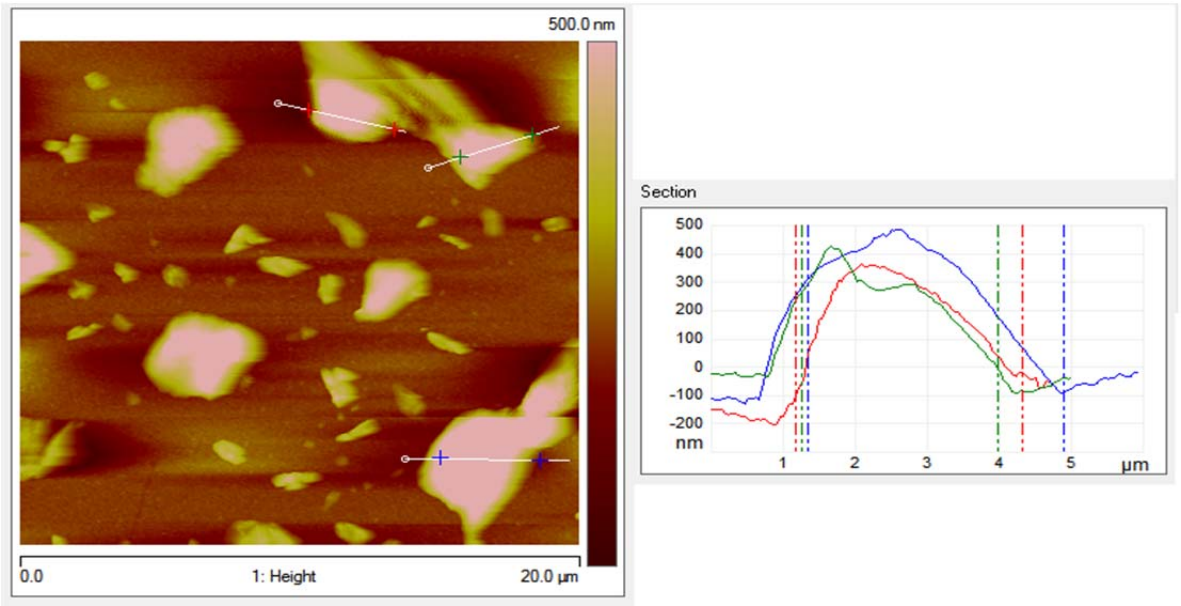

Figure 64: AFM Section profile of the thin film of $Ir(ppy)_2(bpy)^+PF_6^-$ mixed with $BMIm^+PF_6^-$ (approach B) on ITO substrate.

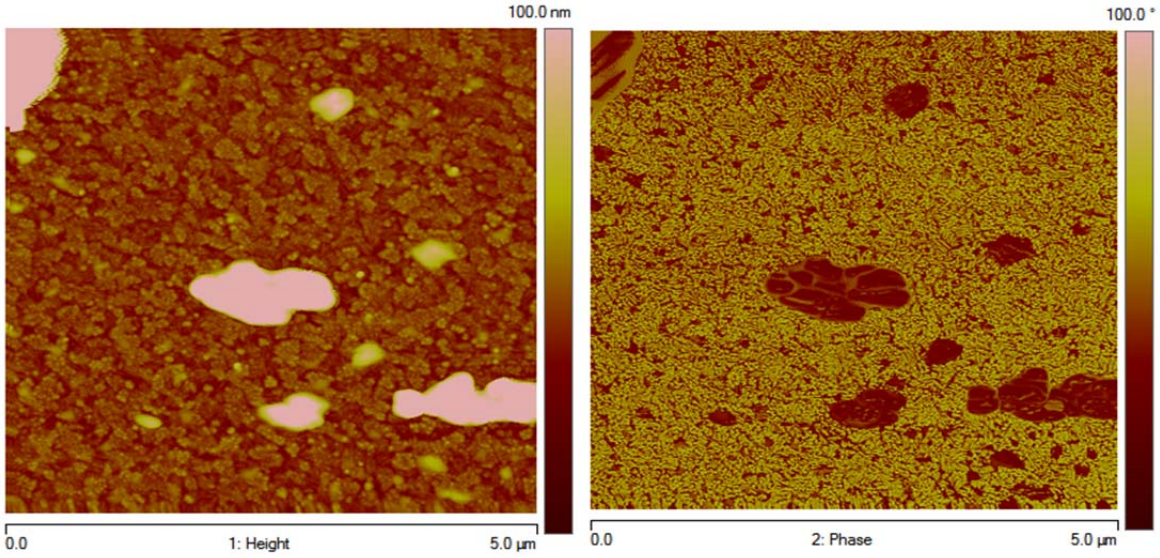

Figure 65: AFM images of of the thin film of $Ir(ppy)_2(bpy)^+PF_6^-$ mixed with $BMIm^+PF_6^-$ (approach B) on ITO substrate

Leakage current

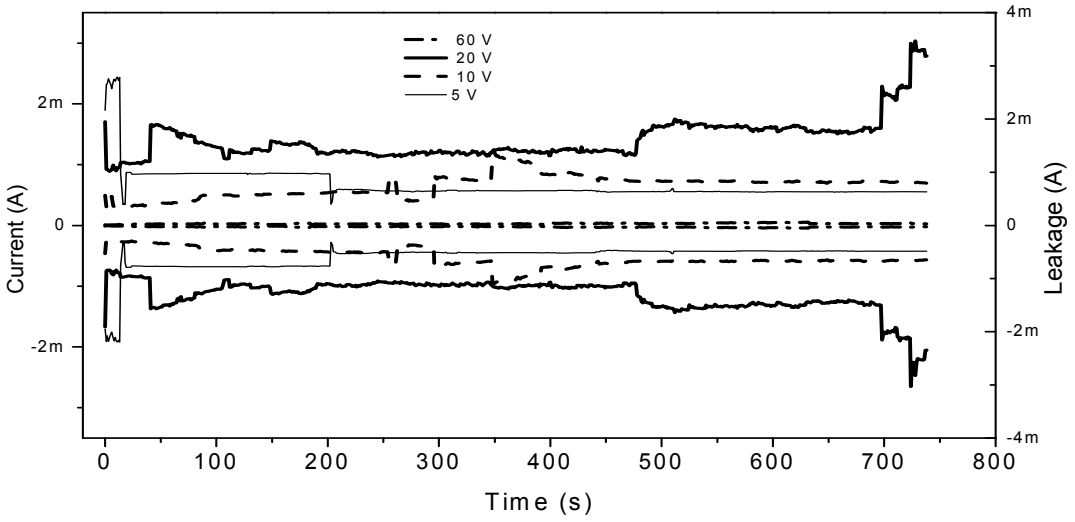

Figure 66: Comparison of the current and leakage current (vertical current) for a thin film of $Ir(ppy)_2(bpy)^+PF_6^-$ mixed with $BMIm^+PF_6^-$ (Approach B) on Au patterned SiO_2 substrate (channel length is 10 microns and width is 4 mm). Positive values of the curves describe the current (left axis) and the negative values represent the leakage current (right axis).